International Scientific-Technical and Production Journal

The Paton WELDING JOURNAL

November 2010 # 11

English translation of the monthly «Avtomaticheskaya Svarka» (Automatic Welding) journal published in Russian since 1948

Founders: *E.O. Paton Electric Welding Institute of the NAS of Ukraine*
International Association «Welding»

Publisher: *International Association «Welding»*

Address:
E.O. Paton Electric Welding Institute,
International Association «Welding»,
11, Bozhenko str., 03680, Kyiv, Ukraine
Tel.: (38044) 287 67 57, 200 82 77
Fax: (38044) 528 04 86, 200 82 77
E-mail: journal@paton.kiev.ua
http://www.nas.gov.ua/pwj

State Registration Certificate
KV 4790 of 09.01.2001

Subscriptions:
$324, 12 issues per year,
postage and packaging included.
Back issues available.

CONTENTS

EFFECT OF NANOFOIL OF THE Ni–NbC SYSTEM ON STRUCTURE OF ELECTRON BEAM WELDS IN HEAT-RESISTANT ALLOYS

K.A. YUSHCHENKO, A.I. USTINOV, B.A. ZADERY, V.S. SAVCHENKO, T.V. MELNICHENKO, V.V. KURENKOVA, A.V. ZVYAGINTSEVA and **I.S. GAKH**
E.O. Paton Electric Welding Institute, NASU, Kiev, Ukraine

The effect of niobium carbide nanoparticles on structure and properties of electron beam welds in nickel alloys was studied. Alloying of the weld metal with niobium carbide nanoparticles was performed by adding composite nanostructured foil of the Ni–NbC system into the weld pool. The foil was produced by electron beam evaporation of the components in vacuum, followed by combined deposition of their vapour flows on the substrate. Adding the niobium carbide nanoparticles into the weld pool was shown to lead to formation of crystalline grains with a cellular structure within the weld zone, with the NbC particles located along the boundaries of the above grains. The effect of this structure of the welds on their mechanical properties was analysed.

Keywords: *electron beam welding, electron beam evaporation, nickel alloy, weld, foil, alloying, modification, niobium monocarbide, nanoparticles, intragranular substructure*

Main difficulties in welding heat-resistant precipitation-hardening nickel-base alloys are associated with the need to prevent hot cracking of the welds and provide the welded joints with a required set of mechanical, technological and service properties. One of the ways of addressing these problems is optimisation of alloying of the weld metal. The alloying elements of choice in this case are those that improve high-temperature ductility of the weld (even at the expense of decreasing its strength compared to that of the base metal). Cracking of the weld metal and HAZ can be avoided by adding molybdenum, vanadium, cobalt, manganese, titanium, boron, rhenium, hafnium and yttrium, as well as their borides, oxides and carbides to the weld metal, and by controlling the welding process [1–5].

However, traditional methods used for alloying the welds have a number of drawbacks. For example, alloying the weld metal with molybdenum and tungsten decreases high-temperature corrosion resistance, presence of boron reduces heat resistance, and adding rhenium, hafnium and yttrium is difficult to implement in terms of technology. In this connection, optimisation of a method of alloying the weld metal in welding heat-resistant precipitation-hardening nickel alloys is a problem of current importance.

One of the most common metallurgical methods for preventing hot cracking is refining of structure of the weld metal and HAZ by alloying the weld pool with modifiers [6–8]. Adding small amounts of nitrides, carbides, oxides and other elements promotes formation of fine-grained structure of the weld metal owing to heterogeneous solidification [9]. Modification also contributes to the intensity of the diffusion processes in the melt and promotes lowering of the level of liquation in the weld metal [7].

Positive results were obtained from using thin composite foils consisting of components of a nanosized scale as a filler metal in fusion welding or as a transition element in pressure welding [10, 11]. Such foils produced by combined condensation of various components from the vapour phase and containing nanoparticles provide activation of the diffusion processes during welding [12–15]. Supposedly, adding refractory nanoparticles to the weld pool will also promote increase in the number of solidification centres and, eventually, grain refining, formation of equiaxed structure and uniform distribution of alloying elements in the weld metal.

By an example of model materials (nickel), this study considers the possibility of modifying structure of the welds by using fillers in the form of foils that contain nanosized carbide phases, and gives estimation of strength properties of the resulting welded joints.

Pure nickel being the base of heat-resistant alloys was used as a model material to evaluate the effect of nanoparticles added to the weld pool on structure of the weld metal. Chemical composition of alloying filler metals was selected allowing for the requirement of filler and base metal matching. From this standpoint, the preference was given to niobium monocarbide, which is characterised by high thermodynamic stability and used as a structural component of many heat-resistant alloys.

The filler metal based on a composite of the Ni–NbC system in the form of foil 50–150 μm thick was produced by electron beam evaporation of components in vacuum using two ingots, followed by combined deposition of their vapour flows on the substrate at a preset temperature. The flow diagram of the deposition process is given in [10, 11]. A layer of CaF_2 was

Microhardness of welds made on nickel by using filler foils of different chemical compositions

NbC in foil	NbC in weld metal	*HV*, MPa
Without foil	0	1200
6.7	0.68	1310
8.8	0.73	1385
20.0	0.87	1475
26.0	0.96	1495
28.0	1.07	1515
35.5	1.37	1735
60.0	2.70	1865

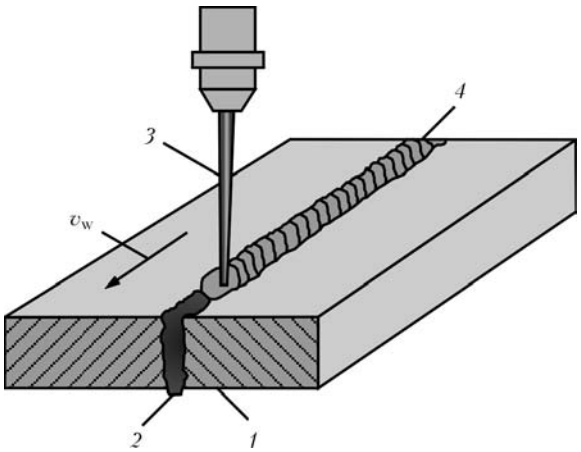

Figure 1. Flow diagram of the EBW process using nanostructured foil as filler metal: *1* — base metal; *2* — filler foil; *3* — electron beam; *4* — weld

preliminarily deposited on the substrate, which provided easy detachment of the foil. Pressure in the chamber during deposition was maintained at a level of $5 \cdot 10^{-3}$ Pa. The temperature of the substrate during deposition was 550–600 °C.

Nickel specimens for the experiment were cut from the billets by the electric spark method. They were polished and then degreased before welding. The filler in the form of foils of different thicknesses and compositions (Figure 1, Table) was butt added between the two halves of the billet to be welded.

The choice of electron beam welding (EBW) was based on the possibility of regulating temperature-time conditions of the process, volume and shape of the weld, and limiting the negative effect of residual atmosphere on the weld metal. EBW was performed by using installation U-212m with a capacity of 30 and 14 kW. For intensive stirring of the filler material with the base metal, welding was carried out at a low speed (about 8–12 m/h) with transverse scanning of the electron beam.

Specimens of the filler foil and welded joints were prepared for metallographic analysis by a standard procedure using grinding-and-polishing machine «Abramin» of the «Struers» Company. Structure and chemical composition of the foil and weld zone were analysed by using scanning microscope «SamScan» equipped with energy-dispersive local analysis system «Energy 200». Microhardness of the weld was measured by using the microhardness measuring attachment to optical microscope «Polyvar-Met» under a load of 0.49 N by the Vickers method. Structure of the filler foil and weld metal in the planar and transverse sections was analysed by using transmission electron microscope «Hitachi H-800» at an accelerating voltage of 200 kV. The foils for these examinations were subjected to mechanical thinning and polishing by using machine «GATAN 656», and then to thinning by bombarding the surface at an angle of 3° with argon ions at the energy of 5 keV and ion gun current of 20 mA using machine «PIPS 691».

X-ray diffraction analysis of the composite filler foil was carried out by using standard geometry θ–2θ with diffractometer «DRON-4» in Cu_{K_α} radiation.

Composite filler foil Ni–(6.7–35.5) wt.% NbC produced by the electron beam evaporation method had a uniform distribution of components through thickness δ (Figure 2). Cross section of the filler foil in the initial state had a columnar structure, width of the columnar crystalline grains being approximately 300 nm (Figure 3). The low condensation temperature provided formation of nano-scale carbide particles in the condensate, which was confirmed by the presence of wide diffraction peaks (indicated by arrows in Figure 4, *a*) of NbC in the diffraction pattern of a specimen of foil Ni–6.7 wt.% NbC after deposition. Narrow peaks of NbC appeared in the diffraction pattern only after annealing of the foil at a temperature of 1100 °C for 2 h, this being indicative of coarsening of the carbide particles (Figure 4, *b*).

The clearly pronounced peaks of nickel and niobium carbide appeared in the diffraction pattern after the content of NbC grew to 35.5 wt.% (Figure 4, *c*), i.e. increase in the niobium carbide content of the composite was accompanied by coarsening of the carbide particles.

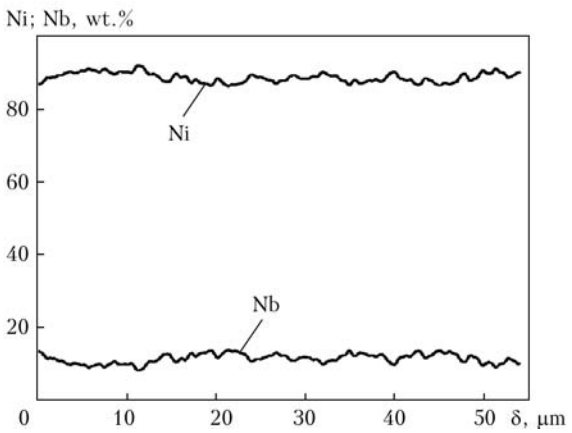

Figure 2. Distribution of elements through thickness δ of composite foil of the Ni–NbC system

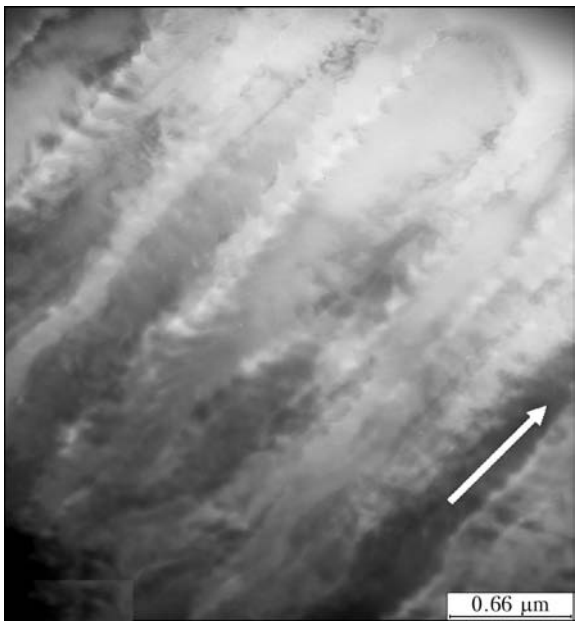

Figure 3. Microstructure of specimen of composite foil Ni–6.7 wt.% NbC (direction of growth of crystalline grains is indicated by arrow)

According to the results of X-ray spectral microanalysis, the use of this foil as a filler metal provides formation of dense defect-free welds with a uniform and regular distribution of carbide particles over the entire volume of the weld (Figure 5). It should be noted that this uniformity of distribution of added particles over the entire weld pool is hard to provide by modifying it with powder modifiers. It can be seen that with the use of the filler foil the nanosized NbC particles are uniformly distributed in the bulk of the forming weld metal during the EBW process and convective stirring of the weld pool. At a NbC content of the foil equal to about 28 wt.%, the average NbC content of the weld metal was approximately 1.07 wt.%. Increase in the NbC content of the filler foil from 6.7 to 35.5 wt.% led to growth of the weight fraction of carbide particles in the weld metal (see the Table). For instance, at the up to 10 wt.% NbC content of the foil the weight fraction of the carbide phase in the weld was 0.68–0.73 %, and at the 20 to 60 wt.% NbC content the weight fraction of this phase grew from 0.87 to 2.70 %.

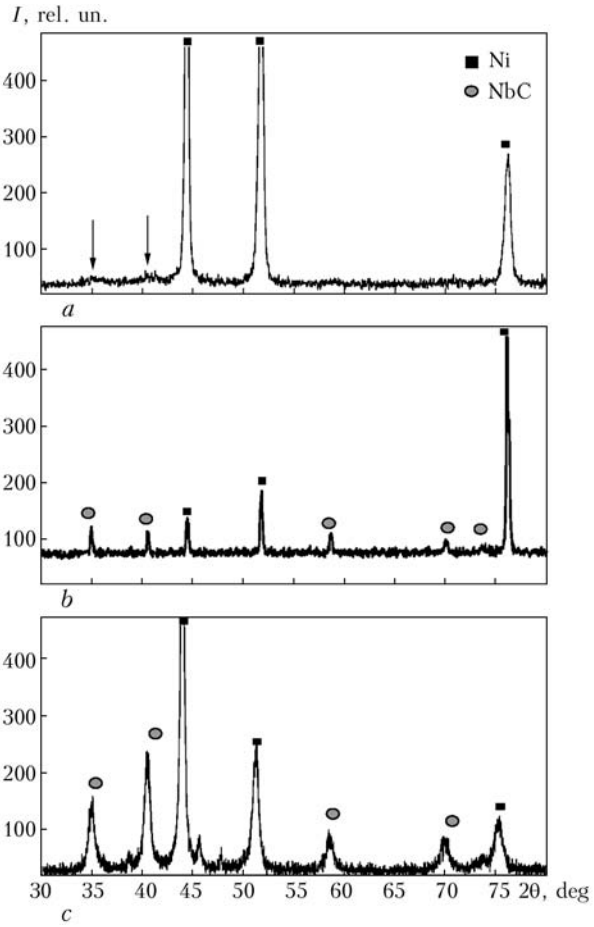

Figure 4. Diffraction patterns of specimens of composite foils Ni–6.7 wt.% NbC after deposition (*a*), subsequent annealing at 1100 °C for 2 h (*b*), and Ni–35.5 wt.% NbC (*c*) in Cu_{K_α} radiation

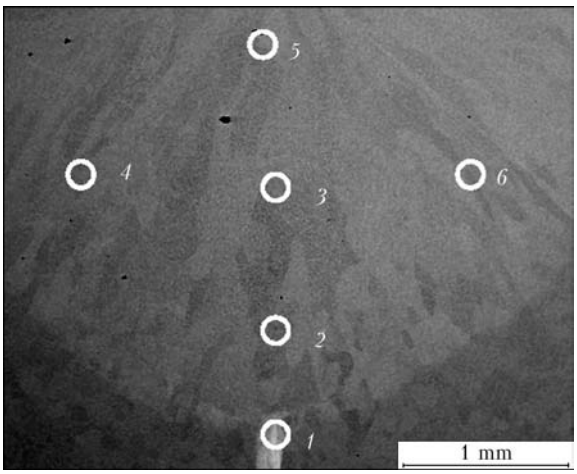

Figure 5. Microstructure of weld metal produced by using composite foil Ni–28 wt.% NbC (the photo was made in the phase contrast mode; numbers show the points of determination of local chemical composition): *1* — 19.90; *2* — 1.11; *3* — 1.15; *4* — 1.00; *5* — 1.47; *6* — 1.05 wt.% NbC

In welding of pure nickel using no filler foil, the structure formed in the joint zone featured a slightly pronounced orientation of primary crystalline grains towards the weld surface (Figure 6, *a*). The size of cross sections of the crystalline grains was 80–200 μm, and their length was 150–500 μm. Grain microstructure of the weld was homogeneous, having no visible precipitates of secondary phases (Figure 6, *a*, *c*).

An insignificant decrease (to 50–120 μm) in the transverse grain size was observed when using filler metal in the form of the Ni–NbC foil with the NbC content of about 6.7 wt.%. In this case, the primary grains had a more equiaxed polyhedral shape (Figure 6, *b*, *d*). The presence of nanosized carbide particles in the weld pool promoted refining of the primary crystalline grains forming along the line of fusion with the substrate (Figure 6, *e*, *f*). The transverse size of the polyhedral grains at the solidification front in metal decreased from 150–300 μm (for the weld produced without filler) to 50–70 μm, which is a positive factor for prevention of formation of the columnar oriented structure of primary crystalline grains.

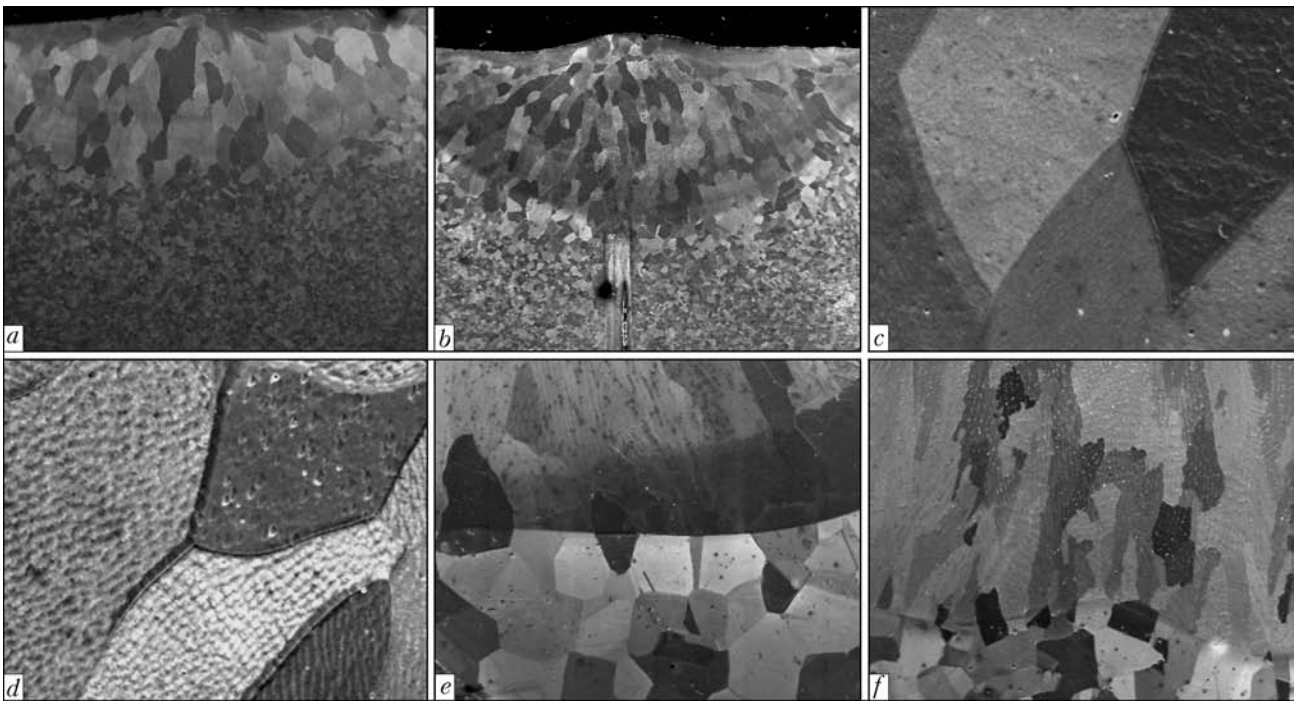

Figure 6. Microstructure of metal of the welds made on nickel without nanostructured filler (*a*, *c*, *e*), and with filler foils Ni–6.7 wt.% NbC (*b*, *d*) and Ni–20 wt.% NbC (*f*)

Metallographic etching revealed an internal substructure of the grains in the form of subboundaries, having certain orientation in the bulk of a given crystalline grain. Substructure became more pronounced with increase in the weight fraction of the NbC particles in the weld pool, i.e. with increase in the NbC content in the filler metal (see the Table). As the second phase content increased, the boundaries of subgrains became more clearly defined and developed (Figure 7, *a*, *b*). X-ray spectral analysis by scanning the area of a single crystalline grain in the weld metal revealed distribution of the niobium-rich phase along the subboundaries of cells of the primary crystalline grains (Figure 7, *c*).

Electron microscopy of central regions of the subgrains showed that they did not contain the NbC particles and were characterised by a low dislocation density (Figure 8, *a*, *c*). The regions located near the subgrains contained the NbC particles (Figure 8, *d*) and featured a high dislocation density (Figure 8, *c*).

Increasing the NbC content of the foil to 60 wt.% caused not only increase in the weight fraction of niobium along the subboundaries of primary crystalline grains of the weld but also precipitation of discrete NbC particles 0.5–1.0 μm in size (light particles), whose structure corresponded to stoichiometric carbide NbC, according to the electron diffraction pattern (Figure 9).

Welding of pure nickel involves no difficulties, as no phase transformations take place in heating or cooling it. It can be assumed that stable groups of atoms are formed in the bulk of the pure nickel melt in overcooling, and some of them act as the solidification centres. Peculiarity of formation of the welds in pure nickel is that the molten metal of the weld pool is characterised by a high sensitivity to impurities located along the boundaries of primary grains and subgrains of the weld metal. The results obtained allow a conclusion that with adding into the weld pool the filler metals that contain refractory carbide particles

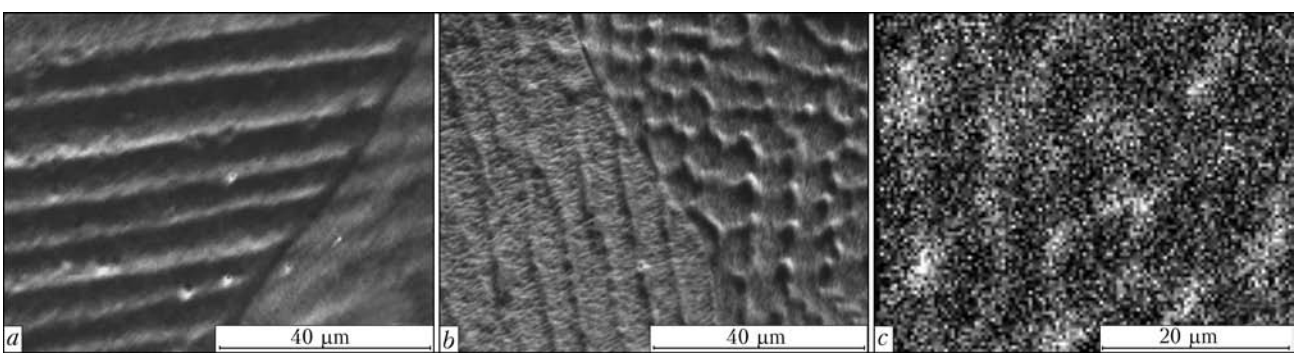

Figure 7. Substructure of primary grains of metal of the welds made on nickel at their 8.86 (*a*) and 35.5 (*b*) wt.% NbC content, and electron microscopic picture of distribution of niobium in one crystalline grain (*c*) (regions with light contrast at subboundaries correspond to 3.04 wt.% NbC)

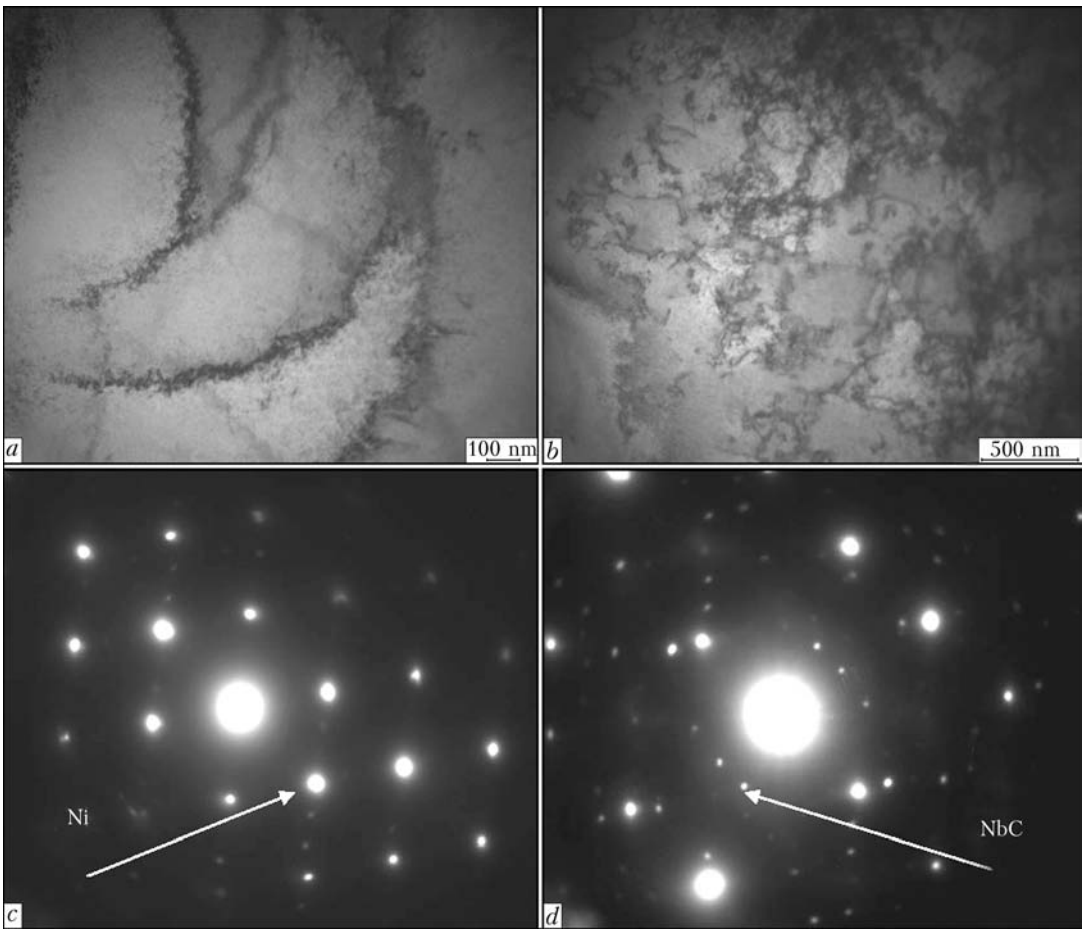

Figure 8. Microstructure (*a*, *b*) and corresponding electron diffraction patterns (*c*, *d*) of regions of the weld metal obtained by using the Ni–NbC filler at centres of crystalline subgrains (*a*, *c*) and at their boundaries (*b*, *d*)

the latter exert a dual effect on structure of the weld metal. Firstly, they can act as centres of nucleation of primary crystalline grains, this providing decrease in their size and change in their shape towards a more equiaxed one, and, secondly, upon getting into the grain body, they can promote formation of a cellular substructure of the primary grains owing to their preferential precipitation at the subgrain boundaries. The set of subgrains, the boundaries of which are rich in the carbide phase and oriented in a certain way within the primary grain, is in fact a reinforced grain structure. The boundaries of such grains are comparable in their characteristics (degree of imperfection and level of stresses) to boundaries of the primary grains, and in deformation of a material they will prevent evolution of the dislocation structure, which may affect mechanical properties of the welded joint.

The investigations conducted to evaluate the effect of the content of the NbC particles on strength properties of the welds showed that microhardness of the

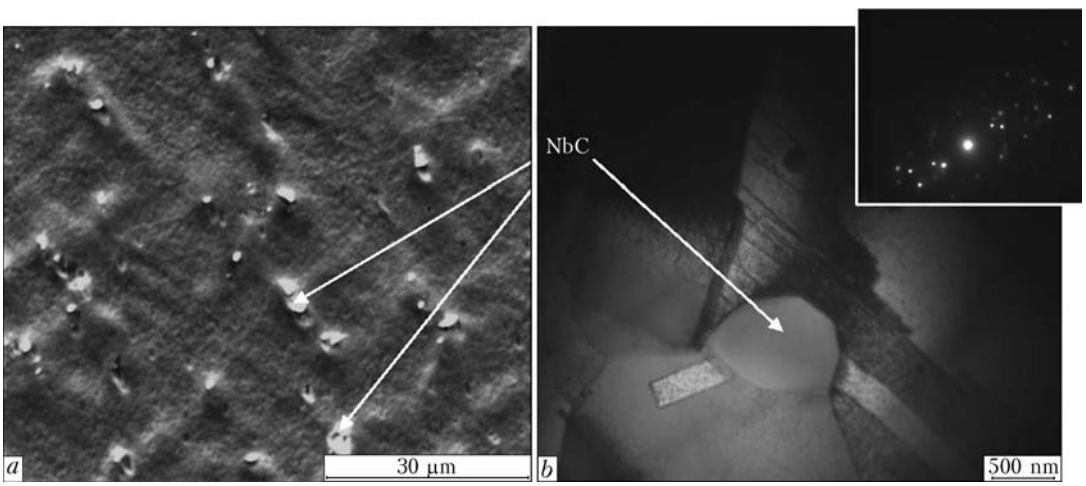

Figure 9. Pattern of distribution of carbide phase NbC in the bulk of primary crystalline grain of the weld metal obtained by using composite filler foil Ni–60 wt.% NbC (*a*), and electron microscope dark-field image of carbide particle obtained in NbC reflex (*b*)

material in the weld zone increased from 1200 (for pure nickel) to 1865 MPa (when using the Ni–35.5 wt.% NbC filler foil) with increase in their weight fraction in the weld pool. The mean value of short-time strength of the welded joints produced by using the Ni–NbC filler foil increases to 343 MPa, compared with strength of the welds (325 MPa) made without the filler foil, whereas the value of yield strength $\sigma_{0.2}$ increases two times (to 248 MPa) compared with pure nickel ($\sigma_{0.2}$ = 126 MPa). Therefore, the modifying effect of the niobium carbide nanoparticles on structure of the welds as a whole provides increase in short-time strength of the welded joints in the as-welded condition at a small decrease in toughness of the joints.

As shown by structural analysis, the highest modifying effect of the niobium carbide particles shows up at their content of the filler foil equal to 15–20 wt.%. Increase in the NbC content of the filler foil to more than 35.5 wt.% leads to precipitation of coarse niobium carbide particles along the primary grain boundaries in the weld metal, which form carbide chains after annealing of the material, while this may have a negative effect on mechanical properties of the welded joints at high temperatures and applied stresses.

Mechanical tests of the EI698 nickel alloy welded joints produced by using composite filler Ni–NbC, which were conducted at a temperature of 600 °C, showed that σ_t = 805 MPa and $\sigma_{0.2}$ = 440 MPa corresponded to the level of properties of the base metal.

Therefore, the preferential distribution of the niobium carbide nanoparticles along the subgrain boundaries promotes strengthening of the weld and increase in its microhardness. Also, it may affect increase in heat and crack resistance of the welded joints [16].

1. Bagryansky, K.V., Kuzmin, G.S. (1963) *Welding of nickel and its alloys*. Moscow: Mashgiz.
2. Yushchenko, K.A., Kvasnitsky, V.F. (1985) Current problems of welding and brazing of heat-resistant alloys. In: *Abstr. of Papers of 2nd All-Union Conf. on Problems of Technology for Welding of Thermostable, High-Temperature and Heat-Resistant Steels and Alloys* (Nikolaev, 24–26 Sept. 1985). Kiev: PWI.
3. Morochko, V.P., Yakushin, B.F., Fedorov, V.G. (1976) Effect of alloying on properties of welded joint on heat-resistant alloy KhN73MBTYu. *Svarochn. Proizvodstvo*, **8**, 24–27.
4. Yushchenko, K.A., Savchenko, V.S., Zvyagintseva, A.V. (2004) Effect of heat treatment and degree of alloying on structural changes in nickel alloys. *The Paton Welding J.*, **7**, 12–14.
5. Zaks, I.A. (1996) *Electrodes for arc welding of steels and nickel alloys*: Refer. Book. St-Petersburg: Welcome.
6. Furman, E.L., Zherebtsov, S.N., Gurdin, V.I. (2007) Modification of heat-resistant nickel alloys by ultra-dispersed powders of refractory particles. *Tekhnologiya Mashinostroeniya*, **1**, 7–9.
7. Eryomin, E.N. (2007) Modification of weld metal in electroslag welding of KhN77TYuR refractory alloy. *The Paton Welding J.*, **9**, 38–41.
8. Yushchenko, K.A., Yarovitsyn, A.V., Zvyagintseva, A.V. (2008) Properties of microplasma powder welded joints on heat-resistant nickel alloys. *Ibid.*, **9**, 5–9.
9. Efimenko, N.G. (2002) Modifying, refining and alloying with yttrium in welding of steels. *Ibid.*, **6**, 8–12.
10. Paton, B.E., Ishchenko, A.Ya., Ustinov, A.I. (2008) Application of nanotechnology of permanent joining of advanced light-weight metallic materials for aerospace engineering. *Ibid.*, **12**, 2–8.
11. Ishchenko, A.Ya., Falchenko, Yu.V., Ustinov, A.I. et al. (2007) Diffusion welding of finely-dispersed AMg5 + 27 % Al_2O_3 composite with application of nanolayered Ni/Al foil. *Ibid.*, **7**, 2–5.
12. Ryabtsev, I.A., Kondratiev, I.A., Gadzyra, N.F. et al. (2009) Effect of ultra-dispersed carbides contained in flux-cored wires on properties of heat-resistant deposited metal. *Ibid.*, **6**, 10–13.
13. Gleiter, H. (2000) Nanostructured materials. Basic concepts and microstructure. *Acta Mater.*, 48(**1**), 1–29.
14. Andrievsky, R.A., Glezer, A.M. (1999) Dimensional effects in nanocrystalline materials. Peculiarities of structure. *Fiz. Met. i Metallovedenie*, 88(**1**), 50–73.
15. Gusev, A.I. (1998) Effects of nanostructural state in compact metals and joints. *Uspekhi Fizich. Nauk*, **168**, 29–58.
16. Valiev, R.Z., Kajbyshev, O.A. (1987) *Grain boundaries and properties of metals*. Moscow: Metallurgiya.

STRUCTURE AND PROPERTIES OF ARC-WELDED JOINTS ON STEEL 10G2FB

S.L. ZHDANOV[1], V.D. POZNYAKOV[1], A.A. MAKSIMENKO[1], V.A. DOVZHENKO[1], V.G. VASILIEV[1], N.V. VYSOKOLYAN[2] and V.A. KOROBKA[2]

[1]E.O. Paton Electric Welding Institute, NASU, Kiev, Ukraine

[2]OJSC «Kryukovsky railway car building works», Kremenchug, Ukraine

Structural transformations in the HAZ metal of steel 10G2FB under the impact of the arc welding thermal cycles and their effects on the mechanical properties of this region of a welded joint were investigated. The range of permissible cooling rates of the HAZ metal at temperatures of 600–500 °C, providing properties of the welded joints at a level of requirements to the base metal and their high resistance to delayed, brittle and laminated fractures, was identified.

Keywords: *arc welding, high-strength steels, welded joints, CCT diagram, martensite and bainite transformations, cooling rate, hardness, diffusion hydrogen, cold cracks*

Intensive development of a container shipment, conditioned by establishment of the international transporting corridors, resulted in a necessity of designing and mastering of a production of special container car platforms which should completely fulfill the requirements on load-carrying capacity and type of transporting containers of a carrier. Besides, such a rolling stock should have an advanced reliability and being economical in running. 72 t load-carrying capacity and 22 t light weight are the optimum parameters for this car taking into account 23.5 t of an allowable axle load.

The shaped and sheet rolled products of 09G2, 09G2D, 16D, St3 and other steels with up to 350 MPa yield strength are used in manufacture of the load-carrying welded structures of a freight rolling stock in Ukraine and CIS countries up to present time. However, an application of higher strength steels is necessary for manufacture of new generation freight cars. The specialists of VNIIZhT [1] believe that the steels with more than 390 MPa yield strength which are characterized by higher ductility ($\delta_5 > 19$ %) and impact toughness ($KCU^{-60} > 29.4$ J/cm^2, $KCV^{-60} >$ > 19.6 J/cm^2) are to be perspective for manufacture of load-carrying welded structures of the rolling stock. Such steels should have good weldability and being mass produced at the domestic metallurgical complexes.

10G2FB grade steel mostly fulfills specified requirements as shown by analysis of roll metal produced by Ukrainian metallurgical enterprises. This steel is widely used in manufacture of large diameter pipes for the main pipelines [2, 3] and produced in accordance with TT 227-21–2008 specification. The requirements to chemical composition of sheets of 10G2FB steel are the following, not more, wt.%: 0.15 C; 0.35 Si; 1.70 Mn; 0.02 P; 0.01 S; 0.02–0.03 Al overall; 0.01–0.03 Ti; 0.08 Nb; 0.01 W; 0.30 Mo. The mechanical properties of 10G2FB steel sheets make not less than $\sigma_y = 490$ MPa; $\sigma_t = 565$ MPa; $\delta_5 = 28.5$ %; $KCV^{-60} = 69$ J/cm^2; $KCU^{-60} = 59$ J/cm^2.

The aim of the present paper consisted in an investigation of weldability of high strength 10G2FB grade steel taking into account special requirements to a steel rolled metal designed for freight car building [1]. Structural transformations in the HAZ metal of 10G2FB steel under the impact of the welding thermal cycles and their influence on the mechanical properties of given region of the welded joint, steel susceptibility to formation of cold and laminated cracks, steel reaction to burnian, and brittle fracture resistance of the welded joints were studied in accordance with these requirements.

The samples cutout from 18.7 mm thick sheets of the following chemical composition, wt.%: 0.08 C; 0.249 Si; 1.57 Mn; 0.05 V; 0.05 Nb; 0.006 [N]; 0.007 S; 0.013 P, were used in the investigations. Such indices as $\sigma_y = 531$–581 MPa; $\sigma_t = 610$–660 MPa; $\delta_5 = 24.8$–26.3 %; $\psi = 62.0$–64.8 %, $KCU^{-60} = 220$–324 J/cm^2; $KCV^{-60} = 204$–300 J/cm^2 are characteristic for the mechanical properties of steel in as received conditions after thermomechanical treatment. The extreme values of mechanical property indices correspond to tests of the samples cutout across and along the rolled metal, respectively. It should be noted that the steel has sufficiently high indices of ductility ($\psi_z = 65.0$–69.7 %) in the axis z direction indicating its high resistance to the laminated fracture.

10G2FB steel differs by high ductile properties. An evidence of this fact is the results of the traditional impact toughness tests as well as steel reaction to burning by welding arc in accordance with GOST 23240–78. The main point of the latter test method, regulated by normative documents for selection of rolled metal in car building, lied in obtaining of a low-plastic lens on the surface of sample under the effect of arc burning and determining its influence on steel susceptibility to transion in a brittle state under the impact load application. The shape and dimensions

of the sample corresponded to a notched specimen for impact bend tests.

The results of given tests correlate with the same indices obtained for the O-notched base metal specimens for impact bend and make $KCU^{-60} = 346$ J/cm^2, i.e. critical temperature of 10G2FB steel transition in the brittle state are below –60 °C.

The analysis of a CCT diagram of austenite decay (Figure 1) and the microstructures of corresponding samples (Figure 2) gives sufficient idea of kinetics of structural transformations in the areas of overheating of the HAZ metal. The investigations were carried out on a high-speed dilatometer of the «Gleeble-3800» complex [4]. Cylindrical samples of 6 mm diameter and 86 mm length were heated up to 1200 °C temperature at 150 °C/s rate and then cooled down with the different cooling rates (from 1.5 up to 55 °C/s) in a temperature range of 600–500 °C in accordance with preset welding thermal cycles character for base modes of low-carbon steel arc welding.

Austenite transformation takes place in a ferrite-bainite area at cooling rates up to $w_{6/5}$ = 20 °C/s (Figure 1, curves *1–3*). Thus, the most coarse-grained structure is formed in the area of HAZ metal overheating at cooling rates $w_{6/5}$ = 1.5 and 3.0 °C/s. The hypoeutectoid polygonal ferrite and pearlite precipitate along the grain boundaries, and globular bainite of two morphological modifications, i.e. 1850–2030 MPa microhardness low-carbon (high-temperature) and 2140–2430 MPa microhardness low-temperature bainite (see, Figure 2, *a*, *b*), is formed inside the grains. Rarely an acicular ferrite with Widmanstaetten orientation is observed inside the grains.

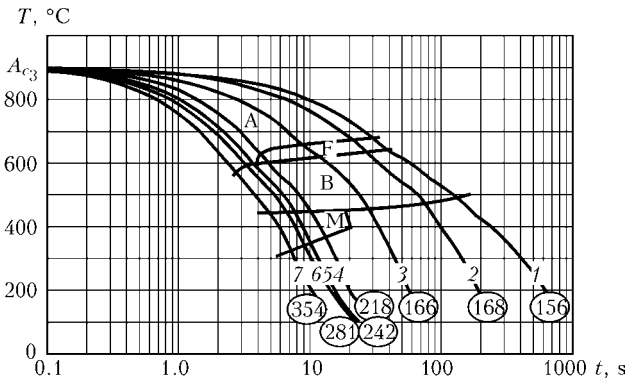

Figure 1. CCT diagram of austenite transformation of 10G2FB steel: *1* — $w_{6/5}$ = 1.5; *2* — 3; *3* — 10; *4* — 30; *5* — 38; *6* — 45; *7* — 55 °C/s; A — austenite; B — bainite; F — ferrite; M — martensite; figures in circles — Vickers hardness

The width of overheating area and size of grain somewhat decrease in cooling with 10 °C/s (see Figure 1, curve *3*). In comparison with 3 °C/s rate the structural changes consist in a reduction of the amount of hypoeutectoid polygonal ferrite and low-carbon bainite (*HV* 1920–1970 MPa) as well as in increase of the amount of higher carbon bainite (*HV* 2360 MPa) (see Figure 2, *c*). It is almost complete suppression of the pearlite transformation and only the single cases of its presence are observed in the structure.

The further decrease of the width of overheating area and size of grain is observed at 20 °C/s cooling rate. The hypoeutectoid polygonal ferrite is rarely found along the grain boundaries in the structure of area of the HAZ metal overheating. The structure of such a metal consists mainly of a low-temperature

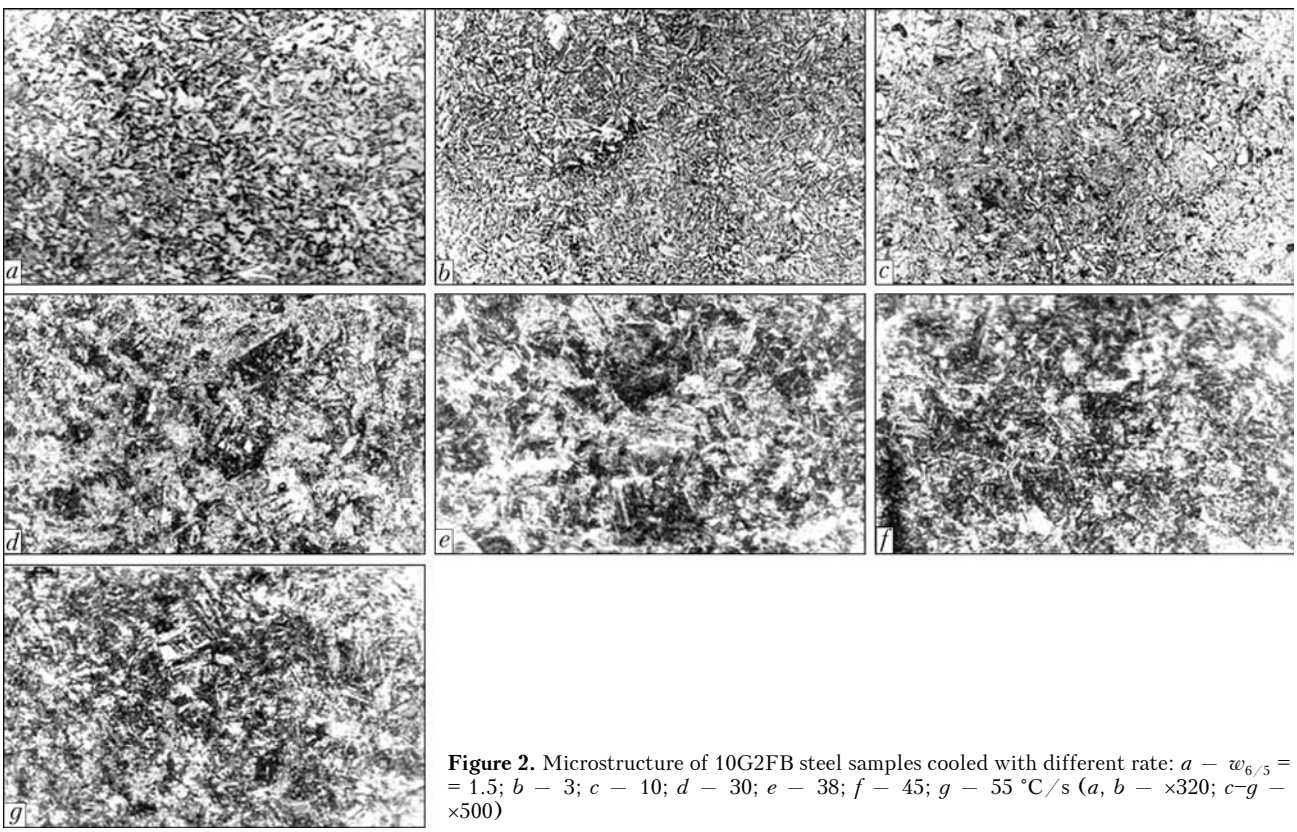

Figure 2. Microstructure of 10G2FB steel samples cooled with different rate: *a* — $w_{6/5}$ = = 1.5; *b* — 3; *c* — 10; *d* — 30; *e* — 38; *f* — 45; *g* — 55 °C/s (*a*, *b* — ×320; *c*–*g* — ×500)

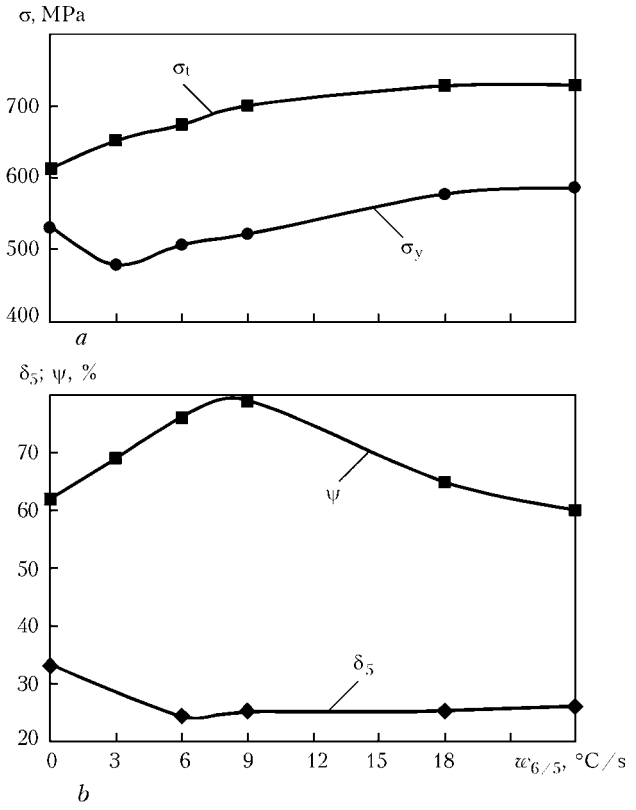

Figure 3. Influence of cooling rate on indices of strength (*a*) and ductility (*b*) of simulated HAZ metal

bainite (globular with *HV* 2100–2360 MPa) plus high-temperature low-carbon bainite (*HV* 1850–2030 MPa) in smaller amount.

The width of overheating area and size of grain at cooling with 30 °C/s rate (see Figure 1, curve *4*) are the same as at $w_{6/5}$ = 20 °C/s. The hypoeutectoid polygonal ferrite is absent in the structure of overheating area and high-temperature bainite (*HV* 1750–2000 MPa) is rarely found. The structure almost completely consists of the globular bainite (*HV* 2140–2280 MPa) (see Figure 2, *d*).

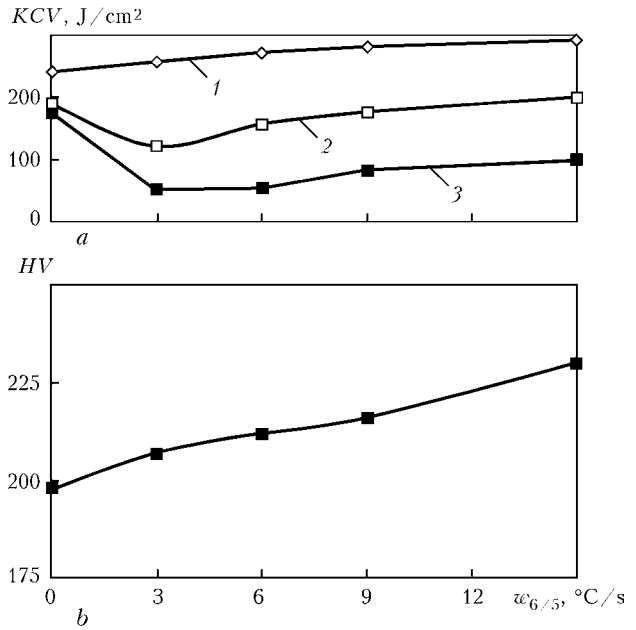

Figure 4. Influence of cooling rate on impact toughness (*1* — +20; *2* — −20; *3* — −40 °C) (*a*) and hardness (*b*) of overheating area of the HAZ metal

An increase of cooling rate from $w_{6/5}$ = 30 up to 55 °C/s (see Figure 1, curves *4–7*) develops the conditions for increasing a level of austenite overcooling and decreasing a temperature of its transformation, respectively. At that the diffusion processes are stopped and austenite transformation takes place on a shear mechanism with formation of a bainite- martensite structure. The temperature of beginning of martensite transformation virtually does not change and makes 440 °C while the temperature of transformation ending decreases from 370 to 310 °C at increase of cooling rates. As a result, it can be claimed that the overcooled austenite has a high strength in 10G2FB steel HAZ metal.

The structural components also change in a percentage ratio. Thus, if at $w_{6/5}$ = 30 °C/s cooling rate the metal structure includes 83 % of bainite, 12 % of martensite and non-equiaxed being the rest with *HV* 218 hardness (see Figure 2, *d*) than the structure will consist of 35 % of martinsite and 65 % of bainite with *HV* 354 hardness at maximum cooling rate $w_{6/5}$ = 55 °C/s (see Figure 2, *g*).

The structural transformation differences in 10G2FB steel set depending on welding thermal cycles have an influence on the mechanical properties of welded joints as well as their resistance to brittle and delayed fracture.

A method described in study [5] was used for evaluation of the mechanical properties and brittle fracture resistance of the welded joints. 150 × 12 × 12 mm samples cut from investigated metal and exposed to the welding thermal cycles (heating up to 1250 °C with 200 °C/s rate and cooling with different rates in the range of 24–2.5 °C/s) were used for tensile and impact bend tests. Obtained results show that at investigated cooling rate range mechanical properties (Figure 3) and *KCV* indices of impact toughness of the HAZ metal (Figure 4, *a*) change insignificantly at $w_{6/5} \geq 6$ °C/s. Hence, in welding of 10G2FB steel the minimal allowable cooling rate of the HAZ metal is reasonable to limit by 6 °C/s value taking into account increasing requirements made to low-alloy steels on the level of international standards ($KCV^{-40} > 47$ J/cm^2).

In the specified range of cooling rates the hardness of metal in the HAZ overheating area changes insignificantly and remains in the limits of *HV* 198–230 (Figure 4, *b*).

The resistance of welded joints to formation of cold cracks was evaluated on Implant samples [6] using rigid T-joint samples [7].

The sample-inserts of 6 mm diameter, having a stress concentrator in a form of spiral groove with 0.8 mm step and 0.1 mm radius of rounding, were tested in the first case. The welding of samples, positioned in the holes of 18.7 mm thick base plate being rigidly fast in a test unit, was carried out in following

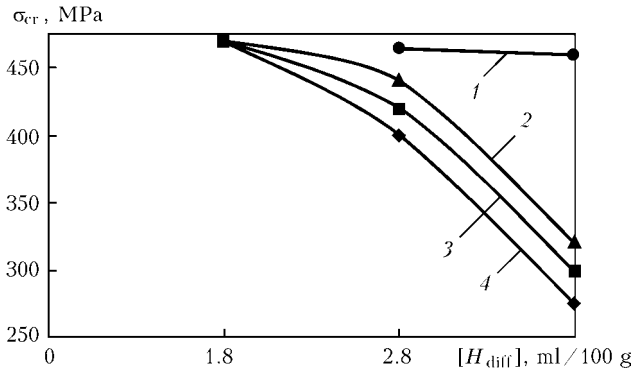

Figure 5. Dependence of critical stresses on concentration of the diffusion hydrogen and cooling conditions of the HAZ metal during testing by Implant method with preheating to 90 (*1*), 60 (*2*), 40 (*3*) °C and without preheating (*4*)

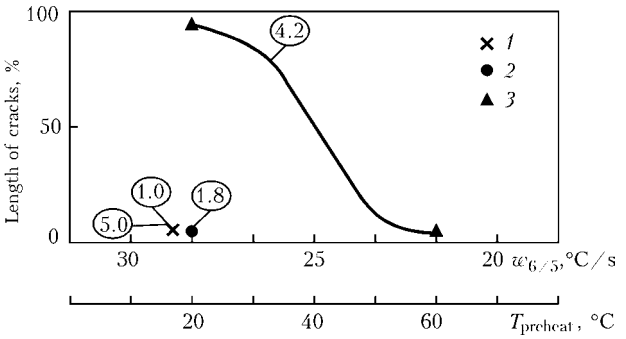

Figure 6. Influence of cooling rate $w_{6/5}$, preheating temperature $T_{preheat}$ and diffusion hydrogen content (figure in circles) on length of cracks in 10G2FB steel joints («rigid T-joint» sample): *1* — flux-cored wire Megafil 821R in CO_2 welding; *2*, *3* — ANP-10 electrodes

mode: I_w = 160 A, U_a = 25 V, v_w = 9 m/h using 4 mm diameter ANP-10 electrodes. The rate of welded joint cooling was varied by changing a preheating temperature of the base plate. Its values were determined on the oscillograms of welding thermal cycles for high-temperature areas of the HAZ metal in the sample-inserts. The amount of diffusion hydrogen in the deposited metal was determined by a pencil test method using a water glycerine solution as a locking liquid. Loading of the sample was performed in a course of its cooling to 100–50 °C temperature after welding.

The welding of «rigid T-joint» samples from 18.7 mm thick steel was performed with ANP-10 electrodes of 4.0 mm diameter as well as in CO_2 with flux-cored wire Megafil 821R of 1.2 mm diameter in modes providing close values of energy input for specified welding methods. The temperature of the samples before welding was changed in the range of 20–90 °C.

The results of Implant samples testing indicate that 10G2FB steel welded joints have a high resistance to cold crack formation in welding without preheating at limited up to 1.8 ml/100 g content of the diffusion hydrogen in the deposited metal. In given case the failure of the samples does not occur under σ_{cr} = = 475 MPa loads (Figure 5) being close to the yield strength of steel. An increase of diffusion hydrogen concentration to 4.2 ml/100 g under given welding conditions leads to a decrease of critical loads to 275 MPa (Figure 5) and, as a consequence, to reduction of welded joint resistance to cold crack formation.

The resistance of welded joints to cold crack formation can be increased using preheating to 90 °C (see Figure 5, curve *1*).

The data of «rigid T-joint» sample tests (Figure 6) correspond well with obtained results. The application of ANP-10 electrodes with low content of diffusion hydrogen up to 1.8 ml/100 g as well as Megafil 821R flux-cored wire in CO_2 welding allows widening the range of cooling rates to $w_{6/5}$ = 20 °C/s providing sufficient resistance to cold crack formation.

Usage of mentioned above welding consumables allows obtaining the weld metal with mechanical properties close to that of 10Kh2FB steel. It is proved by the results of welded joint mechanical tests given in the Table.

The sheets of 10G2FB grade steel was recommended for manufacture of the load-carrying welded metal structures of new generation freight cars based on carried out complex of tests. Specified steel and technological processes for its welding developed together with the specialists of OJSC «Kryukovsky railway car building works» were implemented in manufacture of 13-7024 model flat-car. The high rolling and strength characteristics of given flat model made from 10G2FB steel were confirmed in a course of the full-scale preliminary, acceptance and certification tests carried out by SE «Ukrainian research institute for rail car building». Based on that, it was accepted for serial production and certified in CR of the Certification register system of federal railway transport of Russian Federation by interdepartmental commission.

Mechanical properties of welded joints under investigation

Welding consumable	Weld metal							Welded joint			
	σ_y, MPa	σ_t, MPa	δ_5, %	ψ, %	KCV^{+20}, J/cm^2	KCV^{-20}, J/cm^2	KCV^{-40}, J/cm^2	σ_t, MPa	KCV^{+20}, J/cm^2	KCV^{-20}, J/cm^2	KVC^{-40}, J/cm^2
Electrodes ANP-10	485.4	645.4	27.65	69.7	159.0	84.0	56.0	630.5 (failure along BM)	238.5	150.2	92.8
Flux-cored wire Megafil 821R (CO_2)	533.3	573.2	25.80	78.1	256.0	79.5	23.4	573.3 (the same)	213.6	170.0	143.3

Note. Average values of the test results of not less than three samples are given.

More than 1500 flat-cars, manufactured on OJSC «Kryukovsky railway car building works» are successfully used at the railways of CIS and Baltic countries at present time.

1. *OST 32.153–2000*: Rolled metal for freight car bodies of new generation. Introd. 18.09.2000.
2. Semyonov, S.E., Rybakov, A.A., Goncharenko, L.V. et al. (2005) Deformation ageing of pipes of controlled rolling steel. *Tekhnich. Diagnostika i Nerazrush. Kontrol*, **4**, 39–43.
3. Efron, L.I., Nastich, S.Yu. (2006) State of production of sheet and coiled stocks for spiral-welded pipes of strength category up to X1000. *Chyorn. Metallurgiya*, **11**, 68–81.
4. Grigorenko, G.M., Kostin, V.A., Orlovsky, V.Yu. (2008) Current capabilities of simulation of austenite transformations in low-alloyed steel welds. *The Paton Welding J.*, **3**, 22–24.
5. Sarzhevsky, V.A., Sazonov, V.Ya. (1981) Unit for simulation of welding thermal cycles on the base of MSR-75 machine. *Avtomatich. Svarka*, **5**, 69–70.
6. Makarov, E.L. (1981) *Cold cracks in welding of alloy steels*. Moscow: Mashinostroenie.
7. Hrivnak, I. (1984) *Weldability of steels*. Ed. by E.L. Makarov. Moscow: Mashinostroenie.

STRENGTH OF BRAZED JOINTS ON HEAT-RESISTANT NICKEL ALLOY INCONEL 718 PRODUCED BY USING PALLADIUM BRAZING FILLER METALS

V.F. KHORUNOV[1], **S.V. MAKSYMOVA**[1], **Yu.V. BUTENKO**[2] and **A.B. MALY**[2]
[1]E.O. Paton Electric Welding Institute, NASU, Kiev, Ukraine
[2]State Enterprise «Zarya-Mashproekt», Nikolaev, Ukraine

Comparative investigations were carried out to study strength of high-temperature vacuum brazed joints on heat-resistant nickel alloy Inconel 718, made by using filler metals of the Pd–Ni–Cr–Si, Pd–Ni–Co–Cr–Si and Pd–Ni–Cr–B systems and experimental filler metal of the Pd–Ni–Cr–Ge system. The experimental filler metal was shown to have a high potential for ensuring specified short- and long-time strength of the brazed joints.

Keywords: *brazing, heat-resistant precipitation-hardening nickel alloy Inconel 718, brazing filler metal, nickel, palladium, short- and long-time strength*

Materials for high-temperature applications include heat-resistant high nickel-based alloys (superalloys), whose high mechanical properties are achieved primarily as a result of solid-solution strengthening and intermetallic and carbide reinforcement. The main contribution is made by dispersed inclusions of the phase based on Ni_3Al intermetallic, i.e. the so-called γ'-phase, the amount of which depends on the aluminium and titanium content of an alloy. Alloys with a low content of the γ'-phase have good weldability, whereas those with a high content of the γ'-phase (e.g. over 60 %) are considered unweldable [1]. It is this fact that usually determines the choice of a joining method for this structure or the other.

However, in practice there may be situations where the choice of the joining method is determined not by a material, but by design peculiarities of a product. Such a case is considered in this article.

A workpiece (centrifugal wheel) is a structure of the cylindrical shape with complex-configuration blades milled out on its external surface, and it was necessary to join a 3 mm thick covering disk to the top surface of the blade by the permanent joining methods. The workpiece material was Inconel 718, which is a well-weldable alloy. However, it was impossible to manufacture a product by arc or electron beam welding because of the absence of access inside the workpiece to perform welding. A variant of welding to the blade through the covering disk by its through penetration with the arc or electron beam was unfeasible, as the width of the blade in the zone where it adjoins the covering disk was only 2 mm. A variant of electron beam heating of the surface of the covering disk to melt the filler metal placed in the gap between the sheet and blade was not approved either. As a result, brazing was chosen as the most promising joining method for this application.

Much research efforts in different countries all over the world have been dedicated to development of filler metals for brazing high alloys, and brazing filler metals of different system have been suggested. These filler metals have one feature in common, consisting in the fact that they are the eutectic-containing alloys. Therefore, to achieve high mechanical properties, it is necessary to apply diffusion holding at high temperatures. Moreover, most of these filler metals are intended for repair brazing, rather than for fabrication of complex structures. So, it was desirable to have a filler metal with a solid solution structure, which would have high strength characteristics at any brazing cycle.

Available are such filler metals based on the Mn–Ni and Ni–Pd systems. The second system holds more promise for vacuum brazing, where it is necessary to provide high corrosion resistance of the brazed joints. Known in the art is filler metal PZhK-1000, which is used in industry to braze high-temperature application parts. This filler metal was applied to make specimens for short-time tensile strength tests at 20 and 550 °C,

as well as for long-time strength tests. The specimens were brazed at a temperature of 1230 °C, which is a bit lower than the recommended temperature (1250 °C) for this filler metal [2]. Nevertheless, the short-time strength test results were sufficiently high (Table), whereas the long-time strength values did not always correspond to the specified limit. So, the task was to decrease the brazing temperature by correcting the composition, stabilise the strength values and, what is also very important, improve ductility of the alloy, the rolling of which involves much difficulties. Two ways were tried out: change in alloying of solid solution, and replacement of an element that forms eutectic with palladium. Such an element in filler metal PZhK-1000 is silicon, which does not dissolve in palladium but forms eutectic with it at 4 wt.% (at approximately 810 °C). In this case, three intermetallics Pd_5Si, Pd_9Si_2 and Pd_3Si were formed by peritectic reactions at temperatures of 810, 823 and 1045 °C, respectively [3].

Alloying of palladium with germanium instead of silicon looks more preferable. Solubility of germanium in palladium is approximately 2 % at 775 °C, and is practically absent at 200 °C. Therefore, there are no grounds to fear embrittlement in alloying with germanium within the above limits. At the same time, one might expect strengthening of the palladium-base solid solution in cooling.

Silicon forms solid solution with nickel (approximately up to 5 %) at 700 °C. So, some increase in solubility of silicon when alloying palladium with nickel could be expected. At the same time, solubility of germanium in nickel is approximately 12 % at 200 °C, this evidencing its preference. Solubility of germanium in chromium is also somewhat higher, compared to silicon.

Therefore, germanium can be used as an alloying element in alloys of the Pd–Ni–Cr–Si system in much higher amounts without the risk of embrittlement. It means that these alloys must be more pressure treatable in order to produce thin foils.

The Co–Pd system can be used to produce a filler metal with the solid solution structure. The constitutional diagram of this system comprises minimum at a lower temperature compared to the Ni–Pd system, the range of the concentrations where there is no melting interval being wider. Moreover, no transformations were observed within the melting interval of interest. That is, this diagram looks more favourable on the face of it. In addition, considering an unlimited solubility of nickel and cobalt, one might expect that the partial replacement of nickel by cobalt could also be favourable.

Hence it follows that it would be of interest to study the effect of probable replacement of nickel by cobalt on structure and rolling ability, as well as the effect of germanium on the same parameters.

Short-time tensile strength of brazed joints on alloy Inconel 718 at room and increased temperature

Filler alloy No.	Brazing temperature, °C	Brazing time, min	Tensile strength, MPa, at test temperature, °C	
			20	550
1	1230	5	1275	980
1	1230	10	1310	1060
2	1230	5	1210	950
2	1230	10	1210	970
3	1230	5	1190	
3	1230	10	1260	1030
3	1220	10	1290	1000
4	1080	90	1230	685
4	1085	120	1080	880

This study shows the possibility of producing heat-resistant brazed joints with a high level of static short-time (at room and increased temperature) and long-time strength (at increased temperature and different load values) by an example of precipitation-hardening nickel alloy Inconel 718 and brazing filler metals based on the Ni–Pd system.

The studies were carried out by using multi-component heat-resistant alloy Inconel 718 (IN 718) in the as-received state, having the following nominal composition, wt.%:

(50–55)Ni–(17–21)Cr–18Fe–(4.75–5.50)Nb–
(2.8–3.3)Mo–(0.65–1.15)Ti–
(0.2–0.8)Al–≤1Co–0.06C.

The following consumables were used as filler metals for brazing alloy Inconel 718: commercial filler metal PZhK-1000 (Pd–Ni–Cr–Si system) (filler metal 1), and experimental filler metals based on the Pd–Ni–Co–Cr–Si (filler metal 2), Pd–Ni–Cr–Ge (filler metal 3) and Pd–Ni–Cr–B (filler metal 4) systems (see the Table).

The experimental filler metals were used in the form of rolled foils about 50 μm thick, the standard filler metal — in the form of a foil about 100 μm thick, and filler metal 4 — in the form of a strip (30–50 μm) produced by the super rapid quenching method.

Butt brazed joints were made to conduct metallographic examinations and study mechanical characteristics of the brazed joints. The foil type filler metal was placed in the gap. The specimens were fit up by resistance welding using the TKM-7 machine, with nickel straps fixed to a specimen end face. Brazing of the specimens with the experimental filler metals was carried out at temperatures of 1220–1250 °C for 5–10 min in a vacuum furnace with a work space rarefaction of $1 \cdot 10^{-2}$ Pa by using radiation heating. Brazing parameters were optimised on the butt (Figure 1, *a*,

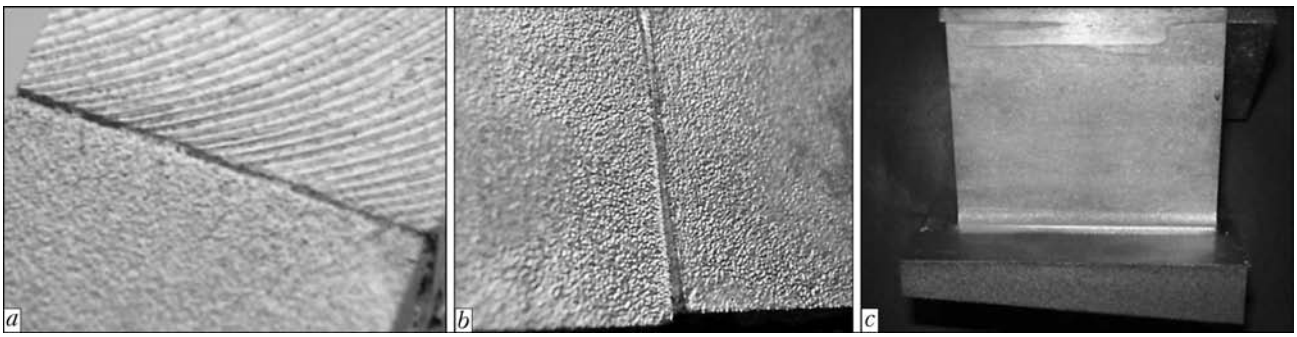

Figure 1. Appearance of butt brazed joints produced, respectively, at T_{br} = 1250, 1230 °C (*a*, *b*), and of T-joint produced at T_{br} = = 1230 °C (*c*)

b) and T-joint specimens (Figure 1, *c*). Standard mechanical test specimens (according to GOST 1497, GOST 9651 and GOST 10145) were turned from the butt joints. The time of brazing using filler metal 4 was increased to 90 and 120 min to ensure diffusion of boron from the seam to the base metal and decrease the amount of borides in the seam.

After brazing and before the mechanical tests the specimens were subjected to heat treatment, leading to strengthening of alloy Inconel 718 as a result of precipitation of the strengthening phases. The heat treatment parameters were as follows: hardening at 1050 °C and holding for 1.5 h, air cooling, ageing at 760 °C and holding for 10.5 h, cooling with furnace to 650 °C at a rate of 55 °C/h, holding at this temperature for 8.5 h, and air cooling. In the strengthened state, the value of tensile strength of alloy Inconel 718 at room temperature was 1338 MPa, and at 650 °C — 965 MPa. Tensile testing machine IMCh-30 was used for short-time tensile tests at room temperature, and machine IM 12A — at 550 °C. Machine MP-3 was used for long-time tensile tests. In the long-time tensile tests the specimens were heated to 550 °C and held for 2 h. And then the required load was applied to them.

As shown by examinations of the brazed butt and T-joint specimens, filler metals 1–3 at a temperature of 1250 °C featured good fluidity and spread well over the substrate of Inconel 718. Flowing out of the filler metal from the brazing gap and its spreading over the surface of the base material was observed. No fillets were formed at the given temperature, and porosity of the brazed seams could be visually observed (see Figure 1, *a*).

The brazing conditions were optimised on butt and T-joint specimens. Decreasing the brazing temperature

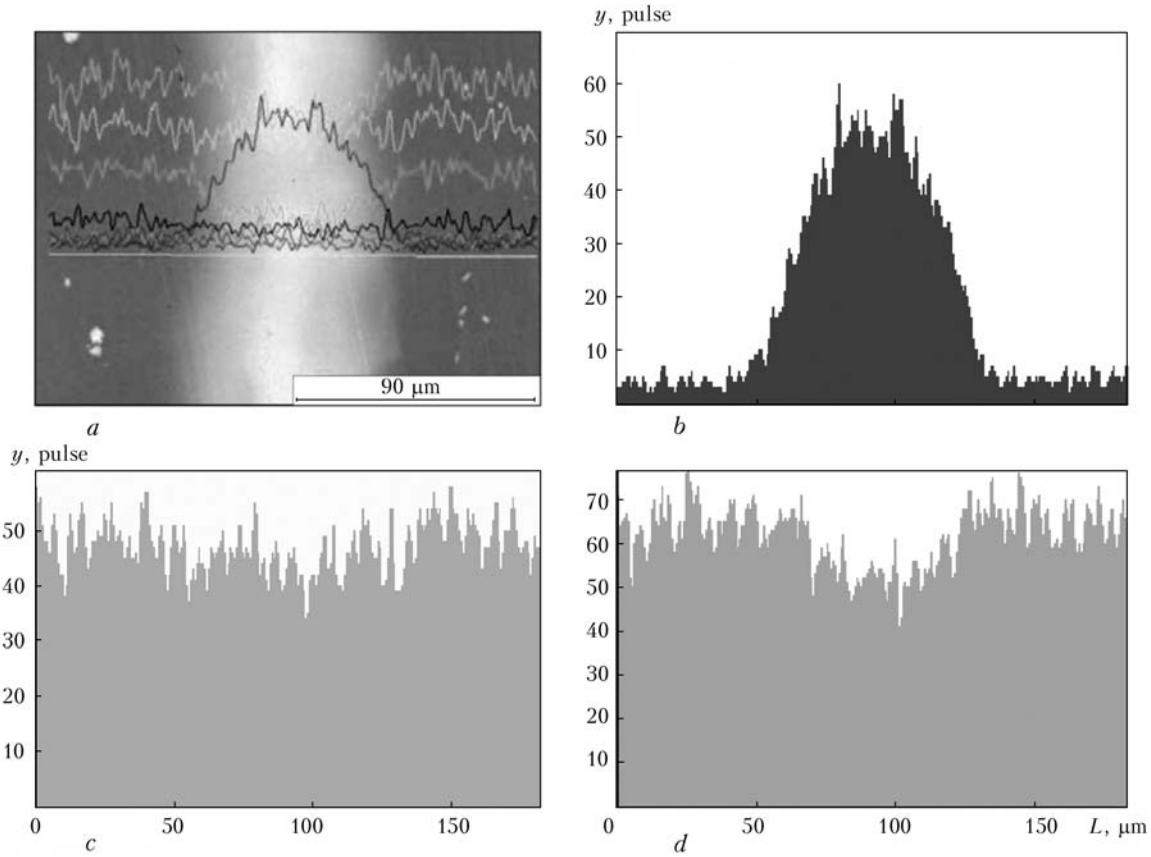

Figure 2. Microstructure of the brazed seam (*a*) and distribution of palladium (*b*), nickel (*c*) and chromium (*d*) in it

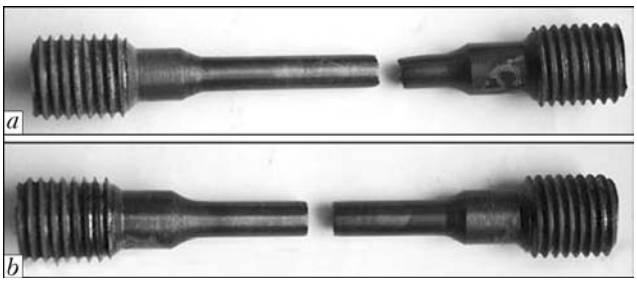

Figure 3. Fracture of brazed specimens after long-time tensile strength tests: *a* — base metal; *b* — seam metal

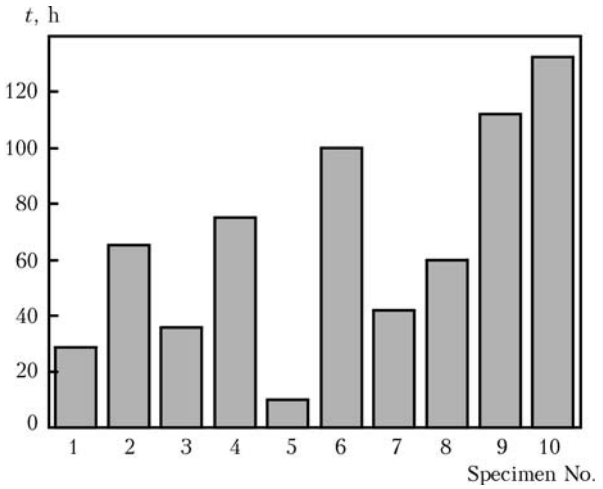

Figure 4. Long-time strength of brazed joints produced by using commercial filler metal Pd–Ni–Cr–Si (specimens 1 and 2) and experimental filler metals Pd–Ni–Co–Cr–Si (3, 4), Pd–Ni–Cr–B (5, 6) and Pd–Ni–Cr–Ge (7–10)

when making the butt joints with brazing filler metals 1 and 2 to 1230 °C, and with brazing filler metal 3 to 1210–1230 °C led to formation of the minimal sizes of the fillets, and caused no erosion of the base metal (see Figure 1, *b*). Brazing of the T-joints featured good formation of thin and dense fillet regions (Figure 1, *c*).

The brazed seams had a homogeneous structure (Figure 2, *a*), nickel was uniformly distributed in the base and seam metals (Figure 2, *c*), the amount of palladium gradually increased in width of the seam from the base metal to the central part of the seam (Figure 2, *b*), and the base metal contained a bit more chromium (Figure 2, *d*).

Results of the short-time tensile strength tests of the brazed joints at room temperature showed that all the brazing filler metals under investigation provided high strength of the joints (from 1080 to 1310 MPa, see the Table). Fracture of the brazed joints occurred in the base metal. The maximal mean values of tensile strength (1292.5 MPa) were obtained by using filler metal 1. The 5 min increase in the brazing time led to a 2.7 and 4.7 % increase in the mean tensile strength values when using filler metals 1 and 3, respectively, the mean tensile strength value for brazing filler metal 3 being 1290 MPa. Filler metal 2 provided the sufficiently consistent strength values, but at a lower level (1210 MPa), independently of the brazing time.

Alloying the Pd–Ni–Cr–Si system filler metal with cobalt increased ductility of the brazed joints approximately twice, this being evidenced by the values of elongation (15.2–16.0 %) and reduction in area (18.0–19.7 %). The high values of ductility and, correspondingly, reduction in area (22.5 %) and elongation (10 %) were obtained by using experimental filler metal 3.

The trend in distribution of strength properties between the filler metals used persisted in the high-temperature tests, which were carried out at a temperature of 550 °C (see the Table). The mean tensile strength values in brazing with filler metals 1 and 3 was approximately identical and equal to 1020 and 1015 MPa, respectively. The lower mean values were obtained when using filler metals 2 (960 MPa) and 4 (783 MPa). The minimal values of strength of the joints brazed with the Pd–Ni–Cr–B system filler metal were caused by the presence of boron, which is characterised by low solubility in nickel. During isothermal brazing it diffused from the seam into the base metal and precipitated along the grain boundaries of the base metal in the form of borides, this having a negative effect on the strength properties.

Maximal ductility at a temperature of 550 °C was provided by the filler metal alloyed with cobalt, the elongation of the brazed specimens ensured by it ranging from 10 to 80 %. Ductility of the brazed joints produced by using the experimental filler metal was a bit lower and equal to 4–12 %.

In the long-time strength tests conducted at a temperature of 550 °C and load of 785 MPa the specimens fractured in the base metal in brazing with filler metal 1 after 29 h, and with filler metal 2 after 75 h (Figure 3, *a*), as well as in the seam metal brazed with filler metals 2–4 (Figure 3, *b*).

The best results were exhibited by the brazed joints produced by using experimental filler metal 3 (Figure 4). Two specimens out of the four ones fractured after the 42 and 60 h tests. Specimens 9 and 10 did not fracture after 112 and 130 h (Figure 4), this being more than two times higher than the required life time.

Filler metal 3 was used to produce the T-joint specimens, which successfully passed the tests under a load of 220 and 300 MPa, their conventional endurance limit being $6.2 \cdot 10^6$ and $8.7 \cdot 10^6$ cycles.

CONCLUSIONS

1. As proved by investigations of the brazed joints on heat-resistant nickel alloy Inconel 718, the boron-containing Pd–Ni–Cr–B filler metal does not allow achieving the required strength and ductility of the brazed joint both at room and increased temperatures.

2. In evaluation of short-time tensile strength at room temperature, an increase in the brazing time (from 5 to 10 min) was found to lead to a 2.7 and 4.7 % increase in mean tensile strength when using

the commercial 1 and experimental 3 filler metals, respectively.

3. The maximal value of short-time tensile strength equal to 1310 MPa (at T_{test} = 20 °C) was achieved in brazing heat-resistant alloy Inconel 718 with the commercial filler metal based on the Pd–Ni–Cr–Si system. However, the brazed joints tested to long-time tensile strength had an insufficient life time within a range of 29–60 h.

4. The experimental Pd–Ni–Cr–Ge filler metal provides the short-time tensile strength value at a level of that of the base metal equal to 1230–1290 MPa, and ensures the consistent results in long-time tensile strength tests at a temperature of 550 °C and load of 785 MPa. The brazed specimens did not fracture after the tests even for 112 and 132 h, this being more than two times in excess of the required life time.

1. Seams, Ch., Hagel, V. (1976) *Heat-resistant alloys*. Moscow: Metallurgiya.
2. (2003) *Reference book on brazing*. Ed. by I.E. Petrunin. Moscow: Mashinostroenie.
3. (1999) *Constitutional diagrams of binary metal system*: Refer. Book. Vol. 3. Ed. by N.P. Lyakishev. Moscow: Mashinostroenie.

FEATURES OF WELD FORMATION AND PROPERTIES OF ALUMINIUM AND MAGNESIUM ALLOY JOINTS UNDER SIMULATED SPACE CONDITIONS

A.A. BONDAREV and **E.G. TERNOVOJ**
E.O. Paton Electric Welding Institute, NASU, Kiev, Ukraine

Features of weld formation in welded joints of aluminium and magnesium alloys made by electron beam welding under the influence of varying gravity forces and low temperatures are given. Influence of the above factors and content of dissolved hydrogen in the base metal on joint strength, defect formation and loss of alloying elements from the weld metal is shown.

Keywords: *electron beam welding, flying laboratory, aluminium alloys, magnesium alloys, gravity conditions, low temperature, liquid nitrogen, dissolved hydrogen, porosity, strength, alloying element evaporation, X-ray microprobe analysis*

Aluminium and magnesium alloys are the main structural materials for aerospace vehicle construction [1–4]. It is probable that already in the near future a real need may arise for application of welding under the conditions of near-earth space or on the Moon surface [5, 6]. These can be mounting-assembly operations in construction of space complexes or repair-preventive operations, associated with guaranteeing long-term service of operating systems [7]. Analysis of the range of welding operations performed in space shows that it will be most often necessary to join materials from 0.5 up to 4.0 mm thick. In this connection, selection of the welding process is an important factor in obtaining an objective assessment of welded joints of aluminium alloys of the mentioned thickness under these conditions. Here it is necessary to apply such a basic criterion as producing high quality welded joints equivalent to the base metal, without pores or cracks, without lowering the ductility of weld or near-weld zone at minimum losses of alloying elements in the welded joint [8]. Taking the above-said into account, application of EBW is the most effective in construction of space structures requiring a high reliability of joints, minimum weight and volume of the used hardware, complete automation of the welding process and its low energy intensity [5].

In fusion welding of aluminium alloys on the ground, the weld and HAZ develop various macro- and microdefects [9], which lead to lowering of joint strength and ductility, and sometimes also to a loss of their tightness [10, 11]. Development of such defects is also possible in welding of these materials under the space flight conditions (presence of microgravity, low temperature, deep vacuum). In addition, initial composition of the used material has a certain influence [12]. The nature of running of a number of physical processes changes significantly: gravity forces are completely or partially absent, role of thermocapillary and chemical convection rises abruptly, phase separation is practically completely absent because of the difference in density, influence of surface tension forces and adhesion increases greatly [13–15].

The purpose of the conducted research consisted in studying the influence of the enumerated factors on the quality of weld formation and properties of welded joints of AD0, AMg3, AMg6, 1201 aluminium alloys and IMV-2 magnesium alloy. Investigations were performed at the change of gravity in the range of g/g_0 from $1 \cdot 10^{-2}$ up to 2 (where g_0 is the free fall acceleration, and g is the effective acceleration) and fixed sample temperature of +20, –100, –120 and –196 °C.

During investigations through-thickness penetration beads on plates and welding of butt joints of the above alloys 2.0 and 2.5 mm thick were performed.

Table 1. Composition (wt.%) and tensile strength of the studied alloys

Alloy grade	Mg	Cu	Al	Mn	Zn	Cd	Fe	σ_t, MPa
AMg6	6.2	0.1	Base	0.60	0.2	–	0.40	320
AMg3	3.5	0.1	Same	0.50	0.2	–	0.50	230
AD0	0.3	0.1	»	0.15	0.2	–	0.30	80
1201	–	6.2	»	0.30	–	–	0.10	370
IMV-2*	Base	–	5.0	0.30	1.4	4.2	0.01	250

*This alloy has 2 wt.% Li.

Composition and ultimate tensile strength of the studied alloys are given in Table 1.

AMg6 alloy was taken from different melts with dissolved hydrogen concentration of 0.2, 0.3, 0.5 and 0.6 $cm^3/100$ g. Before loading into the chamber the samples to be welded were scraped to the depth of 0.05 mm. Time of sample soaking in air did not exceed 10 min. Then they were rigidly fixed to a stationary table, which was cooled by liquid nitrogen after chamber pumping down. Absolute pressure in the chamber, which did not exceed $1.33 \cdot 10^{-3}$ Pa, was maintained by a cryogenic sorption pump. The following parameters were recorded during welding: beam current, focusing current, voltage of powering the power unit from onboard DC system, welding speed, acceleration applied to the weld pool, sample temperature and absolute pressure in the chamber. Welding was performed in the modes given in Table 2 at accelerating voltage of 15 kV and not more than 1.5 mm beam diameter, distance from gun edge to sample surface was 120 mm.

Short-time microgravity conditions were provided by Tu-104A flying laboratory (FL), which carried A-1084M system with high-frequency electron beam power source and small-sized OB 717 gun moving along two coordinates (Figure 1).

During experiments the following accelerations were applied to the weld pool: $-g/g_0 \le 1 \cdot 10^2$ (microgravity), 1/6 (free fall acceleration on the Moon surface), 1 (free fall acceleration on the Earth surface), not less than 2 (more than two-fold acceleration).

Table 2. Modes of EBW when making joints of the studied alloys

Sample No.	Alloy grade	Thickness, mm	Sample type	Beam current, mA	Welding speed, m/h
1	AMg6	2.0	Butt joint with penetration	90	36
2	1201	2.0	Same	100	26
3	AMg3	2.5	Deposited bead with penetration	100	36
4	AD0	2.0	Same	100	30
5	IMB-2	2.5	»	70	36

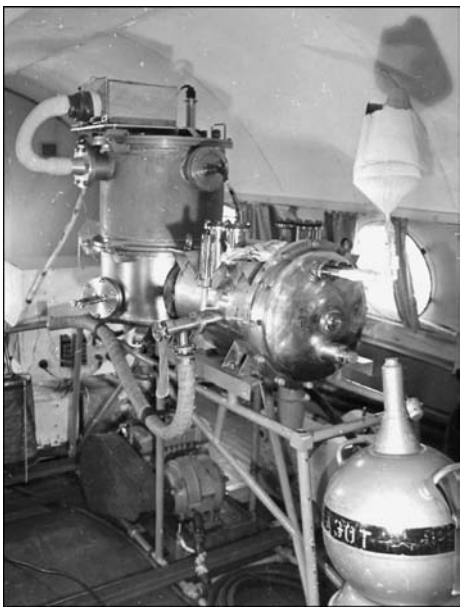

Figure 1. System for EBW of samples at room and low temperatures under the conditions of short-term zero gravity on Tu-104A FL board

Joint quality was assessed by the results of analysis of roentgenograms and macrosections of welds, alloying element distribution and features of weld and HAZ metal structure, as well as by the values of ultimate tensile strength of the joints. With this purpose, small-sized samples were made (Figure 2). Transverse and longitudinal macrosections were revealed by etching in a solution of acids of 72 % NCl, 24 % HNO_3, 4 % HF.

At visual observation of the process of EBW in the entire range of applied accelerations, no cases of liquid metal ejection from the pool or differences in formation of welded joints were registered, compared to the ground conditions. Appearance of welded joints made under the conditions of short-time zero gravity (Figure 3), is indicative of the fact that the nature of their formation does not in any way differ from the ground conditions. It should be noted that in welding under acceleration conditions ($g/g_0 \ge 2$) welds on the studied alloy samples were obtained with a lower technological convexity of the upper part and sagging root (Figure 4). This shows that significant gravity forces have an essential influence on the molten weld pool and, as a consequence, on weld geometry.

Analysis of roentgenograms and layer-by-layer surface sections of welded joint macrosections showed that in all the variants of welding AMg3, AD0, IMV-2

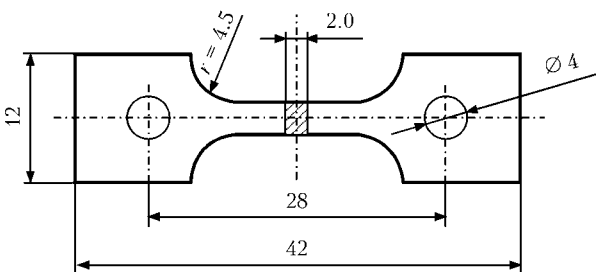

Figure 2. Schematic of a sample for tensile strength testing

Figure 3. Appearance of welded joints of alloys AMg6 (*a*), 1201 (*b*), AMg3 (*c*), AD0 (*d*) and IMV-2 (*e*) made by EBW under the conditions of short-time zero gravity in Tu-104A FL

and AMg6 alloys with dissolved hydrogen concentration of 0.2 $cm^3/100$ g, porosity in weld metal is less than $0.1 \cdot 10^{-2}$ $cm^3/100$ g or is completely absent. In welding AMg6 alloy with dissolved hydrogen concentration of 0.3 $cm^3/100$ g and higher, an increase of porosity is found in welds, which is manifested particularly at lowering of the level of gravity forces ($g/g_0 = 1/6$ and $\leq 1 \cdot 10^{-2}$) (Figure 5). Under these conditions, the total volume of pores sometimes reaches 4.42 $cm^3/100$ g. In addition, the size of individual pores increases considerably, and they can reach 2.0–2.5 mm in diameter (Figure 6, *b*).

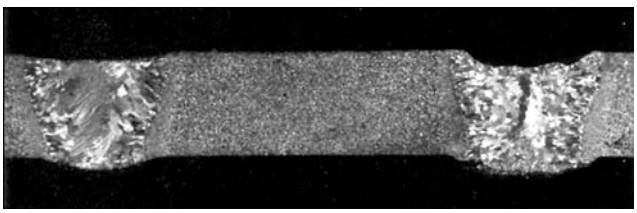

Figure 4. Macrosections of welded joints of AMg6 alloy made by EBW in the same mode at $g/g_0 \leq 1 \cdot 10^{-2}$ (*left*) and ≥ 2 (*right*)

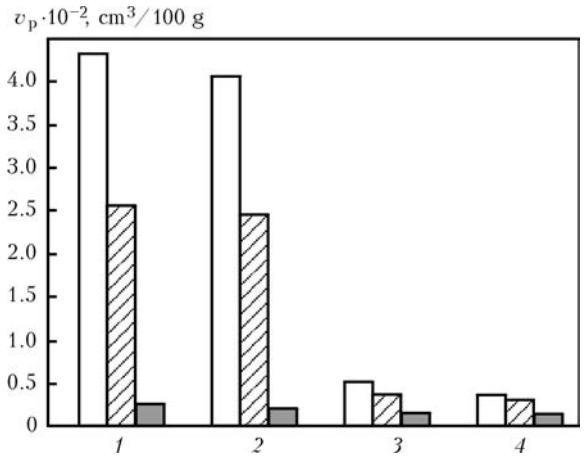

Figure 5. Diagram of susceptibility to porosity, v_p, of welded joints of AMg6 alloy with hydrogen concentration of 0.6 (white bar), 0.4 (hatched) and 0.2 $cm^3/100$ g (gray) at different accelerations: *1* — $g/g_0 \leq 1 \cdot 10^{-2}$; *2* — 1/6; *3* — 1; *4* — ≥ 2

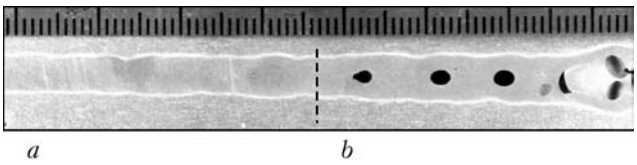

Figure 6. Surface longitudinal section on a joint of AMg6 alloy with hydrogen concentration of 0.4 $cm^3/100$ g made by EBW at $g/g_0 \geq \geq 2$ and $\leq 1 \cdot 10^{-2}$ at acceleration forces (*a*) and zero gravity (*b*)

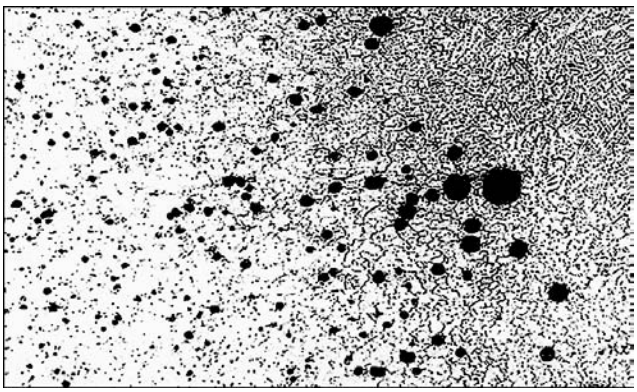

Figure 7. Microstructure (×150) with characteristic porosity in partial melting zone of welded joint of 1201 alloy made by EBW at $g/g_0 \leq 1 \cdot 10^{-2}$

Welded joints of heat-hardenable alloy 1201 made under the conditions close to zero gravity ($g/g_0 \leq \leq 1 \cdot 10^{-2}$) feature an increased number of micropores compared to welded joints made on the ground. These

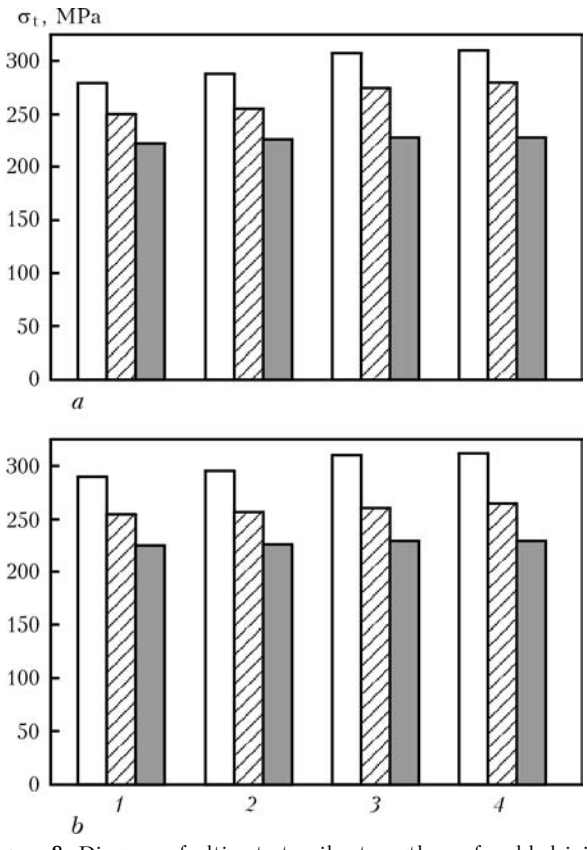

Figure 8. Diagram of ultimate tensile strength σ_t of welded joint of alloys AMg6 (with hydrogen concentration of 0.3 $cm^3/100$ g) (white bar), IMV-2 (hatched) and AMg3 (gray) made at $T = 20$ (*a*) and −196 (*b*) °C depending on gravity level: *1* — $g/g_0 \leq \leq 1 \cdot 10^{-2}$; *2* — 1/6; *3* — 1; *4* — ≥ 2

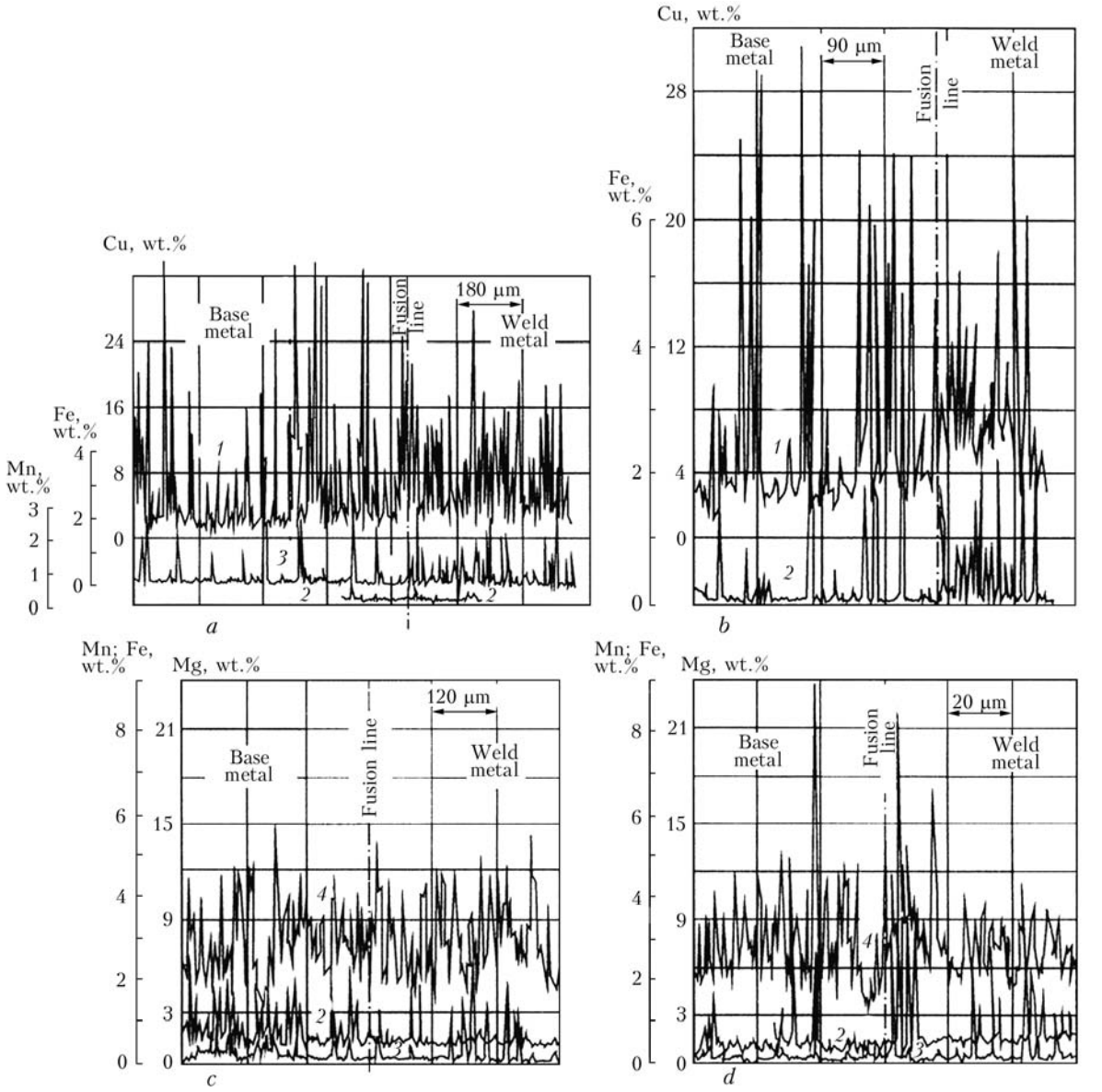

Figure 9. Distribution of alloying and impurity elements in welded joints of alloys 1201 (*a*, *b*) and AMg6 (*c*, *d*) made by EBW on the ground (*a*, *c*) and at zero gravity (*b*, *d*): *1* — copper; *2* — manganese; *3* — iron, *4* — magnesium

micropores are located predominantly in the partial melting section (Figure 7).

It is determined that the density of metal of welded joints made on the studied materials does not depend on temperature conditions of welding. Comparing strength values of welded joints of alloys AMg6 (with hydrogen concentration 0.3 $cm^3/100$ g) and IMV-2 made at the temperature of 20 °C and various values of g/g_0 (Figure 8, *a*), a tendency to lowering of strength at $g/g_0 = 1/6$ and $\leq 1 \cdot 10^{-2}$ should be noted, while these values remained unchanged for AMg3 alloy. In welding under the conditions of low temperature and different g/g_0 values (Figure 8, *b*) a regularity of strength rise with increase of gravity level is also observed. Here, similar strength values are preserved.

Testing for ultimate tensile strength of base metal of heat-hardenable alloy 1201 was performed in as-delivered condition (without heat treatment). Welded joints were tested with heat treatment (T = 180 °C for 12 h) and without it. Values of ultimate tensile strength of 1201 alloy joints are given in Table 3.

Analysis of the results of mechanical testing of 1201 alloy shows that welded joints made under the conditions close to zero gravity ($g/g_0 \leq 1 \cdot 10^{-2}$) are characterized by the lowest strength values (see Table 3). With increase of acceleration the strength of welded joints obtained at the temperature of 20 °C rises from 230 up to 250 MPa, and after artificial ageing — from 240 to 300 MPa. In welding with sample cooling to the temperature of −196 °C strength of joints made at $g/g_0 \leq 1 \cdot 10^{-2}$ also rises up to 270 MPa, and at $g/g_0 \geq 2$ it rises considerably (up to 320 MPa). Thus, increase of gravity and presence of low temperatures promote an increase of the level of ultimate tensile strength of 1201 alloy joints after welding up to 315 MPa, and as a result of artificial ageing — up to 330 MPa.

Table 3. Tensile strength, MPa, at 20 °C of 1201 alloy joints made under different technological conditions

Treatment temperature, °C	Acceleration g/g_0 applied to weld pool			
	$\leq 1 \cdot 10^{-2}$	1/6	1	≥ 2
+20	237/243	228/261	245/292	248/301
−100	259/264	254/281	269/297	303/308
−120	271/273	279/289	282/291	307/312
−196	266/275	291/296	310/328	314/329

Note. 1. Numerator gives the data for welded joint without heat treatment, denominator — those with artificial ageing. 2. Tensile strength of base metal tested in initial condition (quenching + artificial ageing) is equal to σ_t = 454 MPa. 3. Sections without any defects visible at X-ray inspection were selected for testing. 4. Presented data were obtained by averaging the results of five tests.

When studying the weldability of the above alloys by X-ray microprobe structural analysis (SX-50 microanalyzer of Cameca) the influence of the above factors on alloying element evaporation was investigated (Figure 9). Composition of metal of the studied welds made with different technological variants of welding is practically independent on sample temperature and pressure in the chamber and is close to that of base metal. Having analyzed the nature of alloying element distribution in joints of AMg6 alloy made on the ground, it can be noted that the maximum content of magnesium in the base metal and weld metal is equal to about 15 wt.%, and at $g/g_0 \leq 1 \cdot 10^{-2}$ it is above 21 wt.% in the base metal and more than 15 wt.% in the weld metal. In joints of 1201 alloy made on the ground an abrupt increase of copper content (above 28 wt.%) is found both in the base metal, and in the weld metal. A similar increase of copper content occurs also in the welded joint of 1201 alloy made at $g/g_0 \leq 1 \cdot 10^{-2}$. It demonstrates a tendency to increase of copper content in the weld metal by 1.5–2.0 wt.% compared to base metal.

CONCLUSIONS

1. It is established that the adverse influence of zero gravity and accelerative forces on formation of aluminium and magnesium alloy welded joints is not manifested. No ejection of liquid metal from the weld pool was recorded, either.

2. Aluminium alloys AD0, AMg6 and magnesium alloy IMV-2 are readily weldable by EBW under the conditions of low gravity forces and low temperature (down to −196 °C), when concentration of hydrogen dissolved in the base metal does not exceed 0.2 $cm^3/100$ g. Conditions close to zero gravity promote an increase of porosity in the metal of welds made on aluminium alloys with hydrogen concentration of 0.3 $cm^3/100$ g and higher.

3. Increase of values of ultimate tensile strength of welded joints of alloys AMg6, AMg3, AD0 and 1201 by 10–15 % is promoted by increased gravity conditions and low temperature −(100–196) °C.

4. Artificial ageing of welded joints of 1201 alloy made at 20 °C and low temperature at all the accelerations applied to the weld pool, further increases the value of ultimate tensile strength of the joints by 10–15 %.

1. Nikolaev, G.A., Fridlyander, I.N., Arbuzov, Yu.P. (1990) *Weldable aluminium alloys*. Moscow: Metallurgiya.
2. Rabkin, D.M. (1986) *Metallurgy of fusion welding of aluminium and its alloys*. Kiev: Naukova Dumka.
3. Drits, M.E., Sviderskaya, Z.A., Elkin, F.M. (1972) *Superlight structural alloys*. Moscow: Nauka.
4. Osokina, T.N., Karan, A.B., Yakushin, B.F. (1978) Welding of magnesium alloys with lithium. *Avtomatich. Svarka*, **1**, 48–50.
5. Paton, B.E., Lapchinsky, V.F. (1998) *Welding and related technologies in space*. Kiev: Naukova Dumka.
6. Paton, B.E., Dudko, D.A., Lapchinsky, V.F. (1985) *Prospects for applied problems of space technology of metals*. Kiev: Naukova Dumka.
7. Suezava, E. (1989) Space stations and colonies. Welding in space. *Tekhnika Sborki i Soedineniya*, **9**, 66–75.
8. (1974) *Technology of fusion electric welding of metals and alloys*. Ed. by B.E. Paton. Moscow: Mashinostroenie.
9. Nikiforov, G.D. (1972) *Metallurgy of fusion welding of aluminium alloys*. Moscow: Mashinostroenie.
10. Soete, W. (1971) De problematiek van de lasfouten en de moelijkheden van de breukmechanica. *Rev. Soudure*, 27(**3**), 198–203.
11. Ishii, Yu., Iida, K. (1969) Low and intermediate cycle fatigue strength of butt welds containing weld defects. *J. NDI*, 18(**10**), 443–476.
12. (2000) *Space: technologies, materials, strucrures*. Ed. by B.E. Paton. Kiev: PWI.
13. Belyakov, I.T., Borisov, Yu.D. (1974) *Technology in space*. Moscow: Mashinostroenie.
14. Ganiev, R.F., Lapchinsky, V.F. (1978) *Problems of mechanics in space technology*. Moscow: Mashinostroenie.
15. (1989) *Space materials science*. Ed. by V.S. Avduevsky. Moscow: Mir.

IMPROVEMENT OF THE TECHNOLOGY FOR ARC SPOT WELDING OF OVERLAP JOINTS BASED ON THE RESULTS OF MATHEMATICAL MODELLING

O.V. MAKHNENKO, A.N. TIMOSHENKO, A.F. MUZHICHENKO and **P.V. GONCHAROV**
E.O. Paton Electric Welding Institute, NASU, Kiev, Ukraine

Mathematical modelling of the metal-arc spot welding process was carried out by the thermoplasticity method combined with the finite element method to estimate the possibility of improving the welding technology. Performance of a spot welded joint under static and alternating loads was evaluated based on the data on size of the fusion zone and level of residual stresses within the weld spot zone.

Keywords: *arc spot welding, overlap joints, welded frame structures, strength, mathematical modelling*

The technology for arc spot welding (ASW) is well known and has been applied for a long time to produce fillet and butt joints [1–3]. One of the drawbacks of this technology when joining elements more than 1.5 mm thick is the impossibility of ensuring the quality formation of a welded joint in the vertical position and, hence, its serviceability under the effect of working loads. In this case, the joints of a satisfactory quality can be achieved only by ASW through the holes preliminarily made in external elements, this causing a substantial increase in labour intensity of the work. At the absence of holes, for penetration of the lower element of an overlap joint it is necessary to considerably increase the welding current, whereas this leads to increase in volume of the molten metal and its flow down over the vertical plane, thus violating the quality formation of a weld spot (Figure 1).

Study [4] offers an improved technology for gas-shielded metal-arc spot welding of overlap joints in the vertical position without preliminary punching of holes in the external plate being welded. This technology provides spot welded joints of preset sizes and high quality, which is achieved owing to programming of high-cycle welding heating. Welding cycles provide heating up, penetration (burn-through) of the external plate and subsequent formation of a weld spot. The up-to-date automation level allows programming of the sequence of the welding cycles and performing welding in the automatic or semi-automatic mode. However, experimental selection of parameters of high-cycle welding heating for every combination of materials and thicknesses of the elements to be joined is a labour-consuming process.

This study considers the possibilities of applying mathematical modelling to improve the ASW technology. Modelling of the process was carried out by using the thermoplasticity methods combined with the finite element method. Performance of a spot welded joint under static and alternating loads was estimated on the basis of the data on size of the fusion zone and level of residual stresses within the weld spot zone.

The finite element model was developed to model the overlap ASW process (Figure 2). The use was made of the model of a diffuse welding heat source in 2D axisymmetric statement, for which the specific heat flow has the following distribution:

$$q(x, y) = \frac{2q_{ef}}{\pi^{3/2}} k_x\sqrt{k_y} \exp(-k_x x^2 - k_y(y - y_0)^2),$$

where $q_{ef} = \eta I_w U_a$ is the effective thermal power of the welding heat source; I_w is the welding current; U_a is the arc voltage; η is the efficiency of welding heating; and k_x and k_y are the coefficients of distribution of the thermal power.

Figure 1. Poorly formed weld spot because of flow down of the molten metal over the vertical plane

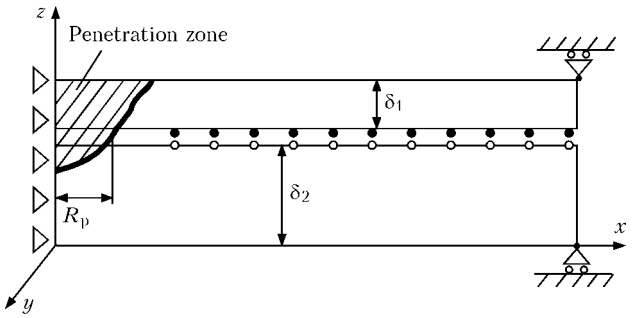

Figure 2. Schematic of finite element model for arc spot welded joint: white and black points — contact elements of surfaces of the upper and lower plates being joined, respectively; δ_1 and δ_2 — thicknesses of the upper and lower plates, respectively

Thermal contact resistance (TCR) between the two plates depends upon the cleanness and roughness of the surfaces, contact pressure and gap between the plates. Therefore, the TCR value may vary within the k_{TCR} = 0.0002–0.0037 W/(mm^2·K) range [5] in each particular case of welding of the plates. However, as shown by the results of calculations with allowance for a short time of the welding process, variation in the TCR values within the above range has no substantial effect on the kinetics of distribution of temperature fields.

In the model developed, variation in TCR between the plates during welding is modelled as follows. If temperature at the contact point at any time step exceeds the melting temperature, at a given time step and at all other steps that follow the k_{TCR} value is equal to the value of heat transfer coefficient at the ideal contact. Therefore, maximal penetration radius R_p between the plates is determined during the process of welding heating. If the contact point is within the penetration zone, at subsequent time steps the k_{TCR} value is equal to the value of heat transfer coefficient at the ideal contact.

Temperature fields in the overlap welded plates in heating and subsequent cooling, as well as a shape and size of the penetration zone are determined as a result of solving the temperature problem. The developed mathematical model describing heating of the overlap welded plates in spatial position on a vertical plane allows for flow out of part of the molten metal during a high-power welding cycle, in which the upper plate is burnt through (Figure 3). Approximate volume of the molten metal that flowed out can be determined on the basis of experimental data.

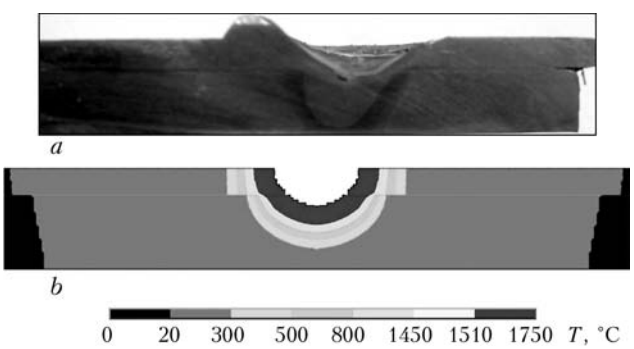

Figure 3. Macrosection of spot welded joint (*a*) and mathematical model that allows for flow out of part of the molten metal after the burn-through welding cycle (*b*)

Table 1. Physical-mechanical properties of steel 09G2S*

T, °C	Thermal conductivity coefficient λ, W/(mm·°C)	Volume enthalpy h_V, J/mm^3	Young modulus $E\cdot10^{-5}$, MPa	Linear thermal expansion coefficient $\alpha\cdot10^5$, 1/°C	Yield stress σ_y, MPa
20	0.040	0	1.97	1.14	435
100	0.040	0.5	1.97	1.14	398
200	0.039	1.0	2.01	1.22	360
300	0.038	1.5	1.95	1.26	323
400	0.036	1.7	1.88	1.30	285
500	0.034	2.0	1.80	1.38	222
600	0.032	2.4	1.69	1.39	97
700	0.029	3.2	1.56	1.41	45
800	0.026	4.0	1.35	1.83	43
900	0.026	5.0	1.25	1.87	43
1000	0.028	6.0	1.25	1.94	43
1100	0.029	7.6	1.25	1.95	43
1200	0.030	9.2	1.25	1.95	43
1400	0.030	10.0	1.25	1.95	43
1510	0.030	15.0	1.25	1.95	43
1750	0.030	17.5	1.25	1.95	43

*Poisson's ratio ν = 0.3.

The temperature and mechanical problems were traced sequentially in time from the beginning of heating to complete cooling of metal. The distribution of temperatures at each time step was used as a load to solve the mechanical problem on evaluation of the stress-strain state at a current time step, allowing for the state at the previous step.

The thermoplasticity problem was solved by using the Prandtl–Reuss theory of plastic flow associated with the Mises yield condition. At each tracing step the linearised problem was solved by the finite element method. Physical non-linearity was realised by the iteration way. The calculation model accounted for the temperature dependence of physical-mechanical properties of steel 09G2S elements (Table 1). To solve the mechanical problem, the finite elements within the penetration zone were fixed to each other, thus modelling fusion of the plates.

The model developed was used to investigate the process of formation of an overlap spot welded joint between two plates of steel 09G2S, 2.5 and 7.0 mm thick, in CO_2 ASW under the conditions consisting of five sequential welding cycles (Table 2, Figure 4). Welding was performed in a spatial position on the vertical plane, this involving certain difficulties with formation of a welded joint.

Table 2. ASW parameters

No. of welding cycle	Arc voltage U_a, V	Welding current I_w, A	Welding wire feed speed v_{feed}, m/h	Welding pulse duration t_w, s	Duration of pause between pulses t_{pause}, s
1	28	200	120	0.4–0.5	0.1
2	42	450	276	1.0–1.3	2.0
3	30	250	138	0.8–1.0	1.5
4	30	250	138	0.8–1.0	1.0
5	26	190	120	0.5	–

The efficiency of welding heating was chosen to be $\eta = 0.7$, based on the data of study [6], as well as on the condition of matching of size of the penetration zone on macrosection of the spot welded joint and calculation results (Figure 5). Thermal power distribution coefficient $k_x = 3.0\ 1/mm^2$ was also corrected on the same condition. Adding a filler material was not modelled in the first heating up welding cycle because of its very short duration and subsequent flow out of the molten metal during the second welding cycle. Volume of the molten metal that flowed out during the second welding cycle was determined from the condition of subsequent filling up with the filler material during the third and fourth welding cycles.

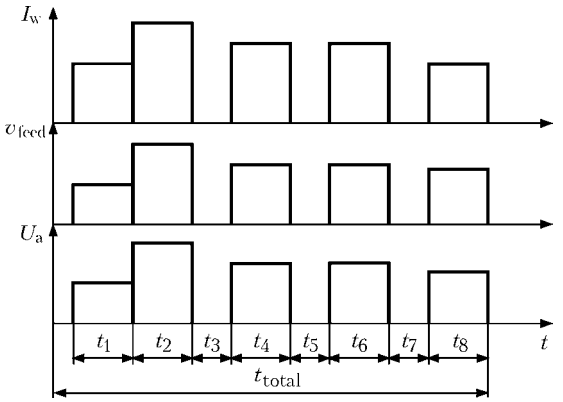

Figure 4. Scheme of variations in parameters of ASW in vertical position: t_1–t_8 — durations of pulses and pauses; t_{total} — total time of ASW cycle

Comparison of the calculation and experimental results shows that the developed mathematical model is adequate for evaluation of formation of the overlap spot welded joint between two plates in ASW in a spatial position on the vertical plane and can be applied to develop the technology for welding such joints with a complex welding cycle.

This mathematical model allowed obtaining the calculation results on the distribution of residual stresses within the welded joint zone. This information can be helpful for estimation of strength of the spot welded joints.

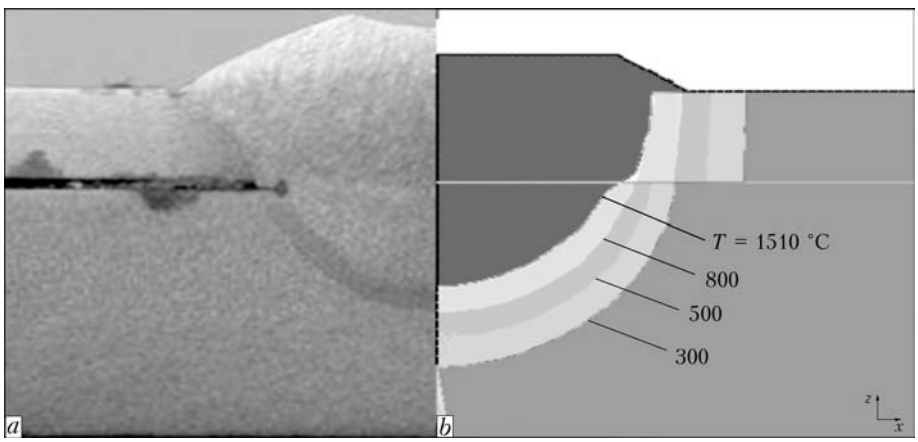

Figure 5. Comparison of size of the penetration zone on macrosection of the spot welded joint (*a*) and calculation results (*b*)

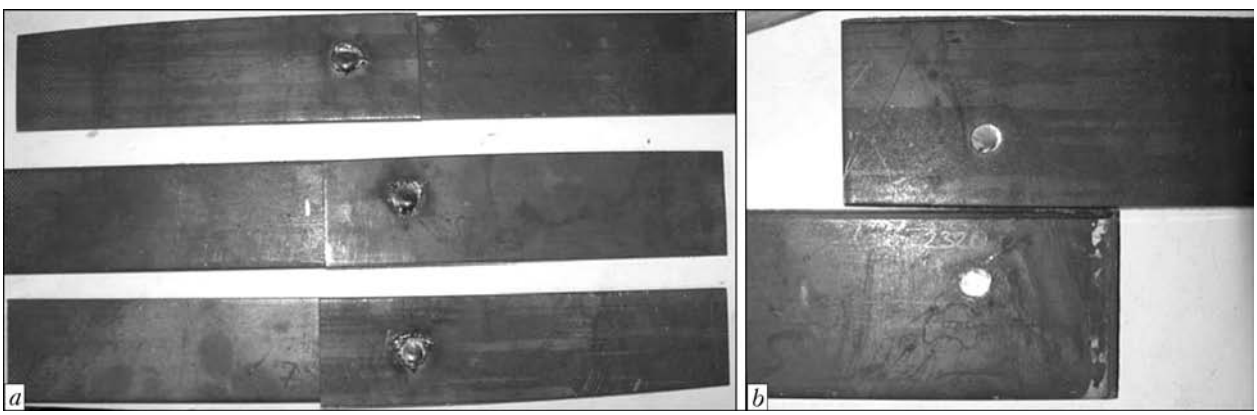

Figure 6. Appearance of samples of spot welded joints before tensile tests (*a*) and after fracture of the weld spots by shear mechanism (*b*)

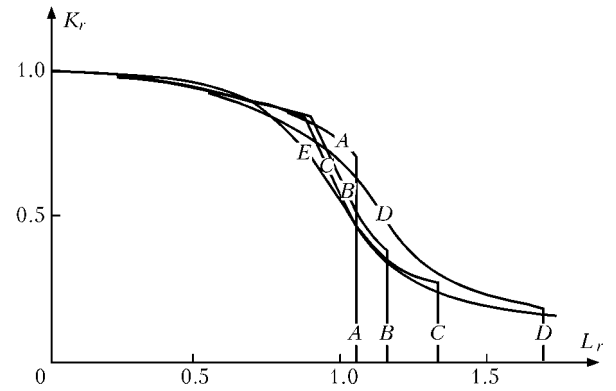

Figure 7. Diagrams of limiting state $K_r \le f_1(L_r)$ for different types of structural steels [3]: *A* — high-strength steel EN408; *B* — pressure vessel steel A533B; *C* — low-carbon steel containing manganese; *D* — austenitic steel; *E* — calculation curve [9]

Welded joints with the spot welds usually fail at fracture of the weld spots by the shear mechanism (Figure 6) [7, 8]. There may be other mechanisms of fracture of the joints both in base metal and HAZ, and because of tear out of a weld spot from the base metal on its perimeter. The determining factor is the fracture that begins at the top of a cavity adjoining the weld spot and propagates either in the bulk of the spot or in the base metal. Therefore, the fracture is initiated by a sharp stress raiser located on the weld spot perimeter. The effect of this raiser can be taken into account on the basis of up-to-date criteria of fracture mechanics, namely the two-parameter criterion of tough-brittle fracture [9, 10]. According to this approach, equilibrium of a crack is not violated, provided that the following condition is met:

$$K_r \le f_1(L_r),$$

where $K_r = K_I / K_{Ic}$ is the ratio of stress intensity factor K_I at the crack apex to the critical value of this parameter K_{Ic}; and $L_r = \sigma_{ref} / \sigma_y$ is the ratio of critical stress σ_{ref} in the weld spot zone that determines fracture by the plastic instability mechanism to yield stress σ_y of the material. The kind of function $f_1(L_r)$ is determined experimentally. Figure 7 gives these data for different structural steels.

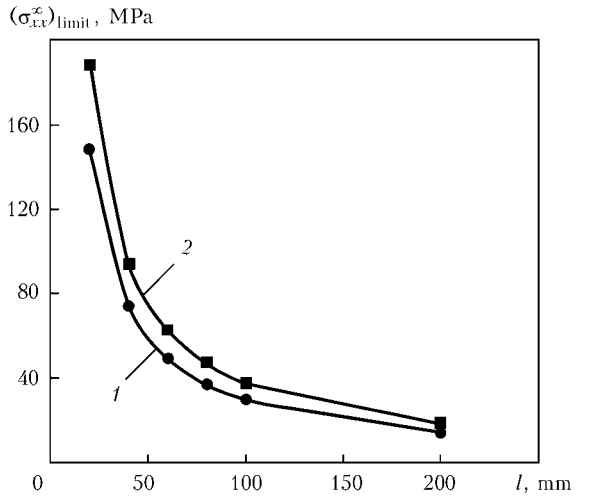

Figure 9. Calculation data on variations in limiting values of stresses $(\sigma^{\infty}_{xx})_{limit}$ in the upper, thinner plate (δ_1 = 2.5 mm, δ_2 = 7.0 mm) under static loading depending on step l of the weld spots $2R$ = = 10 mm in size (shear fracture): *1* — here and in Figures 10 and 11, K_{Ic} = 1025; *2* — 2050 MPa·mm$^{1/2}$

To calculate K_I, it is necessary to account for both external load, i.e. load by force P_x on one spot in plane of the plates welded (Figure 8), and residual non-relaxed stresses within the welded joint zone. When calculating L_r, residual stresses are ignored, as they relax completely.

The P_x values are determined from stresses σ^{∞}_{xx} on the periphery of the elements being joined (Figure 8, *a*), and from values of metal thickness δ_j and step l between the weld spots, i.e. $P_x = \sigma^{\infty}_{xx}\delta_j l$ (j = 1, 2). Loading results in deformation of the joint (Figure 8, *b*). In deformation, the weld spot is affected by shear force $P_x = P_x \cos\beta$, tear force $P_z = P_x \sin\beta$, and momentum

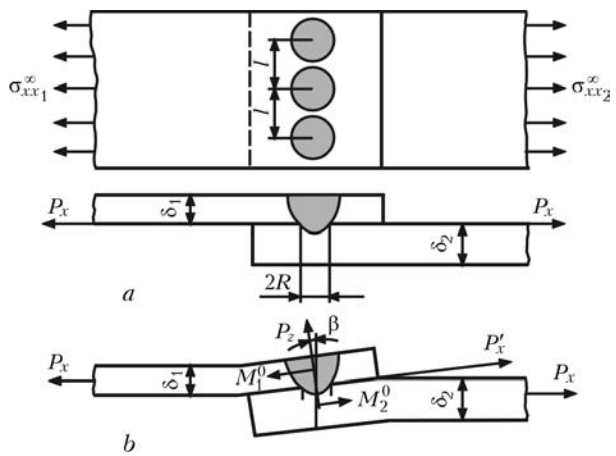

Figure 8. Schematics of welded joint with a single-row weld before loading (*a*) and its deformation at P_x (*b*): l — distance between the weld spot centres (step); P'_x — force acting within the weld spot zone; M^0_1 and M^0_2 — forces acting on the upper and lower plates being joined, respectively; β — bend angle

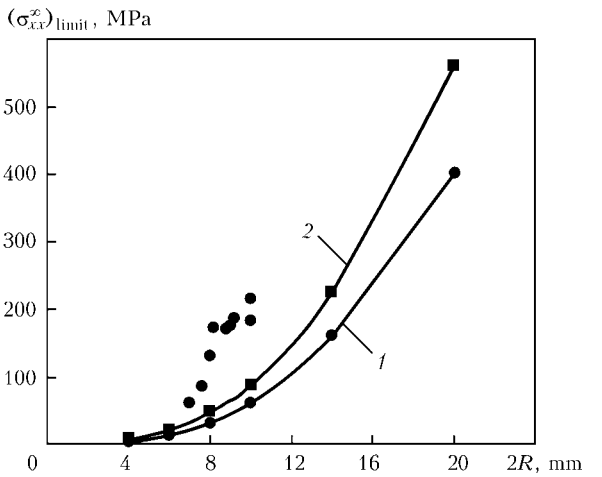

Figure 10. Comparison of calculation (*1*, *2*) and experimental data (points) of limiting values of stresses $(\sigma^{\infty}_{xx})_{limit}$ in the upper, thinner plate (δ_1 = 2.5 mm, δ_2 = 7.0 mm) under static loading depending on size $2R$ of the weld spot with step l = 50 mm

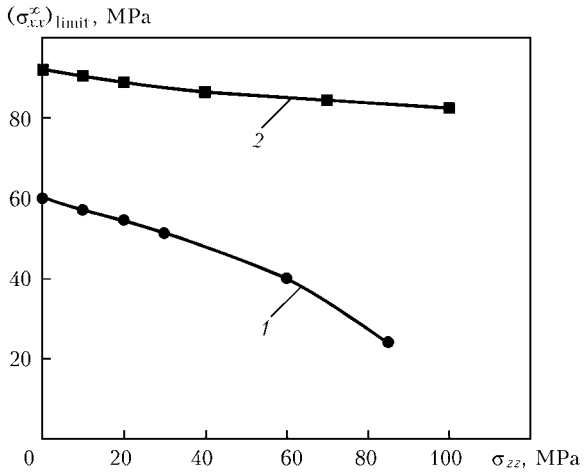

Figure 11. Variations in limiting values of stresses $(\sigma^{\infty}_{xx})_{limit}$ in the upper plate (δ_1 = 2.5 mm, δ_2 = 7.0 mm) under static loading depending on residual stresses σ_{zz} (weld spot size $2R$ = 10 mm, l = = 50 mm)

$$M = M_1^0 + M_2^0 = P_x \frac{\delta_1 + \delta_2}{2} \cos \beta.$$

The values of angle β are in a complex dependence upon the geometric parameters of the welded joint, mechanical properties of the materials and force P_x. Parameters of deformation of the overlap spot welded joint and values of K_I can be calculated from the relationships suggested in studies [11, 12]. The said relationships were used to calculate the limiting values of stresses $(\sigma^{\infty}_{xx})_{limit}$ in the upper, thinner plate under static loading depending on step l of the weld spots $2R$ in size, thicknesses of the upper and lower plates, δ_1 and δ_2, respectively, and residual stresses σ_{zz} within the weld spot zone.

The calculation data given in Figure 9 show that the limiting values of stresses $(\sigma^{\infty}_{xx})_{limit}$ under static loading dramatically decrease with increase in step l of the weld spots.

Size of a weld spot also has a substantial effect on the limiting values of stresses $(\sigma^{\infty}_{xx})_{limit}$ (Figure 10). Increase in size of the weld spot leads to increase in strength of the welded joint under static loading. Comparison of the calculation and experimental data in Figure 10 shows that the applied calculation approach is sufficiently conservative.

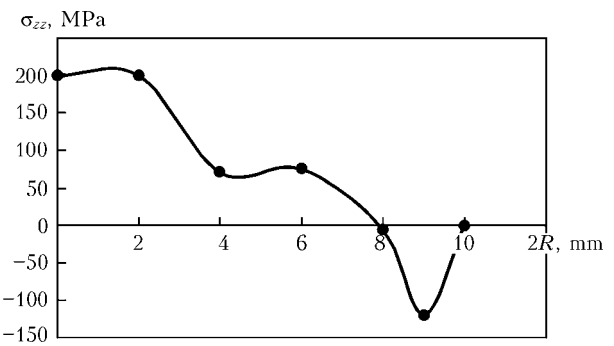

Figure 12. Calculation data on distribution of residual stresses σ_{zz} within the weld spot zone along the fusion line of the plates welded (δ_1 = 2.5 mm, δ_2 = 7.0 mm, weld spot size $2R$ = 10 mm)

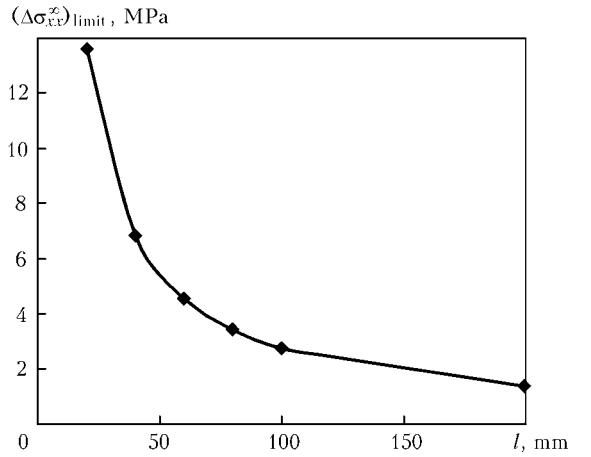

Figure 13. Variations in limiting values of stress range $(\Delta\sigma^{\infty}_{xx})_{limit}$ in the upper, thinner plate (δ_1 = 2.5 mm, δ_2 = 7.0 mm) under cyclic loading on a base of $2 \cdot 10^6$ cycle depending on step l of the weld spot $2R$ = 10 mm in size (shear fracture)

Increase in thickness of both upper and lower plates has a negative effect on strength of the spot welded joint. This factor is negative for the improved ASW technology with high-cycle welding heating, which is used primarily for welding of rather thick plates.

The calculation data in Figure 11 show that the effect of the level of residual stresses σ_{zz} acting through thickness of the plates within the weld spot zone on the limiting values of stresses $(\sigma^{\infty}_{xx})_{limit}$ in the upper, thinner plate under static loading is negligible. As seen from Figure 12, the level of residual stresses σ_{zz} is fairly low. According to the equilibrium equation, the integral of normal stresses σ_{zz} along the fusion line (area) should be equal to zero. This gives grounds to state that the level of residual stresses is not a determining factor for strength of the spot welded joints under static loading.

The limiting state condition for cyclic loading of the spot welded joints can be formulated as follows [13]:

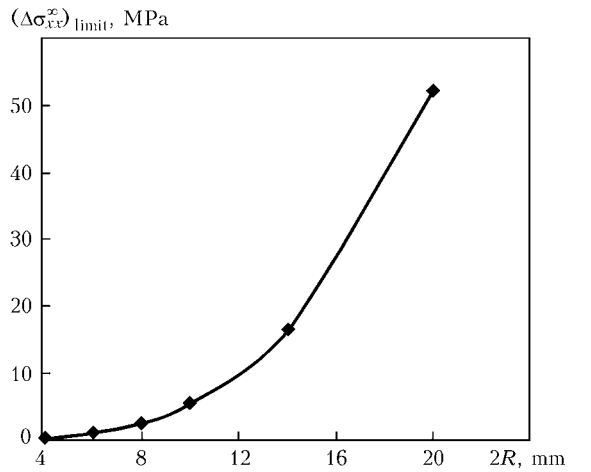

Figure 14. Variations in limiting values of stress range $(\Delta\sigma^{\infty}_{xx})_{limit}$ in the upper, thinner plate (δ_1 = 2.5 mm, δ_2 = 7.0 mm) under cyclic loading on a base of $2 \cdot 10^6$ cycle depending on weld spot size $2R$ at l = 50 mm

$$\Delta K_{\omega^*}^{\max} = K_{\omega^*}^{\max} - K_{\omega^*}^{\min} = \Delta K_{\text{th}}^{0}(1 - \alpha r_\sigma),$$

where the maximal and minimal values $K_{\omega^*}^{\max}$ and $K_{\omega^*}^{\min}$ are determined at $P_x = P_x^{\max}$ and $P_x = P_x^{\min}$, respectively; r_σ is the coefficient of asymmetry of the cycle of variation in force P_x; ΔK_{th}^0 is the threshold value of a range of stress intensity factor K_{I} ($r_\sigma = 0$), at which a normal tear crack does not practically propagate; and α is the experimental characteristic of the material ($\alpha \approx 0.50$–0.85) [13].

Strength of the spot welded joint under cyclic loading was calculated depending on step l and size $2R$ of a weld spot, as well as thickness of the upper and lower plates, δ_1 and δ_2, respectively, at a conservative value of cycle asymmetry coefficient $r_\sigma = 0$ and $\Delta k_{\text{th}}^0 = 190$ MPa·mm$^{1/2}$. As seen from the calculation data shown in Figures 13 and 14, this dependence is of the same character as under static loading. However, as to the limiting values, the stress range under cyclic loading on a base of $2 \cdot 10^6$ cycle is approximately an order of magnitude lower (at a level of 10–20 MPa) than under static loading, this being in agreement with the up-to-date notions of cyclic strength of the welded joints.

CONCLUSIONS

1. High-quality spot welded joints can be provided by regulating parameters of welding cycles in ASW of thin-sheet metal in vertical position. The improved technology offers new possibilities for applying ASW for fabrication of structures in different industries, in particular for fabrication of frame structures of modern freight and passenger railway cars.

2. The developed mathematical model can be efficiently used to develop the technologies for overlap ASW, including with complex welding cycles.

3. As shown by the calculation data, the level of residual stresses σ_{zz} acting through thickness of the plates within the weld spot zone is rather low. According to the equilibrium equation, the integral of normal stresses σ_{zz} along the fusion line (area) is equal to zero. Therefore, the level of residual stresses is not a determining factor for strength of the spot welded joints under static loading.

4. The limiting values of stresses $(\sigma_{xx}^{\infty})_{\text{limit}}$ under static loading and stress range $(\Delta\sigma_{xx}^{\infty})_{\text{limit}}$ under cyclic loading dramatically decrease with increase in step of the weld spots.

5. Increase in size of the weld spot leads to a substantial increase in strength of the welded joint both under static and cyclic loading.

1. Tereshchenko, V.I., Sharovolsky, A.N., Sidorenko, K.A. et al. (1983) Peculiarities of CO_2 metal-arc spot welding. *Avtomatich. Svarka*, **9**, 51–53.
2. Tkachenko, A.N., Voskresensky, A.S. (2005) Application of arc spot welding in fabrication of car bodies. *The Paton Welding J.*, **12**, 22–24.
3. *GOST 14776–79*: Arc welding. Spot welded joints. Main types, design elements and sizes. Introd. 01.07.80.
4. Lobanov, L.M., Timoshenko, A.N., Goncharov, P.V. (2009) Arc spot welding of overlap joints in vertical position. *The Paton Welding J.*, **1**, 26–28.
5. Lienhard, J. et al. (2002) *Heat transfer textbook*. Cambridge, Massachusetts: Phlogiston Press.
6. Rykalin, N.N. (1951) *Calculations of thermal processes in welding*. Moscow: Mashgiz.
7. Dorofeev, A.N. (1964) *Calculation of strength of spot welds*. Moscow: Mashinostroenie.
8. Serenko, A.I., Krumboldt, M.N., Bagryansky, K.V. (1977) *Calculation of welded joints and structures*. Kyiv: Vyshcha Shkola.
9. Harrison, R.P., Looscmore, K., Milne, J. et al. (1980) Assessment of the integrity of structure containing defects. *Central Electricity Generating Board Rep. 6, Rev. 2*. Berkley.
10. Makhnenko, V.I., Pochinok, V.E. (1982) Application of fracture mechanics criteria in calculation of strength of welded joints with specified discontinuities of the crack-like type. *Avtomatich. Svarka*, **1**, 1–6.
11. Makhnenko, V.I., Ryabchuk, T.G., Pochinok, V.E. (1990) Improvement of the strength design procedure for spot welded joints. *Ibid.*, **1**, 9–14.
12. Cherepanov, G.P. (1974) *Brittle fracture mechanics*. Moscow: Nauka.
13. Makhnenko, V.I., Pochinok, V.E. (1984) Cyclic loads resistance of welded joints with incomplete penetration welds. *Avtomatich. Svarka*, **10**, 33–40.

IMPROVEMENT OF CYCLIC FATIGUE LIFE OF METALLIC MATERIALS AND WELDED JOINTS BY TREATMENT BY PULSED ELECTRIC CURRENT

G.V. STEPANOV[1], A.I. BABUTSKY[1], I.A. MAMEEV[1], A.V. CHIZHIK[1], V.V. SAVITSKY[2], G.I. TKACHUK[2] and N.A. PASHCHIN[2]
[1]G.S. Pisarenko Institute for Problems of Strength, NASU, Kiev, Ukraine
[2]E.O. Paton Electric Welding Institute, NASU, Kiev, Ukraine

The paper presents experimental data on improvement of cyclic fatigue life of stainless steel and aluminium alloy samples as a result of treatment based on direct passage of electric current through the material, as well as data of calculation-experimental studies of residual welding stress relaxation under the impact of induced electric current. Results of investigation of the influence of current treatment on residual stresses in the coating and in the material after grinding are given.

Keywords: *metallic materials, welded joints, protective coatings, pulsed electric current, fatigue, residual stresses, relaxation, cyclic fatigue life*

Results of investigation of the influence of treatment by pulsed electric current (PEC) on mechanical properties of metallic materials are indicative of its positive impact on fatigue resistance characteristics [1–3]. However, no significant progress has been achieved in understanding the mechanism of the influence of PEC treatment on these characteristics, so that obtaining new experimental data is urgent.

Also known is the influence of residual stresses (RS), in particular, residual welding stresses (RWS), on fatigue of structural elements: under the conditions of cyclic loading, particularly at loading with a low stress level, RWS influence is manifested in an essential lowering of endurance limit of welded joint material and increase of fatigue crack propagation rate [4, 5].

Operations on lowering of RWS in structures usually are difficult to perform, require considerable expenses, and are reduced mainly to thermal and force (mechanical) impact on welded joint metal or to a combination of these impacts. Each of these methods has certain drawbacks. For instance, local application of high-temperature tempering leads to formation of areas with high residual stresses in the structure after its complete cooling, as such treatment essentially reproduces the thermal cycle of welding. A similar situation arises at heat treatment of some kinds of coatings. Thus, development of new methods to lower RS, devoid of the drawbacks inherent to the currently available methods, also is an urgent task.

This work gives the results of investigation of the influence of PEC treatment on fatigue of 10Kh18N10T steel and D16T aluminium alloy, as well as results of experimental assessment of PEC influence on RWS and RS relaxation in the coating and ground material.

PEC influence on fatigue of 10Kh18N10T steel and D16T aluminium alloy. Investigations were performed on samples of 10Kh18N10T stainless steel (Figure 1, *a*) and similar samples of aluminium alloy D16T 3.7 mm thick (unlike 4 mm for steel). In fatigue testing the sample was supported in cantilever (Figure 1, *b*) in the grip of the machine (electrodynamic vibration testing facility) [6]. Nine sample groups were tested altogether: one each — without treatment (as-delivered) and seven — after PEC treatment in different modes (Table).

At PEC treatment samples were connected to the taps of pulsed current generator [7]. Three current pulses were applied to each of the samples.

Testing results (Figure 2) are indicative of an essential influence of PEC on fracture resistance characteristics of the material. Treatment of steel samples

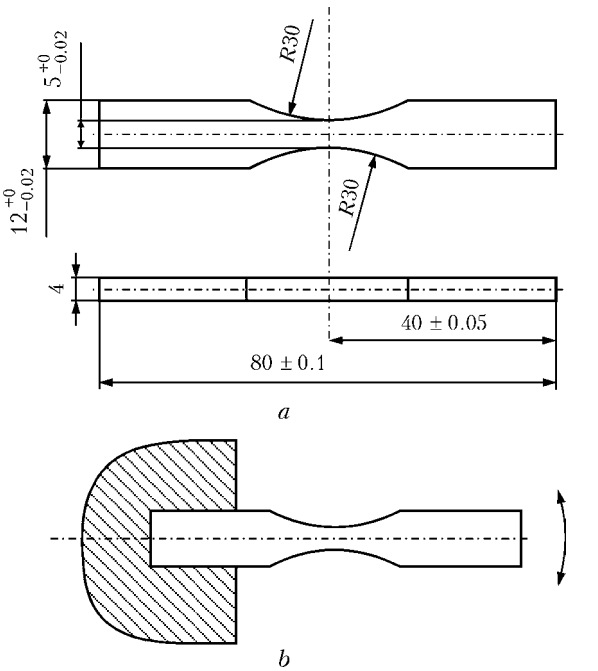

Figure 1. Sketch of a sample for fatigue testing (*a*) and its loading schematic (*b*)

Modes of PEC treatment of samples

Mode No.	j, kA/mm^2	C, μF	U, kV	I, kA
10Kh18N10T steel				
1	1	150	1.8	20
2	2	150	3.63	40
3	4	600	3.46	80
4	5.75	600	5.0	115
D16T alloy				
5	1.35	150	2.25	25
6	2.60	100	5.0	48
7	4.32	600	3.46	80

at current density j = 1 kA/mm^2 (mode 1) leads to a slight increase of these characteristics. At j = = 2 kA/mm^2 (mode 2) endurance limit of steel rises by 30 %. Increase of current density at treatment up to j = 4 kA/mm^2 (mode 3) leads to an increase of endurance limit by more than 50 %. However, further increase of current density up to j = 5.75 kA/mm^2 (mode 4) causes a lowering of fatigue resistance characteristics.

A similar tendency is observed also in the case of treatment of D16T alloy: treatment at j = = 1.35 kA/mm^2 (mode 5) does not change the fatigue characteristics compared to the initial state of the material. At j = 2.60 kA/mm^2 (mode 6) D16T alloy endurance limit increased by 40 %. Further increase of current density up to j = 4.32 kA/mm^2 (mode 7) does not cause any change of fatigue resistance characteristics compared to the initial condition.

It follows from the results of X-ray structural analysis of samples from steel that a certain change of orientation of crystals making up the grains occurs at treatment, which is indicative of ordering of the material crystalline structure in the direction of current action. In addition, according to the data of metallographic investigations, treatment results in precipitation of carbides (complex carbides (Cr, Fe)$_7$C$_3$) in the metal grain bulk (Figure 3). Here, the maximum density of the precipitating carbides in the grain body is observed in mode 3 corresponding to a maximum increase of endurance limit (Figure 3, *c*). Further increase of current density leads to intensive evolution

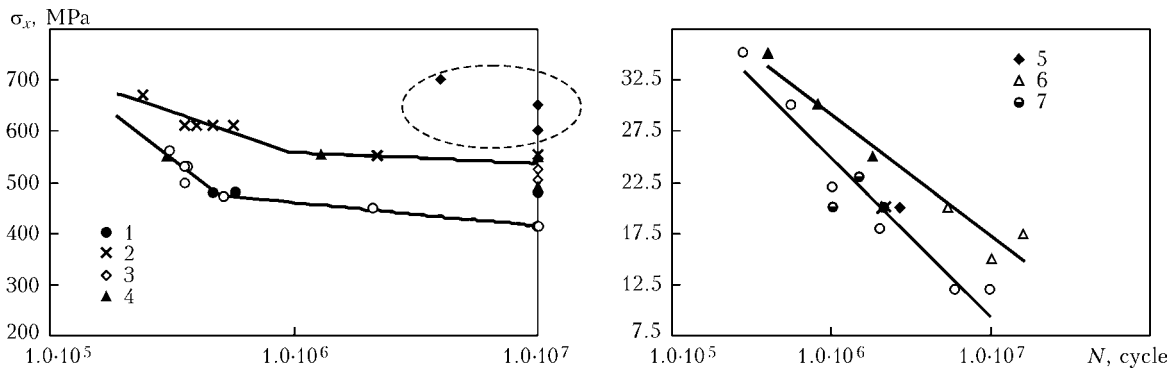

Figure 2. Fatigue curves of samples from steel 10Kh18N10T (*a*) and aluminium alloy D16T (*b*) in the initial condition (light circle) and after PEC treatment in modes 1–7 according to the Table

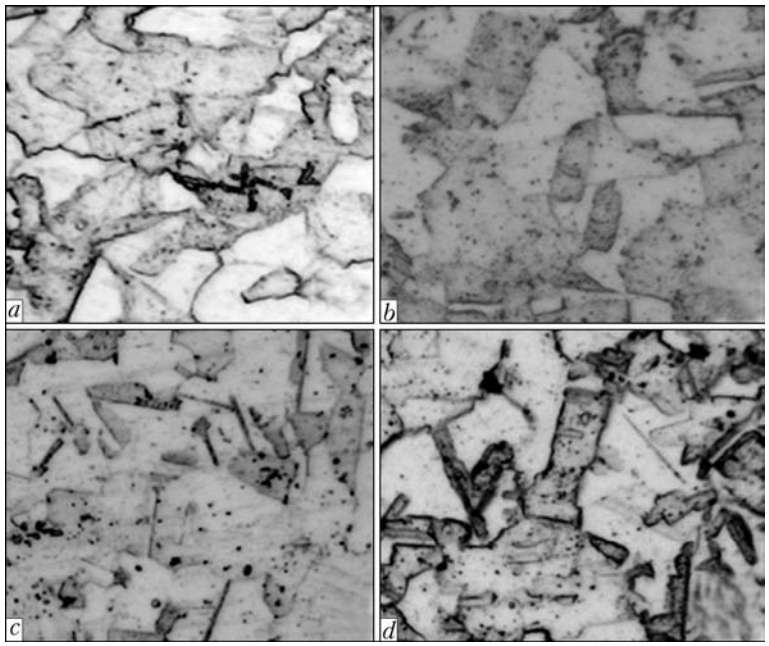

Figure 3. Microstructures (×1000) of a sample of steel 10Kh18N10T depending on PEC treatment parameters: *a* — initial state; *b* — *I* = 40; *c* — 80; *d* — 115 kA

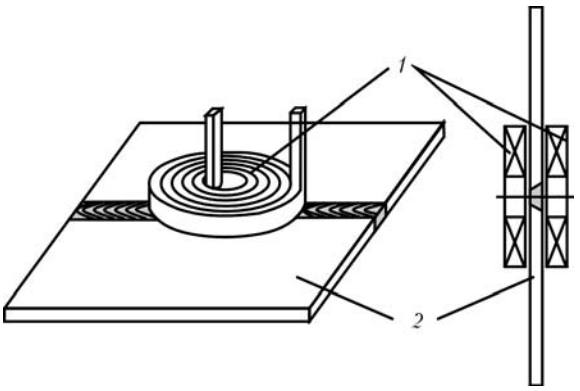

Figure 4. Schematic of PEMF treatment: *1* — inductors; *2* — plate with a weld

of carbides along the grain boundaries (Figure 3, *d*) and, as a consequence, to material softening.

Influence of induced current on RS in the welded joint. Treatment by pulsed electromagnetic field (PEMF) of a plate from aluminium alloy AMg6 made by butt welding of two parts 360 mm long, 250 mm wide and 3.7 mm thick (butt weld is along the long side, melting zone width B is about 12 mm), was made by the schematic given in Figure 4. At treatment the co-axially mounted inductors with outer diameter of 45 mm were shifted along the weld axis by 15 mm after each discharge and the bank of capacitors of 600 μF capacity was discharged through the inductors connected in series, at 3 kV voltage. Results of RWS measurement made by the method of speckle-interferometry are shown in Figure 5.

PEC influence on RS redistribution in the coating. Adverse influence of tensile RS on fatigue and wear resistance of structural elements with coatings is well known. However, considerable compressive RS in the subsurface layer do not always provide the maximum effect of improvement of fatigue life of parts. In study [8] it is shown that lowering of compressive RS induced in the subsurface layer of a titanium alloy after vibration-amplitude strengthening leads to a considerable increase of the number of cycles to fracture.

Therefore, increase of fatigue strength and wear resistance of structural elements ensured at optimum level and distribution of RS for the specified mode of thermomechanical loading and development of effective methods of technological treatment, providing formation of optimum level of RS in the coating–base system, are an urgent task.

Samples in the form of bars 10 mm wide, 80 mm long and 3 mm thick from tool steel of Cr–Mo–V system with one-sided coating from chromium nitride CrN of thickness b_c = 3 μm applied by magnetron sputtering, were studied. Coating was applied in two modes inducing, by the data of sample manufacturer, RS on the level of 0.5 and 1.5 GPa in the coating. At treatment two current pulses with maximum amplitude of about 40 kA (discharge of a bank of capacitors of 300 μF capacity at initial voltage of 2.5 kV) were applied to the sample.

Assessment of PEC influence on the stress-strain state of the coating was performed on samples without

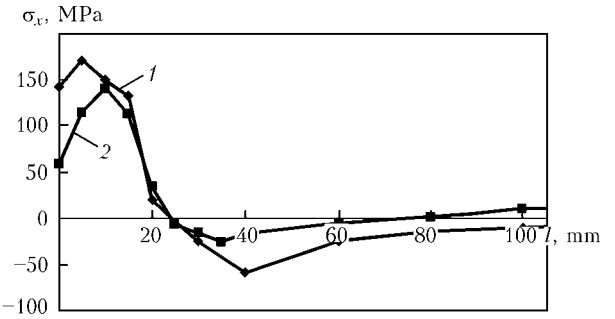

Figure 5. Dependence on RS in a sample of AMg6 alloy (normal to weld axis, plate middle) on distance from weld axis x before (*1*) and after PEMF treatment (*2*)

treatment and after treatment at complete removal of the coating, comparing the data of recording the change of strain on the opposite side relative to the coating. By the results of measurement, sample treatment by PEC application causes a lowering of the level of strain recorded by resistance strain gauges and, therefore, the level of compressive RS in the coating by approximately 20 % (Figure 6).

PEC influence on residual stresses after grinding. Strips from 10Kh18N10T steel 10 mm wide and 2 mm thick were used for investigations. Strips were attached by screws to a rigid pre-ground steel base, which, in its turn, was mounted on the table of a planogrinding machine tool, ensuring the coincidence of the grinding direction with the strip axis. At the first stage pre-grinding of the strips to the thickness of 1.9 mm was performed, using lubricoolant and low feed across the thickness. At the second stage lubricoolant feeding was overlapped and a 0.1 mm layer was removed in two passes at corundum wheel speed of 30 m/s. After such a «tough» grinding and removal from the base, the strips had a pronounced bend — result of action of tensile stresses in the layer adjacent to the ground surface (Figure 7). Strips were cut into samples of about 70 mm length, and then strain gauges were glued onto the sample ground surface in the central part.

At PEC treatment the sample was pressed by current taps of pulsed current generator to the flat surface

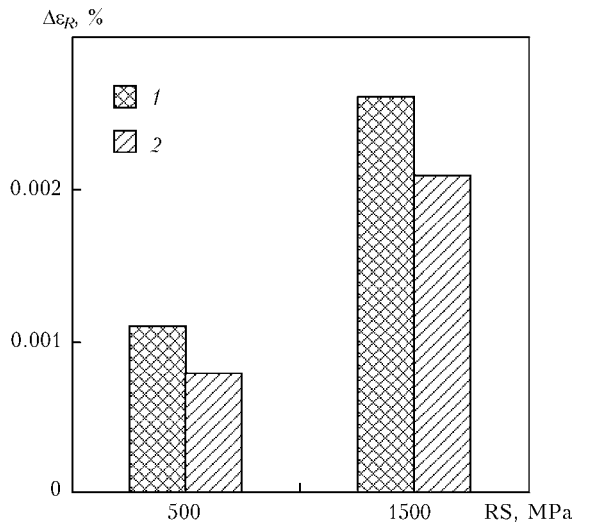

Figure 6. Change of strain in samples with a coating after its removal: *1* — without PEC; *2* — after PEC treatment

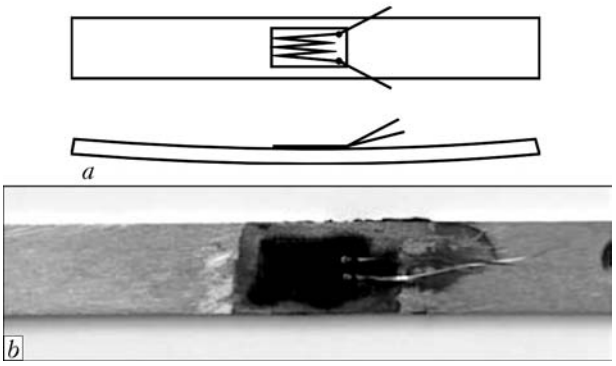

Figure 7. Schematic (*a*) and appearance (*b*) of a sample after grinding

of the massive textolite guide so that there were a sample section of about 40 mm (treated part of the sample) between the current taps with a strain gauge in the central part. One current pulse with 50 kA amplitude was applied, temperature rise being equal to 110 °C, which is essentially lower than the temperature required for RS lowering in regular heat treatment.

During investigations the strain gauge initial resistance was recorded in the free (bent) condition of strip A_1, in its straightened condition, pressed to textolite surface A_2, after PEC treatment (current passing and subsequent cooling) A_3 and in the released state after treatment A_4. Experimental results were used, allowing for calibration coefficient k, to determine the value of tensile strain caused by strip straightening in the initial condition $\varepsilon_b = k(A_2 - A_1)$ and after PEC treatment — $\varepsilon_b^{\text{PEC}} = k(A_3 - A_4)$, as well as treatment-induced longitudinal compression $\Delta\varepsilon = k(A_2 - A_3)$ and lowering of bending deformation in the free state $\Delta\varepsilon_b = \varepsilon_b - \varepsilon_b^{\text{PEC}}$.

The given results of strain recording were used to assess PEC influence on RS in the ground layer. Plastic compression of metal in layer δ_1 overheated as a result of grinding, causes tensile σ_1 (Figure 8) and compressive RS σ_2 in the layer (base metal layer unaffected by overheating) after cooling. From the condition of equality of forces in the layers before and after treatment and compatibility of deformation of the layers as a result of PEC action we can show that the change of stress in the first layer is equal to

$$\sigma_1^{\text{PEC}} = [(\delta - \delta_1)/\delta_1]\Delta\varepsilon E, \qquad (1)$$

where E is the modulus of elasticity.

At the same time, the level of stresses and strains in the surface layer after sample fixing on the flat textolite base is proportional to initial stresses after grinding. It can be shown that the change of bending deformation caused by PEC treatment, is equal to $\Delta\varepsilon_b = [1 - 3(\delta_1/\delta]\sigma_1^{\text{PEC}}/E$, therefore,

$$\sigma_1^{\text{PET}} = \frac{\delta}{\delta - 3\delta_1}\Delta\varepsilon_b E. \qquad (2)$$

Then the thickness of ground layer δ_1 is determined by equating expressions (1) and (2):

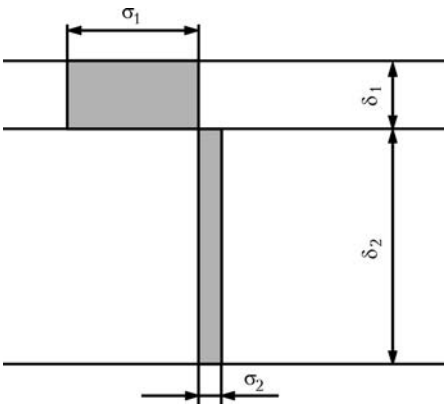

Figure 8. Schematic distribution of RS in a sample straightened after grinding ($\delta_1 + \delta_2 = \delta$)

$$\frac{\delta}{\delta - 3\delta_1}\Delta\varepsilon_b = [(\delta - \delta_1)/\delta_1]\Delta\varepsilon,$$

and finally

$$\delta_1 = \frac{\delta}{6}[\xi + 4 - (\xi^2 + 8\xi + 4)^{1/2}], \qquad (3)$$

where $\xi = \Delta\varepsilon_b/\Delta\varepsilon$.

From the recorded data for $\Delta\varepsilon_b$ and $\Delta\varepsilon$, value ξ can be determined as $\xi = 0.57576$. At strip thickness $\delta = 1.8$ mm using equation (3), thickness of deformed layer can be determined as $\delta_1 = 0.48$ mm, here the calculated lowering of RS as a result of current passage through the sample determined from equation (1) or (2) is equal to $\sigma_1^{\text{PEC}} \approx 40$ MPa.

CONCLUSIONS

1. Treatment modes were determined allowing an essential improvement of the endurance limit of a number of metallic materials at cyclic loading.

2. It is shown that this treatment leads to an essential redistribution of RS in the weld, coating or material after grinding, that in case of its application on structural elements allows their cyclic fatigue life to be extended.

1. Doronin, Yu.L. (1992) *Analysis of possibilities for improvement of structural and service characteristics of aircraft parts with pulse action of high-power electromagnetic field*: Syn. of Thesis for Cand. of Techn. Sci. Degree. Moscow.
2. Popov, O.V., Tanenberg, D.Yu., Vlasenkov, S.V. et al. (1990) Effect of pulse electric current treatment on strength and plastic properties of titanium alloys. In: *Abstr. of Pap. of 2nd All-Union Conf. on Action of Electromagnetic Fields on Plasticity and Strength of Materisls*. Pt 1. Nikolaev: RIO Oblpoligrafizdat.
3. Konovalov, S.V., Sosnin, O.I., Gronov, V.E. et al. (2002) Increase in reliability of products of medium-alloy steels with pulse current action. *Remont, Vosstanovlenie, Modernizatsiya*, **3**, 19–23.
4. Trufyakov, V.I. (1973) *Fatigue of welded joints*. Kiev: Naukova Dumka.
5. Trufyakov, V.I., Mikheev, P.P., Kuzmenko, A.Z. (1980) Effect of scale factor and residual stresses on rate of fatigue crack propagation. *Problemy Prochnosti*, **6**, 20–22, 30.
6. Gryaznov, B.A., Gorodetsky, S.S., Nalimov, Yu.S. et al. (1992) *Fatigue of refractory alloys and blades of gas turbine engines*. Kiev: Naukova Dumka.
7. Stepanov, G.V., Babutsky, A.I., Mameev, I.A. (2004) Nonstationary stress-strain state in long rods induced by electric current pulse of high density. *Problemy Prochnosti*, **4**, 60–67.
8. Loskutov, S.V., Levitin, V.V. (2002) Effect of electric pulse treatment on structure and service life of titanium alloys. *Zhurnal Tekhnich. Fiziki*, **72**, 133–135.

TRENDS IN IMPROVEMENT OF AUXILIARY EQUIPMENT FOR WELDING PRODUCTION

V.A. LEBEDEV[1], **I.V. LENDEL**[2], **V.I. LENDEL**[2] and **V.G. PICHAK**[1]
[1]E.O. Paton Electric Welding Institute, NASU, Kiev, Ukraine
[2]Ilnitsa Plant of Mechanical Welding Equipment, Ilnitsa, Ukraine

Main trends in development of mechanized welding equipment for fabrication of structures made in and outside Ukraine are analyzed, and basic requirements to them are indicated. Versatile rotators comprising a new generation of drives with computer numerical control and commutatorless motors are considered. Specific features of their operation are pointed out, and their advantages are noted. Also, the article analyzes the methods for reinstalling roller supports in a driving roller device, and considers some methods for elimination of drift of a workpiece in welding or surfacing.

Keywords: *welding, surfacing, cutting, workplace, organization, equipment, rotator, manipulators, new solutions*

Successful performance of operations of welding, reconditioning and strengthening surfacing, as well as cutting of different metal structures, ensuring of their quality and efficiency of operations greatly depend on arrangement and fitting of workplaces. Various means and equipment making the welders' work easier and allowing a considerable improvement of the efficiency and accuracy of the performed operations have a great role here. As a rule, this equipment includes means of welding production mechanization, in particular, various types of rotators, tilters, columns for welding and surfacing automatic machines.

The purpose of this work is discussion of the directions of development and production of auxiliary mechanical equipment for welding and surfacing both in Ukraine (specialized plant (Ilnitsa Plant of Mechanical Welding Equipment), and beyond it (by the materials of 2009 Essen Exhibition).

Technical publications have descriptions of various mechanization means for organization of welding and surfacing productions [1, 2], which provide guidelines for selection and design of various equipment of this type.

As before, the main requirement made of mechanical auxiliary welding equipment, is the stability of the workpiece rotation, i.e. maintaining the welding speed. Great importance is attached to the smoothness of the workpiece rotation (without vibrations, jerks, jamming, etc.) that is achieved, first of all, due to rigidity of the rotator bed, accuracy of manufacturing the tooth gears, minimum clearances in the seats, reliability of fastening the workpiece in the rotator faceplate.

Recently much higher requirements have been made to the quality of work performed using mechanized arc processes, realized by semi-automatic and automatic machines of varying degrees of technical perfection, also with additional movements (degree of automation, use of groove following, devices for arrangement of deposited beads, etc.). All this requires widening the capabilities of equipment for organization of modern workplaces for welding, surfacing and cutting of steels and aluminium alloys in the following directions: stabilization of welding and surfacing speed, solving the problems of positioning of the workpiece or welding tool, improvement of the processes, associated with making the weld start and crater welding up. Most of these problems are solved without application of any additional equipment, for instance, without position sensors at positioning or organizing repeated cycles in wide-band surfacing, etc. Equipment of this type should have systems of programming and acquisition of data bases. Particularly urgent are the problems of energy- and resource-saving, solved by optimization of the systems of control and adjustment for them that provide optimum paths of motion of the workpiece or welding tool.

An interesting direction of improvement of the considered type of equipment is that, which it directly involves the modes of welding equipment operation (welding speed is functionally dependent on welding current) $v_w - f(I_w)$. Realization of this direction also requires the availability of a certain data base, providing the following advantages:

- accurate setting and maintaining of the correspondence of energy characteristics of the arc and welding displacement;
- mechanized welding and surfacing station being independent of the operator's qualifications;
- quality performance of welding or surfacing with a uniformly formed bead, having a marketable appearance immediately after performance of the arc process cycle.

Realization of such capabilities in operation of auxiliary equipment for welding and surfacing requires application of adjustable electric drives of working displacement with sufficiently large adjustment range, and, what is highly important, high response. Here the main problems for mechanical welding equipment remain to be ensuring rotation of the welded

Figure 1. All-purpose manipulators with asynchronous electric motor in the rotation drive

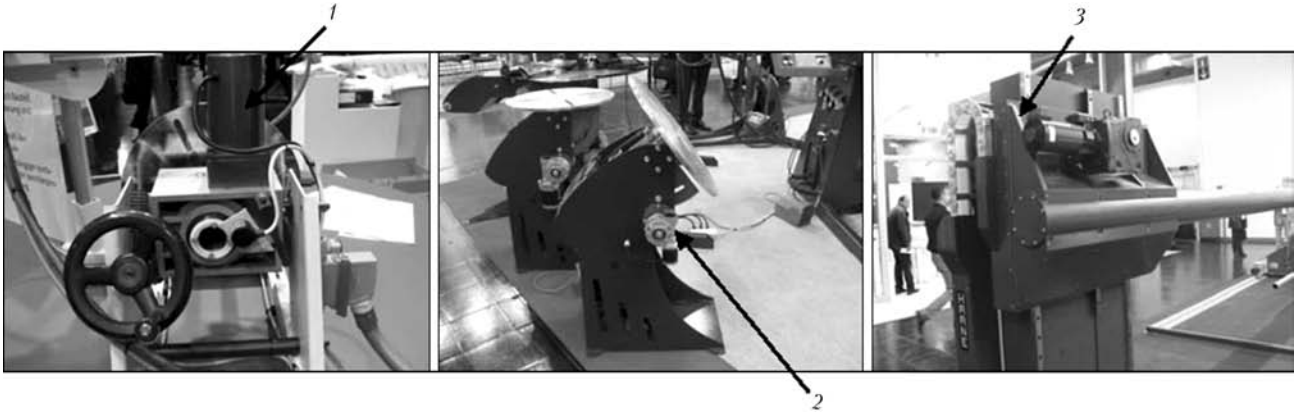

Figure 2. All-purpose manipulators with valve electric motors (*1–3*)

(surfaced) workpiece with the set speed during automatic or semi-automatic welding (surfacing) and moving the workpiece at travel speed into a position convenient for welding.

At present the auxiliary equipment systems use electric drives based on commutator and commutatorless (as a rule, valve) DC electric motors with thyristor or transistor regulators of the frequency of shaft rotation, and the recently becoming accepted asynchronous electric motors with frequency regulators.

Let us consider some types of modern mechanical welding equipment. In the Essen Exhibition this equipment was presented by various manufacturing companies from Hong-Kong, Taiwan, China, as well as Germany, France, Great Britain, Italy, Sweden, Greece, etc.

Figure 3. Control unit of valve electric motor

In mechanical welding equipment of the leading companies (JAVAC, Germany; Key Plant, Great Britain; ESAB, Sweden; Lambert Jouty, France, etc.) asynchronous motors in a set with standard reduction gears or reduction gears produced in-house, as well as motor drives, are mainly applied as the rotation drive (Figure 1). Frequency converters of asynchronous electric motors manufactured by different companies are applied for adjustment of the speed of rotation.

Companies involved in manufacture of mechanical welding equipment also displayed in the exhibition manipulators, in which the rotation drive uses a valve electric motor (Figure 2).

Valve electric motor is a synchronous motor the operation of which is based on the principle of frequency regulation with self-synchronization. The controller of valve electric drive (Figure 3) controls the moment applied to the rotor, and unlike the DC brush-type motor, switching in the valve electric motor is performed and controlled by electronic devices.

Valve electric motors with electronic control systems often combine the best properties of contactless motors: high response and dynamics; positioning accuracy; wide range of rotation frequency variation; absence of components requiring maintenance; high overload capacity by moment; high energy values (efficiency > 90 %, cos $\varphi > 0.95$); long service life, high reliability and increased operating life owing to absence of sliding electric contacts; low heating of electric motor in operation in modes with possible overloads.

Local manufacturer of diverse mechanical auxiliary welding equipment — Ilnitsa Plant of Mechanical

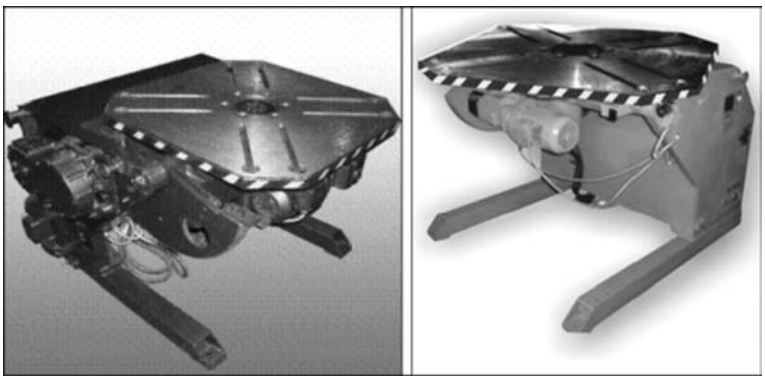

Figure 4. All-purpose manipulators manufactured by IPMWE

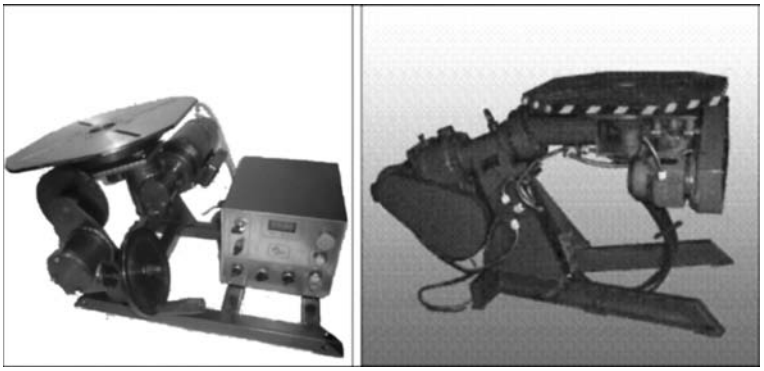

Figure 5. New models of IPMWE manipulators based on drives with valve electric motors

Welding Equipment (IPMWE) pays a lot of attention to various rotation drives. Starting from 2001, the plant during two years had transferred to application of converters of asynchronous motor rotation frequency (Figure 4). Foreign developments, in particular, General Electric electric drive (VAT-200 model) are used as asynchronous electric drives.

IPMWE is working towards introduction of new generation electric drives of valve type. At the beginning of 2009, a number of experimental manipulators were developed which are based on local electric drives. Today IPMWE is ready for commercial production of manipulators with new generation electric drives (Figure 5) that will allow programming some elements of workpiece rotation both by rotation speed, and by angle of workpiece rotation. In addition, at all the same characteristics, the overall dimensions and weight of valve electric drives are smaller than those of electric drives with an asynchronous electric motor. Comparative technical characteristics of these rotators with adjustable electric drives based on asynchronous and valve electric motors are shown in the Table.

There exists a great diversity of driving roller devices (Figure 6) with the same requirements to the speed of rotation, accuracy of mounting the rollers relative to workpiece axis, time required for readjustment of the rollers for the required workpiece diameter. At inaccurate position of roller axis relative to the axis of workpiece rotation, such a phenomenon as shifting of the workpiece being welded along its axis (drift) is observed, leading, in its turn to deviation of the weld from the welding position. Shifting depends on workpiece diameter and angle of non-paral-

Comparative technical characteristics of rotators with adjustable electric drives based on asynchronous and valve electric motors

Parameter	SPS 150-150S (Figure 1)	PRO 1 (Figure 2)	M211080 (Figure 4)
Maximum lifting capacity, kg	125	120	125
Faceplate rotation frequency, min^{-1}	0.5–9.0	0.5–5.0	0.16–5.0
Faceplate angle of inclination, deg	0–180	0–90	0–135
Faceplate diameter, mm	500	350	450
Rated welding current (duty cycle = 100 %), A	500	300	500
Mains voltage, voltage/frequency, Hz	230/50	230/50	230/50
Setting the inclination	Manually		
Overall dimensions ($L \times B \times H$), mm	1050 × 880 × 1080	480 × 325 × 470	850 × 695 × 400
Weight, kg, not more than	100	50	75

Figure 6. Driving roller rotators with different drive layouts

Figure 7. Retaining roller

Figure 8. Working body of the following system mounted on the welding head

lelism of the axes of workpiece and rollers. Different companies have different solutions for this problem. Lampert Jouty mounts a system for following the deviation of the workpiece and depending on this value, the system gives a signal in the automatic mode to the drive of final rotation of roller axes.

IPMWE solves this problem by mounting mechanical rotating rests (Figure 7), as well as displacement of the actuator (weld following) of the welding head, using the following system (Figure 8).

There are several methods for reinstallation of the roller supports, the driving roller device sections into the required position, but from those displayed in the exhibition, the following can be singled out:

• using screw–nut transmissions. It enables simultaneous displacement of two roller supports and elimination of small misalignments by height between roller support sections;

• using rests of different designs, the most widely spread here is fixing of roller supports by holes and displacement of roller supports — a faster, but more labour-consuming process.

Introduction of the new generation of roller supports will be actively pursued further on, as they have a number of advantages, namely possibility of reducing the power inputs and widening the capabilities of mechanical auxiliary equipment, as well as considerable improvement of the quality of manufactured products. New systems of regulation with feedbacks by welding equipment parameters will be also developed.

1. Evstifeev, G.A., Veretennikov, I.S. (1977) *Means of mechanization of welding production: design and calculation*. Moscow: Mashinostroenie.
2. Kurkin, S.L., Khovov, V.M., Rybachuk, A.M. (1989) *Technology, mechanization and automation of production of welded structures*: Atlas. Manual. Moscow: Mashinostroenie.

IMAGE PROCESSING FOR AUTOMATED ROBOTIC WELDING

P. SEYFFARTH and **R. GAEDE**
Ingenieurtechnik und Maschinenbau GmbH, Rostock, Germany

The new developed by IMG and used by WADAN yards MTW image processing system for welding robots delivers a very fast automatically generated program. A laser line scanner with a scanning rate of 1 m/s and a fast working calculation unit gives a 3D picture in less than 3 min all over the 16 × 4 m panel. The accuracy of the robotic positioning is ±0.5 mm after the shake hand process between the image processing system and the robot programming system. This new developed 3D geometrically recognising and robot programming system allows a very fast and flexible production system for micropanels without any link to the central computer aided yard system. This «stand alone system» is independent, more flexible and shows beside of other advantages a high productivity.

Keywords: *robot welding, fillet welding, image processing, robot programming, micropanel welding, welding in shipbuilding*

The main parts in the prefabrication of ship hulls are flat and curved panels with dimensions up to 20 × × 40 m or more and so named micropanels. We meet especially the last one, the micropanels, in a large number of different forms an sizes beginning from 2 × × 2 up to 4 × 16 m. In a medium sized container freighter for 2000 containers there are about 2500 or more various micropanels. There are different production technologies for micropanels, consisting from plates and stiffeners. A modern micropanel production at a shipyard uses robots for mounting and welding as well. This is shown as an example in Figures 1 and 2. Due to the various construction types of micropanels and their large range from unique single construction up to minimum series there is a high demand on the programming of robot systems including the movement of the robots in the 3D coordinates and the various welding parameter. In shipbuilding each micropanel needs its own welding program. All of the known programming procedures require either additional information on the workpiece in the shape of CAD data or they need manual interaction. The classical programming of weld robots for micropanels takes places regardless of the really existing workpiece and production scenario by a partly automatic analysis of CAD data in combination with demanding manual interactions. The programming takes place temporally very much in advance of the production and needs a high quality and relevance of the available construction data. Unfortunately this is in contrast to the flexibility of the production flow and can not take in account some changes of construction. That means we have to take in account that normally the programming is done a long time before production and very often the NC construction data are changed in the meantime.

Refitting of an existing micropanel line by image processing. To meet the needs for a very high flexibility and for an automated programming on demand for the existing panel line (see Figures 1 and 2), the enterprise Ingenieurtechnik und Maschinenbau

Figure 1. Mounting gantry for stiffeners in micropanel line

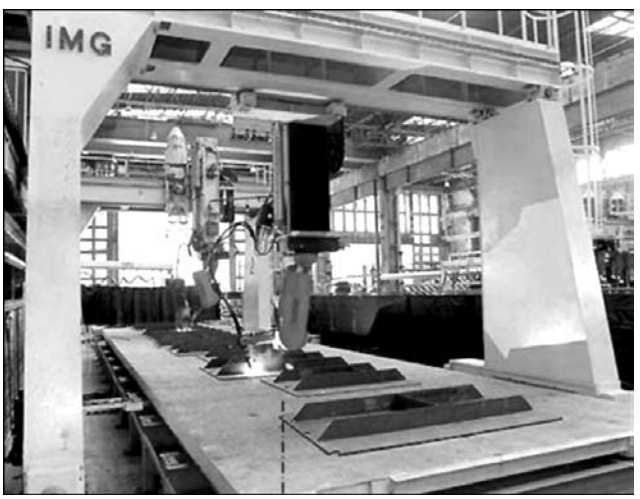

Figure 2. Welding station in micropanel line using two robots before refitting

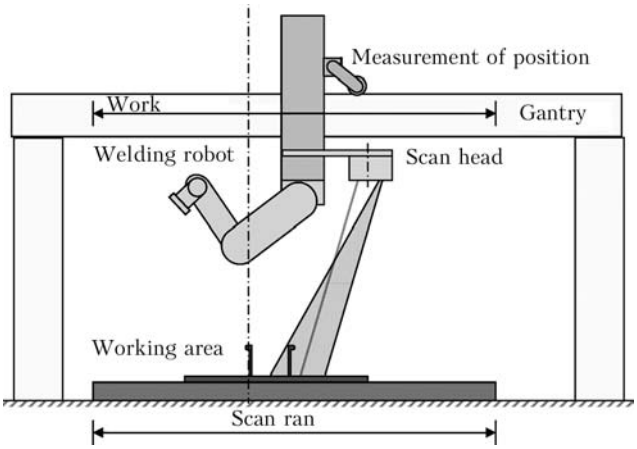

Figure 3. Principle of 3D image processing for robot programming

GmbH (IMG) designed, constructed and delivered recently a very fast working 3D image processing system in cooperation with the company's aviCOM and TSWE.

The principle of this 3D image processing system is shown in Figure 3, and Figure 4 gives an overview about the system controlling units.

The heart of the new industrial 3D scanner measuring system for micropanels is a camera head based on modern camera technology. The scan head measures 3D data according to the laser triangulation principle. Hence, to be able to measure 3D shape, an external line-generating laser source is used. The laser generator is mounted to the robot and projects its laser line on the working area from a distance of about 2 m in the height. The camera, that views the line from a different angle, sees a curve that follows the height profile of the object. By measuring the laser line deviations from a straight imaginary reference line, the height of the object can be computed.

The robot moves for scanning with the scan head and the laser line along the working area, contour slices of the object are generated. The collection of such slices, or 3D profiles, is a description of the complete object shape as seen from the upper side of the object. The unique camera technology is capable of finding the position of the laser line by itself and reducing to whole image information into compact laser coordinates. These laser coordinates are transmitted to the PC. That is what the mounted 3D imaging technology makes very fast and reliable.

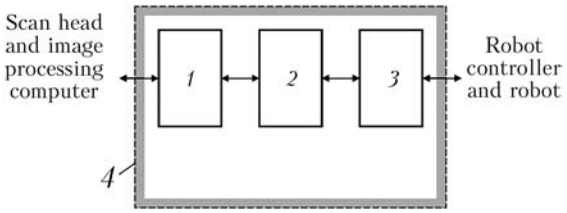

Figure 4. Controlling units of the image processing and robot programming system: *1* — image processing software; *2* — online programming system; *3* — server macroadministration; *4* — system controlling by industrial PC

Inside the scan head the camera offers several different methods for the generation of 3D profiles which differs in speed and height resolution. This flexibility of the camera was used to optimize results for the specific scanning task and material.

The measurement principle gives geometrical limitation concerning the measurement of hidden parts in relation to the camera view. There are two kinds of limitations, camera occlusion and laser occlusion. Camera occlusion occurs when the laser line is hidden from the camera by an object and laser occlusions occur when the laser cannot properly illuminate parts of an object because of its projection angle. Adjusting the angles of the scan head and the laser can reduce the effects of occlusion. Additionally we use two scan heads with two laser sources illuminating the micropanels and especially the profiles from opposite sides.

The measurement system 3D field-of-view (FOV) is a trapezoid-shaped region where the laser line intercepts the FOV of the camera. It is only in this region that the camera generates 3D measurements. The camera FOV is given by the selected lens and camera software parameters. The height resolution of the measurements is dependent on the angle between the laser and the camera — as the angle is increased, the resolution is also increased — and on the selected 3D method. Generally, if the precision of the profiling algorithm is high, the maximum profile rate is limited compared to a less precise but fast algorithm.

The maximum profile rate is dependent on a combination of the selected 3D method, the required meas-

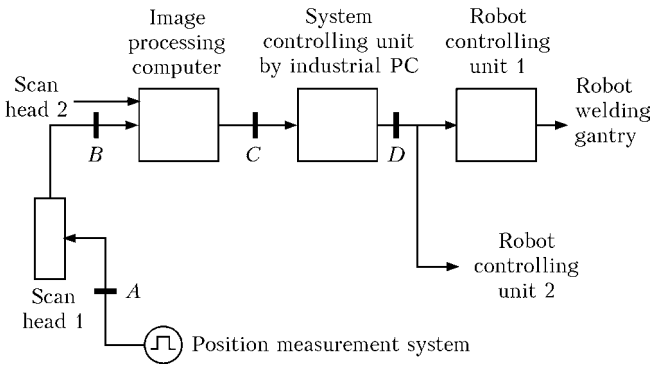

Figure 5. Concept of data processing for two robots from scan head to the welding robot

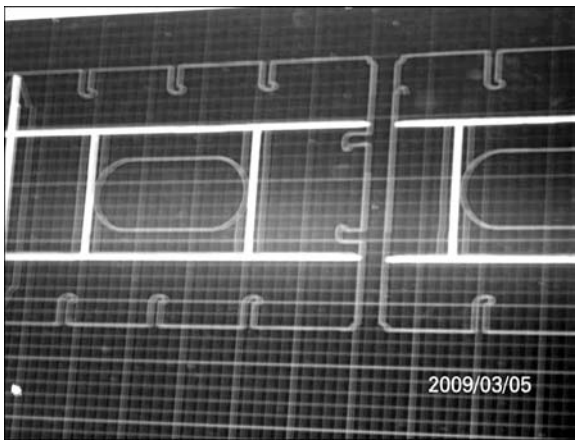

Figure 6. Visualization of micropanel on the user screen, ready for further high level processing

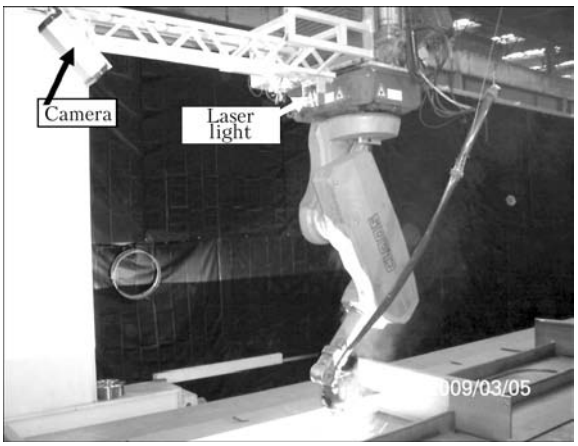

Figure 7. Refitted robot with automated programming system by image processing in operation at the yard

urement resolution, and the required height of the measurement region. By for instance decreasing the height region used for object inspection the profile rate can be increased. Note, however, that the maximal usable profile rate also depends on the amount of light reflected from the object.

The data stream of profiles was synchronized with the robot movement using an external encoder. This functionality will ensure that the length measurement and object scale in the movement direction is correct, even if the object speed varies (Figure 5).

All parameters were optimized for the application of scanning micropanels under production conditions. The result is a scanning speed of 0.5 m/s with a maximum of independence from surrounding light conditions. The resolution of the 3D points is about 1 mm in x- and y-direction and 2 mm in z- (height). It is to consider that the resolution differs over the field of view in the relation to the height of points. The measurement range in z-direction is actually 400 mm.

The design goal was to optimize the overall scanning time, the sum of time to scan and process data. Although the scanning speed could be higher (up to 1 m/s) it is shown that the shortest process time is reached by processing the data parallel to the scanning process.

The scanning is done in stripes of 1.2 m width and 16 m length in reversing order of forward and backward movement. Hence, the whole working area consists of a maximum of four stripes for each scanning head.

The measured 3D points in the laser plane of the scanner have to be processed with complex mathematical algorithms to calculate real world coordinates. This is done mostly during the scanning process parallel to the capture of 3D points. Additionally a first step of data reduction is done to extract object shape information as panel planes, profile planes and contours. The whole working area is scanned after about 3.5 min. At this time the extracted object shape information is available for high level processing in the final geometry extraction (Figure 6).

Figure 7 shows the scan jib together with the two laser sources and the camera fixed at the refitted robot.

The process of geometry extraction calculates the matching of all scanning stripes separately for each scan head. Additionally it calculates the matching of both scan heads to one description of the scene. This description consists of panels with 3D contour polygons, a plane approximation for profiles distinguishing different types such as HP, Flat, T- or L-profiles and an information which profile belongs to which panel.

Advantages of the new installed 3D image processing system. The main advantages of the recently installed new programming system by 3D image processing are the following:

- programming on demand guarantees a very high production flexibility;
- programming is a very fast process, there is no remarkable production time lost;
- the scan rate depending on the profile height is 0.5 up to 1 m/s;
- the process time for the whole process depending on the size of the panel and the number of stiffeners is 3.5 up to 12 min. This is very fast in comparison with some hours of welding time;
- the accuracy with 1 mm in x- and y-direction and 2 mm in z-direction is very high;
- it needs no operator for programming.

CONCLUSION

The micropanel is now successful in operation more than one year at one German shipyard. It needs only one operator for all processes including mounting and tacking of the stiffeners, changing the filler material for the two robots and so on. The automated micropanel line provides a high level of automation utilisation, production flexibility and an increase in efficiency. The experience at the yard shows that the play-back-time for the investment is in a range of one year.

OPTIMISATION OF PARAMETERS OF ADDITIONAL GAS SHIELDING IN SUBMERGED ARC WELDING AND SURFACING OF COPPER AND ITS ALLOYS

V.N. KOLEDA and **V.M. ILYUSHENKO**
E.O. Paton Electric Welding Institute, NASU, Kiev, Ukraine

The paper presents the results of evaluation of influence of a combined shielding on gas saturation of metal at the stage of a drop and a pool in welding and surfacing of copper and its alloys. Parameters of the process of submerged arc welding and surfacing using an additional gas shielding were optimized. A new method of a pulsed supply of shielding gas into the arc zone in submerged arc welding and surfacing was developed.

Keywords: *arc welding, submerged arc surfacing, copper and copper alloys, gas shielding, hydrogen, porosity prevention*

Automatic submerged arc welding and surfacing of copper and its alloys is one of the prospective methods of manufacturing both elements of metallurgy equipment as well as producing of bimetallic products from copper–bronze and steel–bronze [1–4].

Nowadays, for welding and surfacing of copper and copper alloys the fused fluxes AN-60, AN-20P, AN-26P, AN-348-A, OSTs-45 and other, developed for welding of steels, are used. However, even keeping all technological recommendations (calcination of fluxes, mechanical cleaning, degreasing of wire and base metal) they do not always provide the required density of metal. It is known that efficient measure of preventing porosity is the decrease of a partial pressure of hydrogen in the arc atmosphere. It can be achieved due to both its binding into compounds and also adding of other gases into the arc atmosphere [5, 6].

This wok evaluates the influence of additional gas shielding on gas saturation of metal at the stage of a drop and a pool, quality of welds of copper, copper with steel and surfacing of copper alloys on steel and copper.

To select the optimal scheme of gas supply to the arc zone, two methods were tested: through the copper nozzle and through a copper tube located horizontally. As an additional shielding the nitrogen was used (300–700 l/h consumption), which was supplied in a continuous mode. During supply of shielding gas using the first method the diameter of a nozzle (from 10 to 20 mm) and distance from its end to the base metal (from 10 to 30 mm) were changed, while at the second method the diameter of tube (from 3 to 10 mm), inclination angle (from 0 to 30°) to the horizon, distance from the outlet hole to the electrode (from 10 to 30 mm), to the base metal (from 5 to 15 mm) were changed. The external pores were determined visually. The presence and character of location of inner defects were studied on macro- and microsections. Tendency of deposited metal to the porosity was estimated according to the quantity of dense beads.

As the carried out experiments showed, during supply of shielding gas through the nozzle the positive effect was achieved only when the lower edge of nozzle was in a molten slag and favorable conditions were created for shielding gas to get into the zone of arc. However it leads to shunting of welding current, violation of the process stability and deterioration of bead formation.

During supply of shielding gas through the gas-supplying copper tube the best results were obtained when it was positioned ahead the arc or on the side at the angle of not more than 5–10° to the horizon, its end was located in the molten slag. The optimal diameter of the tube was 4–6 mm. While selecting the most effective shielding environment the nitrogen, argon and carbon dioxide were tested.

To study mechanism of influence of additional gas shielding on the porosity, the gas saturation of metal at the stages of a drop and a pool was determined. For this purpose the content of hydrogen was determined in drops of electrode metal, remaining at the ends of electrode after interruption of welding, and in «pencil samples» after sampling by drain of a pool metal through a hole in the specimen. The liquid metal entered the dismountable copper mould of 10 mm inner hole diameter. Fixation of gases dissolved in liquid metal occurs as a result of high rate of samples crystallization. Specimens manufactured of «pencil samples» and drops of electrode metal were analyzed in the LECO unit RH-2 to determine the content of residual hydrogen in them. The surfacing was performed using wire of the BrAMts9-2 grade under flux AN-26P on 10 mm thick plates of bronze of the BrAMts9-2 grade. During welding of copper of 10 mm thickness the wire of the BrKh07 grade and flux AN-348-A were used, in welding of copper with steel of 10 mm thickness the wire of the MNZhKT5-1-0.2-0.2

grade and AN-60 flux were used. The consumption of argon, nitrogen and carbon dioxide was 500 l/h. Gas was supplied in a continuous mode through the 5 mm diameter copper tube, positioned ahead the arc at the angle of 10° to the horizon. The distance from the outlet hole to the electrode was 12 mm, and to the surface of specimens — 7 mm.

It was established that application of additional gas shielding allows reduction of saturation of liquid metal with hydrogen at the stage of a drop and a pool (Figure 1) that stipulates the decrease of porosity in welds and deposits.

In welds and deposits performed with additional gas shielding the porosity was absent in all cases. Without application of additional gas shielding in welding copper and copper with steel the single pores were observed in welds, and in surfacing of bronze the noticeable porosity was observed.

Figure 1 shows that the content of hydrogen in a molten pool is much lower than in electrode metal drops that is probably due to a partial degassing of the pool.

To study the effect of additional gas shielding on the porosity of deposited metal, the method of multilayer deposition was applied, when in each next bead the tendency of deposited metal to porosity is increased. The deposits were made with wire of the BRAMts9-2 grade under the flux AN-26P on copper and steel specimens of 15 mm thickness. A copper tube of 5 mm diameter was set at the distance of 10 mm from the electrode ahead the arc. The angle of inclination to the horizon was 5°, and distance from outlet hole to the surface of specimens was 5 mm. As an additional shielding, the argon, nitrogen and carbon dioxide were used which were supplied in a continuous mode, changing the consumption from 100 to 900 l/h. The data about the effect of additional gas shielding on the porosity of deposited metal are given in Figure 2.

As the carried out experiments showed, with increase of gas consumption the resistance of deposited metal against pores formation was increased. However, at consumption of more than 800 l/h the breaks of slag bubble are observed, that leads to the violation of stability of arc burning process, increased spattering of metal and deterioration of beads formation. During consumptions of less than 200 l/h the uniform gas

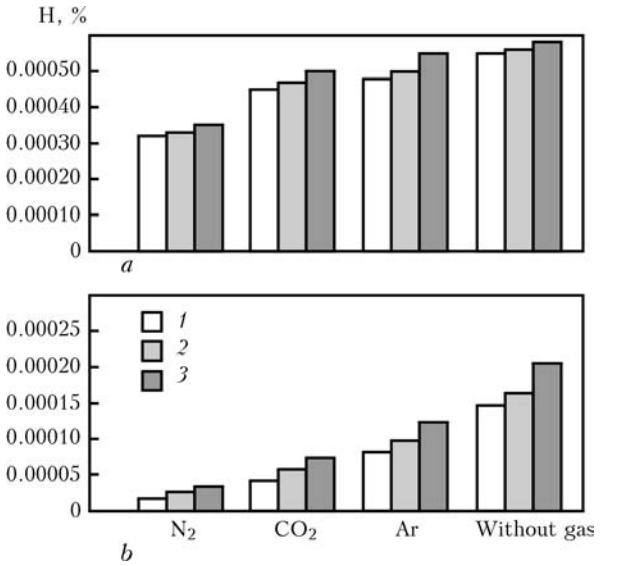

Figure 1. Influence of shielding gas on the hydrogen content in drops of electrode metal (*a*) and metal of weld pool (*b*): *1* — wire of the BrAMts9-2 grade; *2* — BrKh07; *3* — MNZhKT5-1-0.2-0.2

supply is not provided due to the tube sealing with a slag.

The best density of the deposited metal is achieved in use of carbon dioxide as an additional shielding, which does not only dilute the arc atmosphere, but also, having oxidation ability, it binds hydrogen additionally.

The high efficiency of nitrogen as a shielding gas, as compared to argon, is probably can be explained, on the one hand, by a content of admixtures of oxygen in commercial nitrogen (from 0.5 to 5 %), which binds hydrogen, and on the other hand — by the better conditions of degassing the weld pool. Here the evolution of nitrogen bubbles is possible which can serve as nuclei of pores and leads to porosity at lower hydrogen contents in liquid metal.

To decrease consumption of shielding gas the comparative tests on supply of shielding gas in pulsed and continuous modes were carried out. In experiments the inclination angle of gas pipeline was changed from 0 to 15°, the distance from outlet hole of gas pipeline to the base metal — from 3 to 9 mm, frequency of pulses — from 0 to 1.5 Hz, consumption of shielding gas — from 250 to 800 l/h.

The testing of method of shielding gas supply through the copper tube in a pulsed mode showed that

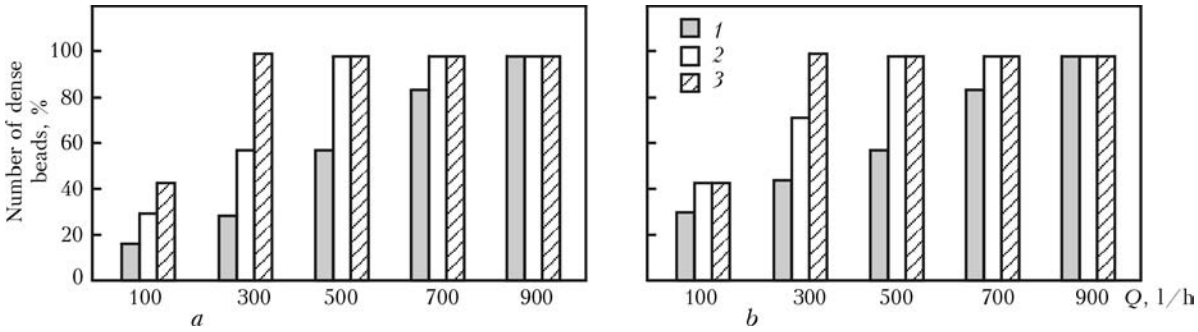

Figure 2. Influence of gases content and their consumption on the resistance to porosity in surfacing of bronze BrAMts9-2 under the flux AN-26P on the copper (*a*) and steel (*b*): *1* — Ar ; *2* — N_2; *3* — CO_2

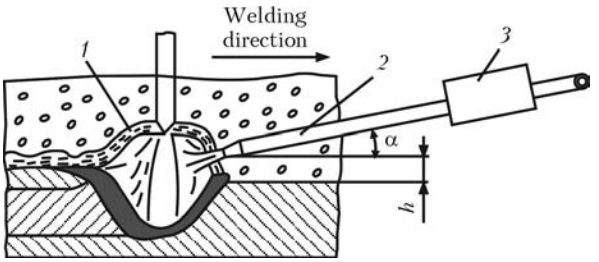

Figure 3. Scheme of the method of shielding gas supply (designations see in the text)

at certain parameters of a pulsed supply, a significant decrease in consumption of shielding gases, improvement of stability of welding and surfacing processes at a guaranteed absence of pores in welds and deposited metal can be reached.

On the basis of carried out experiments the method of shielding gas supply to the arc zone in a pulsed mode, schematically shown in Figure 3, was developed. A gas pipeline *2*, made in the form of a tube, is arranged on the boundary of flux fusion *1*. Gas can be supplied to the welding zone both in continuous and pulsed modes by means of device *3*.

The output diameter of gas pipeline is selected in the limits of one diameter of electrode and positioned at the distance of 5–7 mm from the surface of a part being welded, and gas pipeline is arranged at the angle of 5–1° to the horizontal plane. The duration of a pulse of gas supply is set in the volume of 40–60 % of duration of a selected period of gas supply. The increase or decrease of inclination angle of gas pipeline to the horizontal plane leads to deterioration of weld formation, spattering of metal in welding and surfacing, overlap formation, violation of stability of welding and surfacing process, and also appearing of porosity in welds and deposited metal. At setting the distance from outlet hole of a gas pipeline up to the surface of a part being welded of less than 5 mm the cases of its sticking to the metal surface are possible and with increase of this distance by more than 7 mm a jet of shielding gas can be spread in the flux above the molten film of a slag. Here, the partial pressure of hydrogen is not reduced, which results in appearance of porosity in deposited metal. The frequency of gas pulsation is set in the limits of 0.75–1.25 Hz. Decrease in pulses frequency leads to appearing of porosity in deposited metal, and increase in frequency leads practically to continuous gas supply and increase of its consumption. Decrease or increase in ratio of duration of a pulse to the duration of the whole period of pulsation from 40–60 % leads to porosity in the deposited metal of a weld.

The experimental data are generalized in the Table, where results of surfacing by the bronze wire BrAMts9-2 of 4 mm diameter on the specimens of copper of M1 grade under flux AN-26P at different consumptions of argon shielding gas are given.

At a pulsed shielding gas supply the periodical break of a film of molten flux is achieved and gas, directly getting into the arc zone, decreases the partial pressure of hydrogen in it with a dynamic effect on the molten metal and thus facilitating the evolution of hydrogen, dissolved in it.

As is seen from the Table, the keeping of the abovementioned optimal parameters of a pulsed gas supply through the copper tube allows obtaining the stable process of surfacing, dense beads with a good formation at lower consumptions of shielding gas in comparison with its supply in a continuous mode.

Influence of parameters of shielding gas supply and technological factors on the quality of welds

Pulse frequency f, Hz	Angle of inclination of gas pipeline α, deg	Height of gas pipeline over base metal, mm	Shielding gas consumption Q, l/h	Quality		Presence of pores
				Stability of process	Bead formation	
0.50	5	5	250	Satisfactory	Satisfactory	Pores
0.75	7	5	250	Good	Good	No pores
1.00	5	6	250	Excellent	Excellent	Same
1.25	5	7	250	Same	Good	»
1.50	5	5	250	»	Same	Single pores
1.00	0	5	250	Satisfactory	Unsatisfactory	No pores
1.00	10	5	250	Good	Good	Same
1.00	15	5	250	Satisfactory	Satisfactory	Single pores
1.00	7	3	250	Unsatisfactory	Unsatisfactory	Pores
1.00	7	9	250	Good	Satisfactory	Same
–	5	5	250	Excellent	Excellent	»
–	5	5	300	Same	Same	»
–	5	5	400	»	»	»
–	5	5	500	»	»	»
–	5	5	600	»	»	Single pores
–	5	5	700	»	»	Same
–	5	5	800	»	»	No pores

Comprehensive testing of this method in welding of copper and copper with steel, multilayer surfacing on copper and steel, bronzes of the BrAMts9-2, BrKMts3-1 types under the fluxes of AN-26P, AN-20P, AN-60, AN-348-A, OSTs-45 grades showed that application of combined shielding provides dense welds and deposited metal in all cases.

The method of combined shielding has passed the industrial tests in welding of copper with steel under flux as applied to the manufacturing of blast furnace tuyeres with thickness of edges being welded of 5–10 mm, and also in deposition of bronze on steel under flux on circumferential surfaces with the purpose to increase the operability and service characteristics of bimetal products, that allows it to be recommended for the industrial implementation.

1. Gurevich, S.M. (1990) *Reference book on welding of nonferrous metals*. Kiev: Naukova Dumka.
2. Paton, B.E. (1974) *Technology of fusion electric welding of metals and alloys*. Moscow: Mashinostroenie.
3. (2006) *Machine building*: Encyclopedia. Vol. 4: Welding of nonferrous metals and alloys. Ed. by B.E. Paton. Moscow: Mashinostroenie.
4. Monnean, P. (2000) Les liaisons du cuivre. *Vide Sci., Techn. et Appl.*, 55(**296**), 147–158.
5. Podgaetsky, V.V., Mandelberg, S.M., Bender, V.S. et al. (1973) Submerged-arc welding using gas-saturated flux. *Avtomatich. Svarka*, **6**, 28–31.
6. Ilyushenko, V.M., Bosak, L.K. (1984) Influence of oxidation level of flux on porosity in welding of copper. *Ibid.*, **4**, 67–68.

HALF-CENTURY ANNIVERSARY OF THE FIRST EXHIBITION OF ACHIEVEMENTS OF WELDING PRODUCTION

A.N. KORNIENKO

E.O. Paton Electric Welding Institute, NASU, Kiev, Ukraine

50 years ago (since 12 July till 3 October, 1960) the exhibition «Implementation of advanced welding technology into national economy of the USSR» took place in Moscow at the Exhibition of Achievements of National Economy in the pavilion «Machine building» at the area of above 6000 m^2, where more than a thousand of exhibits (full-scale specimens, mockups and posters) was shown. According to the scales of demonstration of development of welding production in the single country the exposition had no equals. By that time in the USSR not only world-famous methods of welding and related technologies were successfully applied, but also a number of principally new methods of joining were developed. Therefore, it can be considered that the exposition illustrated the world level of welding technology for the end of the first half of the XX century. It was namely the period when welding became the most widely applied in mak-

ing the permanent joints. In the 1930s the welding production made the great contribution into the industrialization of the USSR. In the USA and a number of other countries the welding also continued to replace riveting in machine building, industrial building in spite of depression and delayed rates of economic development.

During those years the fundamentals of welding were based. In particular, under the leadership of Evgeny O. Paton the methods of calculation and designing of sub-assemblies of welded structures were developed, the strength of welded specimens was studied, high-quality electrodes for manual arc welding were manufactured, the development of high-efficient method of automatic submerged arc welding was finalized and its implementation at the plants of the USSR started. During the years of the Great Patriotic War the specialists of the Electric Welding Institute at the evacuation to the Urals developed first in the world the automatic submerged arc welding of armored steels, proved experimentally the presence of arc discharge under flux, new designs of welding heads were created on the basis of discovery of self-adjusting of arc processes, dozens of installations for welding the components of tanks, aircraft bombs were designed and mounted. In other countries, the same as in the USSR, implementation of welding accelerated the production of armament, transport vehicles, construction and restoration of metallic structures.

In the postwar period the rates of development of welding preserved. The Electric Welding Institute started conversion of the submerged arc welding. Already in 1944 the works on mechanization of welding processes in site, widening of application of the automatic welding in different fields of civil production began, two-arc welding at high speeds was suggested, mobile welding tractor-automatic machines, hose semi-automatic machines and other were offered. In that period Evgeny O. Paton laid grounds of combining the theoretical and experimental research works with applied developments which led to foundation of investigations of a principally new class, i.e. purposeful fundamental studies.

The works, carried out at the E.O. Paton Electric Welding Institute, promoted the facilitated acceleration of restoration of destroyed industry of the country, first of all metallurgy and fuel-power complex. The technologies of pipes production and construction of pipelines, large-block building of ships, production and repair of railroad transport were developed. For the first time in the world the automatic submerged arc welding of vertical welds was performed, implemented into the building of blast furnaces, bridges and other structures, the production of tanks of flat panels was created, the assembly-welding automatic machines for manufacturing mining cars, standpipes, miner's lamps, etc. were designed. The remarkable achievement of the E.O. Paton Electric Welding Institute, awarded by Grand Prix at the International Exhibition in Brussels (1958), was the development of electroslag welding, the technology of joining metals (steels, aluminium, copper, titanium and their alloys) of unlimited thickness. Basing on this technology the electroslag surfacing and remelting were developed. The world achievement became the development at the E.O. Paton Electric Welding Institute of a circumferential transformer for the flash-butt welding in the field conditions of rails, butts of pipes including main pipelines of large diameter. At the end of the 1940s TsNIITMASh, E.O. Paton Electric Welding Institute, NIAT, IMET and a number of other institutes developed for the first time in the world the arc welding in CO_2, the implementation of which allowed considerable mechanization of welding production of steel structures. To manufacture critical products of non-ferrous metals the arc welding in ar-

gon, plasma welding, ultrasonic, friction, electron beam, diffusion, magnetically-impelled arc butt welding and other were used. New technological possibilities of gas-plasma treatment, in particular, cutting were achieved due to the works of such organizations as VNIIAVTOGEN and VNIIESO.

It should be noted that before the organizing of exhibition the USSR leaders studied the status of welding science and technology. On June 5, 1958 the Decree of Central Committee of Communist Party of the Soviet Union and Council of Ministers of the USSR «About the further implementation of welding technology into the production» outlined the main trends in the development of welding in the USSR for seven years. For the first time welding was recognized as an independent type of production, the state planning of production of welded structures and level of mechanization of welding works were established. On 23–24 February, 1959 the first session of the Council on coordination of research works in the field of welding, which included 70 leading specialists of the country, scientists and managers of production, took place in Kiev under the chairmanship of Boris E. Paton. 15 commissions on different problems of welding science and technology were organized which began to conduct independent operative work on coordination. The July plenum of Central Committee of Communist Party of the Soviet Union of 1959 outlined the building of specialized welding plants in different regions of the country. On 13 July, 1960 at the next plenum B.E. Paton presented the paper «Welding, its importance in industry and construction and prospects of its further development». The exhibition served as visual illustration of the paper made on behalf of all welders of the country. It consisted of the following chapters: introduction, welded structures, automatic and semi-automatic submerged arc welding, welding in shielded gases, power sources for arc welding, surfacing, electroslag welding, flash-butt welding, innovative methods of welding and cutting, welding consumables, gas-flame treatment, mechanization of assembly-welding works, inspection of welded joints and welding consumables. The achievements were demonstrated by the enterprises of 43 councils of national economy of all regions of the country, 18 ministries, establishments and committees, 22 scientific and research, design and technological organizations. At the exhibition one could get acquainted with innovative technological processes, equipment, rational welded structures, automation and mechanization of assembly-welding, surfacing and other works.

In the section «Welded structures» on the example of crane beam of Chelyabinsk plant of metal structures the advantages of welding in comparison with riveting were shown. In the exposition the mock-up of two-tier stand was shown for manufacture of flat sheet panels, coiled into a coil in accordance with the Paton method of industrial manufacturing of large tanks. The gasholder at the stage of manufacturing using method of coiling was presented at the exhibition. This method allowed several times reducing the time of site works, decreasing the total cost of tanks construction. Besides, the technology of manufacturing of flat-coiled pipes of strips welded on edges was developed. Liquid or gas, supplied among the strips under pressure, form the cylindrical shape of the pipe. Thus, in Tatarstan

the laying of 100 km of pipelines of these pipes allowed saving more than thousands of tons of metal and reducing the cost of construction by 1700 thousand roubles. The results of implementation of new welding technologies of critical engineering products were presented at the exhibition. The unique sample of welded structure was also the exhibition pavilion itself, the dome of which consisted of rings connected between each other in the meridian sections by stiffeners.

One of the most metal-intensive branches is ship building where large block method of building is widely used. At the exhibition the single sub-assemblies, mockups of atomic ice-breaker «Lenin», large-tonnage tankers, dry cargo ships and others were presented.

Electroslag welding was already applied in the 1950s for manufacture of high-capacity power units, forge-press, hoisting-transport and other equipment, equipment for chemical, nuclear and other branches at the Novo-Kramatorsk plant, Taganrog plant «Krasny Kotelshchik», Uralmashzavod, Leningrad Metal plant and other plants and organizations, which presented over 80 exhibits-products and mockups.

CO_2 welding found the wide spreading in our country. The high economic effect of the process was proved by mockups and full-scale samples of products of automotive industry, turbo-generator and turbo-motor plants of Kharkov, Novosibirsk, Leningrad, shipbuilding yards of Kherson and Nikolaev, other machine- building plants, mockups and units of blast furnaces, industrial constructions, etc. In the demonstration of achievements in this field of welding technology more than 30 organizations took part, including NIAT, VNIIESO, E.O. Paton Electric Welding Institute, TsNIITMASh, NIIKhIMMASh.

Maximum mechanization of assembly-welding works in transport machine building, boiler, instrument industries, and also in a number of other branches was provided due to application of all methods of resistance welding. A wide application of repair technologies of restoration of worn-out parts using hardfacing was also reflected at the exhibition. In this section a series of special surfacing mechanized equipment attracted attention. With the development of new types of machinery and more strict requirements to the quality of materials and their joints an attention to related processes and special electric metallurgy was intensified. Surfacing and other technologies of deposition of coatings belong to the methods allowing considerable increasing of service properties of parts and mechanisms.

The successful implementation of new technological processes became possible due to an abrupt increase of production of the modern welding equipment. In the section «Power sources for arc welding» many types of welding transformers, mechanic converters of direct current and semi-conductor rectifiers, developed by VNIIESO, E.O. Paton Electric Welding Institute, NIAT, plant «Elektrik» and other were presented. Hundreds of models of machines for arc welding, machines for resistance welding, machine-tools, holders, different machines of welding stations and other equipment were widely presented. At the exhibition the E.O. Paton Electric Welding Institute presented a welding tractor TS-32 with a sliding water-cooled copper shoe, providing a forced formation of a lower weld bead; tractor TS-33 for automatic welding of butt and fillet welds of aluminium of thickness of up to 40 mm using semi-open arc along the layer of flux with universal set up for layout of a weld between the wheels and near the tractor (including also circumferential welds on the vessels of diameter of 1000 mm and higher); rails machine A-372r and magnetically-walking machine A-501M, which were successfully demonstrated in Brussels and New York; gun A-564 for stud welding under flux in lower, vertical and overhead positions; universal tractor TS-17M, semi-automatic machines PSh-5 and other. Semi-automatic machine A-547r of the E.O. Paton Electric Welding Institute was designed for CO_2 welding of metal of small thickness in all spatial positions using wire of 0.6–1.2 mm diameter at currents of 20–200 A. A set was demonstrated, consisting of a hose holder, feed mechanism together with a wire reel in a common casing, control panel, gas equipment and rectifier VS-200. For resistance spot welding the E.O. Paton Electric Welding Institute developed small-sized tongs K-165 with a built-in transformer, suspended machines for flash-butt welding of rails (K-155) and pipes (KTSA-1). A large amount of versatile and specialized machines and tongs for all methods of resistance welding was presented by VNIIESO and plant «Elektrik». Other technological processes were also provided by high-efficient equipment. According to technical data the domestic equipment was not inferior to the best foreign models, and design solutions were the basis for the development of the new equipment.

The exhibition attracted attention of specialists of many branches of industry, demonstrated high level of welding production in the USSR and had considerable influence on the further development of welding.

SELECTION OF CURRENT SENSOR POSITION IN HIGH-VOLTAGE POWER SOURCES OF WELDING GUNS

O.K. NAZARENKO and **S.A. SHEVCHUK**
E.O. Paton Electric Welding Institute, NASU, Kiev, Ukraine

Studied were spectral characteristics of current flowing in the plus circuit of electron beam sources of accelerating voltage operating on industrial frequency or with high-frequency transformation. Recommendations on the position of resistive current sensor are given.

Keywords: *electron beam welding, accelerating voltage sources, inverter voltage converter, resistive sensor of electron beam current*

A feature of most of the accelerating voltage sources designed for powering welding electron guns is application of resistive current sensors to close the beam current feedback.

Numerous attempts to mount this sensor in the plus circuit of the traditional power sources, generating rectified voltage directly from the mains of frequency f = 50 Hz without frequency transformation, failed, as the feedback signal is quite noisy, because of the flowing in this circuit parasitic capacitive currents of the high-voltage transformer and currents of recharging the filter capacities. Figure 1, *a* gives current oscillogram in the plus circuit of ELA-60 source, in which the high-voltage rectifier is assembled by the Larionov star-triangle connection diagram. Up to 30–50 % of total current, particularly in the range of small current values (from one to several percent of rated current) are made up of low-frequency (f = 50–600 Hz) variable components, for which the results of Fourier analysis are given in Figure 1, *b*. Suppression of these noises requires application of filters with cutoff frequency f_{cutoff} < 10 Hz. For first order filters,

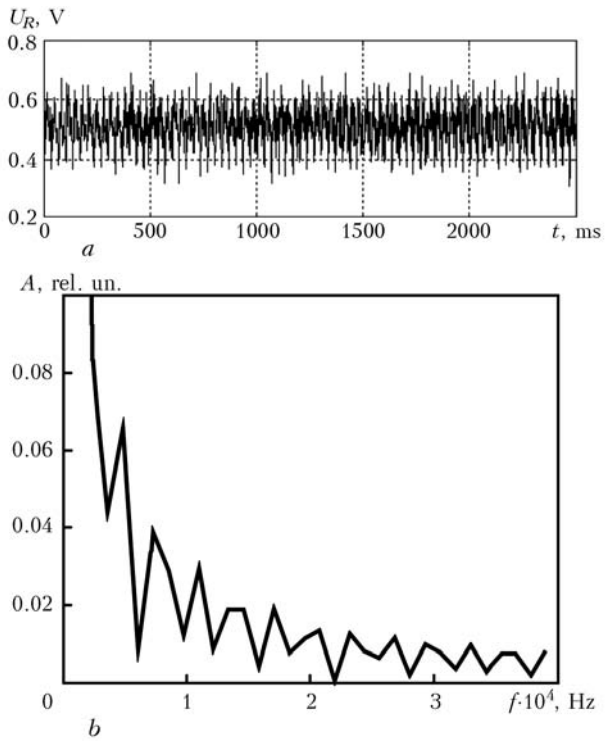

Figure 1. Oscillogram of voltage drop U_R on resistive current sensor with resistance R = 10 Ohm mounted in the plus circuit of accelerating voltage source ELA-60 (*a*), and spectrum of its variable component at load current 50 mA (*b*): A — voltage amplitude

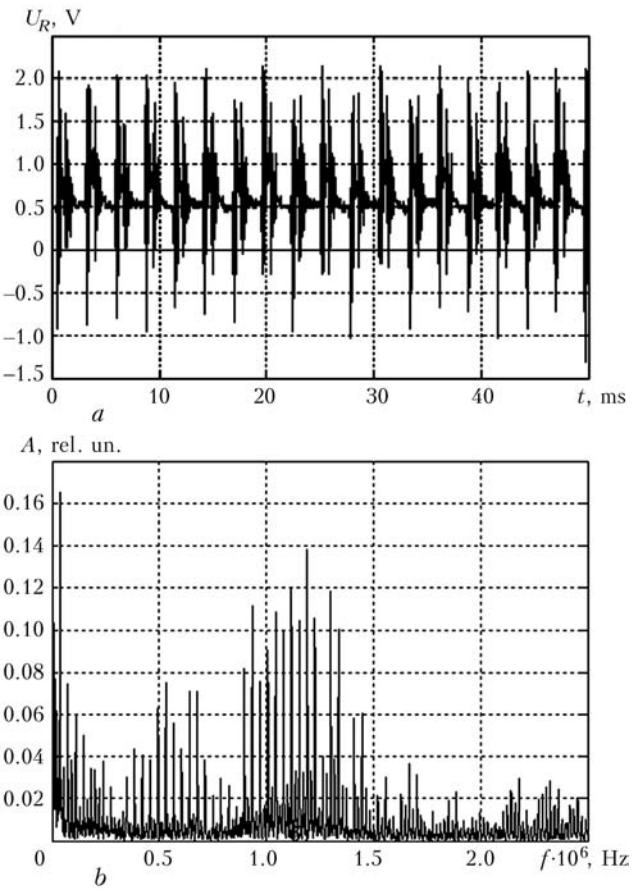

Figure 2. Oscillogram of voltage drop U_R across resistor with resistance R = 10 Ohm of current feedback in the plus circuit of inverter source of accelerating voltage ELAI-120/18 (*a*), and spectrum of its variable component at 50 mA load current (*b*)

in which $f_{cutoff} = (2\pi fRC)^{-1}$ (here, R, C are the resistance and capacity of the component elements), time constant is not less than 100 ms [1]. Here it turns out to be impossible to achieve the required fast control of beam current for welding with pulsed modulation of beam current, or apply secondary-electron systems of following the butt of the edges being welded in real time, when it is necessary to set and stabilize beam current during 5 ms pulse.

When resistive current sensor is mounted in the high-voltage circuit of these power sources, the feedback signal has a low noise level, the need for its filtration is eliminated, and fast control of beam current becomes possible. Such a solution, however, makes the equipment more complicated and less reliable [2].

In inverter power sources with high-frequency transformation of mains voltage mounting current feedback resistor in the plus circuit of the power source is applicable due to the fact that frequencies of the variable component lie in the high frequency region (f = 20–30 kHz) (Figure 2). Filters with 2–3 kHz cutoff frequency can be applied for filtering these components that corresponds to time constant $t <$ < 0.2 ms.

Thus, current feedback resistor in electron beam sources of accelerating voltage operating at industrial frequency should be mounted in the rectifier high-voltage circuit, and in inverter power sources with high-frequency transformation of mains voltage, it is rational to place it in the rectifier plus circuit.

1. Moshits, G., Khorn, P. (1984) *Design of active filters*. Moscow: Mir.
2. Nazarenko, O.K., Lanbin, V.S. (2007) Investigation of high-voltage control circuits of welding electron beam current. *The Paton Welding J.*, **5**, 17–20.

THESES FOR A SCIENTIFIC DEGREE

E.O. Paton Electric Welding Institute of the NAS of Ukraine

On October 6, 2010, V.I. Dzykovich defended his thesis for Candidate of Sciences on «Investigations and development of the materials for wear-resistant surfacing based on spheroidized granules of the tungsten carbides».

The analysis of existing materials for surfacing of wear-resistant composite alloys based on fragmented particles of the tungsten carbide was carried out. It is shown that the spherical shape of particles due to maximum volume of spherical particle at minimum specific surface area is the most perspective for improvement of quality of deposited layer, decrease of a level of dissolution of reinforcing particles during surfacing, enhancement of operating abilities of the composite coatings and increase of a volume fraction of wear-resistant granules in the deposited layer.

The thesis substantiates selection of a method of thermocentrifugal sputtering of refractory materials for obtaining spherical tungsten carbide particles for their application as a wear-resistant phase in a composition of the materials for composite surfacing.

Using mathematical modeling of a method of thermocentrifugal sputtering of tungsten carbide the corresponding equations connecting the main parameters (thermal characteristics of heat source, speed of rotation) with the process efficiency and dimension of the forming tungsten carbide (relite) granules are proposed, and, as a result, the mechanism for control of granulometric composition of tungsten carbide WC–W_2C spheroidized granules was developed. A formula for calculation of a rotation speed of spindle assembly of the unit for sputtering of material of the necessary granulometric composition was obtained.

The technology for melting of source materials with application of induction heating was developed that allows obtaining the ingots for the thermocentrifugal sputtering of high quality eutectic composition.

Investigations of influence of ingot quality for sputtering on structure, properties and stochiometric composition of obtained spherical particles of the tungsten carbides were carried out. In comparison of the spheroidized granules of tungsten carbides with analogues of the well-known foreign companies it was determined that the particles made using the thermocentrifugal sputtering have the maximum values of microhardness and uniformity of chemical and phase composition.

The technology for thermocentrifugal sputtering of refractory materials using plasma arc as a heat source, and commercial equipment were developed on the basis of obtained theoretical and experimental results. The optimum mode for sputtering of tungsten carbide ingots is welding current of 550–600 A at arc voltage of 38–40 V. At that, the optimum speed of vertical feed for ingot makes 0.12–0.18 mm/s. A speed of ingot rotation is the basic parameter influencing

granulometric composition of the spherical sputtering particles. At that, a change of the frequency of rotation from 1200 up to 10000 rpm allows obtaining particles of 1000–50 μm in size.

The investigations of morphometry characteristics of spheroidized granules of the tungsten carbides WC–W_2C were carried out for the first time, and it was determined that all testing powders have very stable and uniform indices on shape of particles. A yield of the tungsten carbide spheroidized granules by 15–20 % higher than that of the source material in separation of a nonspheric constituent from the composition of finished material that has positive influence on the operation of dosing units in some methods of surfacing.

Surfacing materials for deposition by different methods of wear-resistant composite layers based on the tungsten carbide spheroidized granules were developed. The maximum concentration of reinforcing phase in the deposited layer (up to 50 %) was achieved in surfacing of the test samples owing to the biggest volume of spherical particles at minimum specific surface area as compared to the fragmented particles. The minimum dissolution of the particles (up to 5–10 %) in the deposited layer is achieved due to absence of the concentrators of non-uniform heating of particles (spherical shape has no sharp angles). At the same time, there are no secondary iron-tungsten carbides which, significantly, embrittle deposited layer, in the alloy matrix, in particular, based on nickel and copper. Wear resistance of the samples, deposited by different methods using spheroidized granules, on average is 25 % higher of that of the samples with fragmented particles of the tungsten carbides. This is explained by increased microhardness of spheroidized granules, absence of the defects in a form of pores and cracks in them, as well as minimum content of the brittle phases in the alloy matrix.

E.O. Paton Electric Welding Institute of the NAS of Ukraine

On October 6, 2010, T.R. Ganeev (Chernigov State University of Technology) defended his thesis for Candidate of Sciences on «Advancement of a technology for copper to molybdenum diffusion welding».

The thesis is dedicated to development of the technology for a vacuum diffusion welding of molybdenum to copper.

The thesis proposes to apply a low-energy ion treatment in glow-discharge plasma to the molybdenum surface preliminary coated with a copper layer for development of intermediate layer during it welding with copper. This will increase a static strength and heat resistance as well as reduce electric resistance of the welded assemblies.

The methods of molecular dynamics were used in the thesis for detection of the ways of influence of low-energy ions on properties of near-surface molybdenum layers. A relationship between energy of ions bombarding metal surface and location of displacement maximum of molybdenum atoms was determined through mathematical modeling of the process that allowed calculating a mode providing the best conditions for implantation of the atoms of covered with copper layer in the molybdenum.

The thesis presents a mode of ionic etching determined by the methods of polarization resistance and limiting wetting angle allowing increasing the quality of molybdenum surface preparation before thermal vacuum spraying on it of copper layer. The mode providing spraying of a layer of necessary thickness is proposed.

A range of modes for the ion treatment of molybdenum surface covered with copper layer was found at which a modified layer with mechanical properties providing welded sample with a smooth changing of microhardness from copper to molybdenum is formed.

Series of investigations for determination of influence of proposed series of operations on service characteristics of the welded joint was carried out. At application of modified layer 15 % increase of the width of copper diffusion zone in molybdenum is shown with the help of a method of X-ray spectrum analysis. The mode of copper to molybdenum welding was determined providing increase of shear strength of the joint up to 110 MPa, i.e. full-strength copper.

Using experimental X-ray method and method of mathematic modeling 30–35 % reduction of residual equivalent stresses in obtained welded joints, 5 time increase of strength at thermal cycling in comparison with pure Cu–Mo joint as well as 20 % reduction of specific electric resistance are shown in comparison with the welded joint obtained on traditional technology with nickel interlayer application.

The technology for manufacture of the molybdenum anodes by vacuum diffusion welding method was developed on the basis of carried out investigations.

NEWS

CONSUMABLE-NOZZLE ARC-POOL WELDING OF RAILS

During 2009–2010 the specialists of the E.O. Paton Electric Welding Institute developed a special technology, equipment and welding consumables allowing carry out a high-performance quality welding of the rails of different dimension-types in field conditions. New technology, developed on the basis of the method of embedded-electrode arc welding previously proposed in PWI, was named as consumable-nozzle arc-pool welding. Its distinctive feature is usage of a self-shielded flux-cored wire fed through a longitudinal channel in special flat consumable nozzle. This allows welding at 15–18 mm and in certain cases up to 22 mm joint gap. Developed special welding apparatus ARS-4 differs by portability (weight 36 kg) and can be easily adjusted to welding of different rails. Inverter FORSAZh-500 of the Ryazan State Instrument Plant was used as a welding current source. Electricity is supplied by two-phase circuit of 380 V as well as independent diesel generator of 25 kV·A power, at that the power consumed in welding made up to 10 kV·A. An average production time of welding of R65 type rail joint makes around 20 min that allows achieving efficiency of up to 15 joints per shift. Present technology was widely used in reconstruction of a high-speed tram line in Kiev. Around 900 joints of R65, T-62 type rails and web-free tram rails were welded.

Carried out work showed that the consumable-nozzle arc-pool welding of rails is a high-performance process in comparison with manual arc-pool welding method and aluminothermic welding and can be used for welding of railway, tram and crane rails of different application.

MEE'2010

INTERNATIONAL CONFERENCE «MEE-2010»

The 6th International Conference «Materials and coatings under extreme conditions: investigation, application, environmentally appropriate technologies for manufacture and recycling of products» took place in Big Yalta, Crimea, Ukraine, in September 20–24, 2010. It was dedicated to the 80th birth anniversary of Viktor I. Trefilov, a well-known scientist and materials engineer.

The Conference was organized by the National Academy of Sciences of Ukraine (NASU), Russian Academy of Sciences (RAS), National Academy of Sciences of Belarus (NASB), Ukrainian Society for Materials Science, I.M. Frantsevich Institute of Problems of Materials Science, Joint Institute of High Temperatures of the RAS, A.A. Baykov Institute of Metallurgy and Materials Science of the RAS, N.E. Bauman Moscow State Technical University, A.V. Lykov Institute of Heat and Mass Transfer of the NASB and INTERM Ltd. (Ukraine).

The Conference was held under the auspices of the Headquarters of United Stated Air Force in Europe, Secretariat of European program EUREKA, JNR Global and Federation of European Societies for Materials Science. European Office of Airspace Research and Development, Air Force Office Scientific Research, United States Air Force Research Laboratory, U.S. Office of Naval Research Global, I.M. Frantsevich Institute of Problems of Materials Science of the NASU, National Academy of Sciences of Ukraine, companies «Virial» (St.-Petersburg, Russia), «Diskom» (Kiev, Ukraine) and «Eltekhmash» (Vinnitsa, Ukraine) were sponsors of the Conference.

More than 150 scientists, researchers, post-graduate students and engineers of world leading research centres, research institutes, universities, academies, branch laboratories and other organizations from 17 countries participated in the Conference work.

The Conference was opened by a welcoming speech of academician of the NASU V.V. Skorokhod. He wished all the participant a successful work and business-like co-operation as well as read out the tasks of the Conference and stated organizing issues.

The problems of the Conference were discussed in nine sections:

- *A*: Principles of designing of the materials and coatings for operation under extreme conditions;
- *B*: Scientific principles and computer modeling of the processes for obtaining materials and coatings operating under extreme conditions;
- *C*: Perspective technologies for obtaining and joining of the materials and parts operating under extreme conditions;
- *D*: Structure and properties of the materials and coatings for operation under extreme conditions;
- *E*: Special session «Heat-protection coatings»;
- *F:* Experimental results of application of the materials and coatings under natural extreme conditions;
- *G*: Possibilities and up-to-date technologies of recycling of industrial waste in order to obtain structural, heat-insulating, covering and other materials;
- *H:* Research and organization and information issues of cooperation of the materials engineer scientists;
- *I*: Round-table discussion «Effective transfer of the technologies — a catalyst of innovative development of the society».

The themes of papers, being under consideration in sections B and C, included the welding technologies and technologies classified as related to welding as well as structures of the materials and their properties, obtained through welding heating. The following papers, in our opinion, can be interesting for the welding specialists: «Obtaining of titanium-based functionally gradient coatings by laser surfacing method» (V.K. Narva, A.V. Marani, Moscow Institute of Steel and Alloys, Russia); «Advantages of electron beam technology in development of reinforcing coatings» (N.K. Galchenko, S.I. Belyuk, K.A. Kolesnikova, Institute of Strength Physics and Materials Science of RAS SD, Tomsk, Russia); «Technology and equipment for diffusion welding of high-precision parts on dissimilar materials» (A.V. Lyushinsky, OJSC «Ramenskoe Instrument Engineering Design Bureau», Russia); «Development of resource-saving repair technology for the turbine rotor blades on alloy KhN65VMYuT (EI893)» (Yu.P. Tarasenko, O.B. Berdnik, V.A. Sorokin, Nizhny Novgorod Branch of the A.A. Blagonravov Institute of Machine Science of the RAS, Russia); «Damageability of long-term running welded joints of the steam lines» (V.V. Dmitrik, S.N. Bartash, NTU-KhPI, Kharkov, Ukraine) and series of others.

After plenary papers the participants of the Conference listened to oral presentations and examined poster papers. In total around 200 papers and oral presentations were made.

In course of the Conference work the ways of further development of the materials science for solving specific tasks on development of the structural materials and coatings and their application under extreme conditions were discussed. The participants of the Conference exchanged scientific information, established business contacts and drew up the plans of joint scientific activities.

In our opinion, the Conference was of interest not only for the materials science researchers, but also for the welders studying structure of the materials and coatings made by means of welding as well as related technologies.

Prof. V.V. Dmitrik, KhPI

TECHNICAL SEMINAR «AIRCRAFT CONSTRUCTION — TECHNOLOGIES AND EQUIPMENT FOR WELDING»

On October 7, 2010, a one day seminar on «Aircraft construction — technologies and equipment for welding» was held in the Technology Center of OSJC «Fronius Ukraine» in Knyazhichi village, Kiev District. The seminar that is becoming a tradition was organized by the directorship and specialists of OSJC «Fronius Ukraine». The idea of holding the seminar was suggested by the lately increased interest to developments of «Fronius» Company from the Ukrainian companies working in the field of aircraft construction and repair of aircraft equipment, as well as the need for familiarization of the leading specialists of these companies with operation of Company equipment in the plants.

Seminar participants included representatives of SE «Antonov» and its affiliate «Antonov Commercial Plant», Kharkov State Aircraft Manufacturing Plant, SE «PA Yuzhny Mashinostroitelny Zavod im. A.M. Makarova», OJSC «Motor Sich», Kharkov National University «KhNU», «Aeroprakt» Ltd., PC «Anisimov», «Lugansky aviatsionno-remontny zavod» Ltd., Lvov and Nikolaev Aircraft Repair Plants of MD of Ukraine, OJSC «Linder Gas Ukraina», «Favorit Ltd.», E.O. Paton Electric Welding Institute of the NAS of Ukraine, OJSC «Severodonetsky zavod khimicheskogo nestandartizirovannogo oborudovaniya». Seminar was opened by V.L. Bondarenko, Sales Manager of OJSC «Fronius Ukraine».

Program of the seminar held in the mode of a dialogue between managers of «Fronius Ukraine» and its participants, included the theoretical and demonstration parts on the following subjects:

- technological features of application of «Fronius» equipment for welding stainless steels and aluminium alloys by TIG process (V. Shkurenko, Manager of Sales Department of «Fronius Ukraine»);
- welding helmets of Vizor 3000 series (A. Pindyura, SD Manager);
- technological capabilities of CMT process and its application (D. Bojko, Advertising Manager);
- welding process automation. Orbital welding systems (V. Onishchuk, engineer);
- equipment for plasma cutting Trans Cut300 (A. Tarajmovich, engineer).

In addition, the following presentations were made in the seminar: by G. Kovalenko, Chief Welder of SE «Antonov» affiliate — «Antonov Commercial Plant», on the subject «Experience of application of «Fronius» equipment in aircraft construction» and by A. Grinuyk, PWI Junior Staff Scientist, on the subject «Technology and equipment for plasma welding and its application».

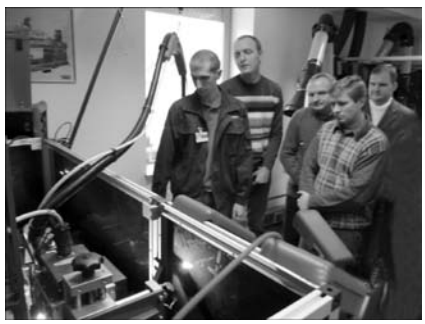

Presentations made in the seminar, aroused lively interest of the participants. The dynamic form of their presentation, good illustration material, questions and answers during the presentations allowed satisfying the inquiries of seminar participants. Subsequent practical familiarization with the equipment during demonstration of operation in various modes and on a range of materials, effectively complemented the theoretical discussion. All the seminar participants expressed their gratitude to seminar organizers for an intensive program and possibility of detailed familiarization with advanced samples of equipment and technologies.

Seminar participants were invited to the International Industrial Forum (Kiev, IEC, 23.26.2010), to the booth of «Fronius Ukraine».

Prof. V.N. Lipodaev, PWI